Carlsbad Programs Group
Waste Isolation Pilot Plant

BRAGFLO Results For the Technical Baseline Migration

Revision 0

Author:	Clifford Hansen (6823)		August 15, 2002
	Print	Signature For Cliff Hansen	Date
Author:	Christi Leigh (6852)		August 15, 2002
	Print	Signature	Date
Author:	David Lord (6821)	David L Lord	8/15/2002
	Print	Signature	Date
Author:	Joshua Stein (6821)	David L Lord For Joshua Stein	8/15/2002
	Print	Signature	Date
Technical Review:	Palmer Vaughn (6840)	For Palmer Vaughn	August 15, 2002
	Print	Signature	Date
Management Review:	M. Kathryn Knowles (6821)		15 August 2002
	Print	Signature	Date
QA Review:	Mario Chavez (6820)	Mario Chavez	15 Aug 02
	Print	Signature	Date

Acknowledgements

The authors would like to recognize the contributions of Rodger Coman (Hewlett Packard Corporation), Kari Cox (Sandia National Laboratories, Department 6821), Jim Garner (Piru Associates), Teklu Hadgu (Sandia National Laboratories, Department 6821), Dave Lechel (Lechel Inc), Jennifer Long (Sandia National Laboratories, Department 6821) to the development of this report.

TABLE OF CONTENTS

Page

FIGURES

TABLES

ACRONYMS

CCA	Compliance Certification Application
CCDF	Complementary Cumulative Distribution Function
CFR	Code of Federal Regulations
CMS	Code Management System
DOE	U.S. Department of Energy
DRZ	Disturbed Rock Zone
EPA	U.S. Environmental Protection Agency
LWB	Land Withdrawal Boundary
MB	Marker Bed
PA	Performance Assessment
PAVT	Performance Assessment Verification Test
PCS	Panel Closure System
SMC	Salado Mass Concrete
SNL	Sandia National Laboratories
SRS	Savannah River Site
TBM	Technical Baseline Migration
TRU	Transuranic Waste
WIPP	Waste Isolation Pilot Plant

REFERENCED VARIABLE NAMES

BNBHDNUZ	Brine flow down the borehole at the top of the upper disturbed rock zone
BNBHLDRZ	Brine flow up the borehole at the bottom of the lower disturbed rock zone
BNBHUDRZ	Brine flow up the borehole at the top of the upper disturbed rock zone
BRNREPTC	Cumulative brine flow into the waste regions
BRNVOL_A	Total brine volume in excavated areas
CELL_KG	Remaining mass of cellulose
CONC_PCS	Material representing panel closure concrete
CONC_T1	Material representing salt saturated concrete designed for the shaft (initial conditions)
CPCS_F	Material representing panel closure concrete at low pressures
DRF_PCS	Material representing the empty drift and explosion wall
DRZ_1	Material representing the disturbed rock zone above and below the repository excluding the DRZ above the panel closure
DRZ_PCS	Material representing the disturbed rock zone above the panel closure
EXP_POR	Porosity in the experimental area
EXP_PRES	Volume-averaged pressure in the experimental area
EXP_SATB	Brine saturation in the experimental area
FE_KG	Remaining mass of steel
GAS_MOLE	Total moles of gas generated
PRMX_LOG	Log of permeability in the x direction
PRMY_LOG	Log of permeability in the y direction
PRMZ_LOG	Log of permeability in the z direction
REP_POR	Volume-averaged porosity in the rest of repository
REP_PRES	Volume-averaged pressure in the rest of repository
REP_SATB	Volume-averaged brine saturation in the rest of repository
WAS_POR	Volume-averaged porosity in the waste panel
WAS_PRES	Volume-averaged pressure in the waste panel

WAS_SATB	Volume-averaged brine saturation in the waste panel

GLOSSARY OF TERMS

Carbon-normalized molecular weight: The carbon-normalized molecular weight is the molecular weight of the molecule divided by the number of carbon atoms in the molecule.

Correlation Coefficient:

Excavated Area: This term is used to refer to the WIPP excavated regions together.

Horsetail Plot: A plot showing the value of a single variable over time for a full replicate (100 vectors).

Intruded Panel: The single waste panel located at the south end of the repository. The borehole is represented as intersecting this panel in disturbed scenarios. Same as "Waste Panel."

Replicate Analysis: For this report, a replicate analysis is used to understand how certain changes affect model results over a full replicate (100 vectors). The analysis examines results from a full replicate that incorporates the changes and compares these results on a vector-by-vector basis to other calculations that only differ in the changes being examined (sampled input variables must be equal among calculations).

Rest Of Repository: In the CCA and PAVT this is the region in the BRAGFLO grid that represents nine waste panels with no panel closures. In the TBM this region is divided into a North and South Rest of Repository region separated by a panel closure. For the present analysis, the North and South Rest of Repository regions are volume averaged in order that they can be compared with the PAVT results.

Scatter Plot: For the replicate analyses, scatter plots illustrate the differences between calculations. They plot a variable's value at a certain time in one calculation against another calculation for each vector. If the values are similar between calculations (and the plots have the same axis limits), the symbols lie on the diagonal 1 to 1 line dividing the plot in half. Deviations from this trend indicate differences between the calculations.

Sensitivity Analysis:

Volume-Averaged Brine Saturation: The volume-averaged brine saturation of a particular repository region is the total volume of brine in that region divided by the total pore volume of the region.

Volume-Averaged Porosity: The volume-averaged porosity of a particular repository region is the total pore volume in that region divided by the total volume of the region (including the rock).

Volume-Averaged Pressure: The volume-averaged pressure in a particular region is the sum of the products of pressure and grid cell volume for each grid cell in the region divided by the total volume of the region.

Waste Panel: The single waste panel located at the south end of the repository. The borehole is represented as intersecting this panel in disturbed scenarios. Same as "Intruded Panel."

Waste Region: The combination of the Waste Panel and the Rest of Repository. These regions are where all the waste resides.

1. INTRODUCTION

The Technical Baseline Migration (TBM) refers to a series of modifications and corrections made to parameters, conceptual models, and the computational grid used in the Waste Isolation Pilot Plant (WIPP) Performance Assessment (PA). In May, 2002, these changes were presented to the Salado Flow Peer Review Panel and were conditionally approved (Caporuscio et al., 2002). The panel withheld its final approval until after the full PA is run and the final Complementary Cumulative Distribution Function (CCDF) results are available.

This report describes the effects of the changes made for the TBM on the brine and gas flow (BRAGFLO) model in the baseline PA. It completes the analysis outlined in SNL AP-086 (Stein, 2002a). This analysis compares results from the BRAGFLO model run with the TBM changes to those obtained in the Performance Assessment Verification Test (PAVT). The PAVT is the current baseline. For this reason there is no need to compare TBM results to the CCA.

TRANSURANIC WASTE

TRU waste is defined as "waste containing more than 100 nanocuries of alpha-emitting transuranic isotopes, per gram of waste, with half-lives greater than 20 years, except for (A) high-level radioactive waste, (B) waste that the Secretary has determined, with concurrence of the Administrator, does not need the degree of isolation required by the disposal regulations; or (C) waste that the Nuclear Regulatory Commission has approved for disposal on a case-by-case basis in accordance with part 61 of title 10, Code of Federal Regulations" (WIPP Land Withdrawal Act, Public Law 102-579).

TRU elements, each having several isotopes, are radioactive and typically man-made. The half-lives of many are considerably longer than 20 years. For instance, the half-life of one isotope of plutonium is 24,000 years.

TRU waste is further classified as contact-handled or remote-handled. Contact-handled waste has radioactive levels that are low enough to permit workers to directly handle the containers in which the waste is kept. This level of radioactivity is specified as a dose rate of no more than 200 millirems per hour at the outside surface of the container. Remote-handled waste has a surface dose rate greater than 200 millirems per hour, so workers use remote manipulators to handle containers of remote-handled waste.

1.1 BACKGROUND

The WIPP is a deep geologic repository for the disposal of transuranic (TRU) waste generated by national defense activities. The WIPP site is located in Eddy County in southeastern New Mexico about 26 miles southeast of the City of Carlsbad. The WIPP underground disposal area is mined at a depth of about 2,160 feet beneath the surface in ancient salt beds of the Salado Formation (Figure 1). The WIPP facility has been designed to dispose of up to 175,600 cubic meters of contact-handled and 7,080 cubic meters of remote-handled TRU waste.

The WIPP, which is owned and managed by the U.S. Department of Energy (DOE), is operated by Westinghouse TRU Solutions, LLC. Sandia National Laboratories (SNL), as a scientific advisor to the DOE, is primarily responsible for the conduct of various field experiments and for the development and maintenance of the analytic tools needed for the demonstration of compliance with TRU waste disposal regulations.

In October 1996, the DOE submitted its CCA to the EPA (DOE, 1996). The CCA, which is DOE's request that EPA certify the WIPP for the disposal of TRU waste, was prepared in response to the

requirements promulgated by the EPA at 40 Code of Federal Regulations (CFR) Part 191, the criteria in 40 CFR Part 194, and the guidance in the EPA's *Compliance Application Guidance for 40 CFR Part 191* (EPA, 1996). The CCA included a Performance Assessment (PA), which evaluated the potential for radioactive materials to migrate to the accessible environment over a 10,000-year period (i.e., repository performance). The PA was based on a compendium of conceptual models for features, events, and processes that could affect repository performance, software applications that implement the conceptual models, and parameter values and their associated distributions that form inputs to the software applications.

The WIPP PA

The WIPP PA is based on a compendium of conceptual models for features, events, and processes that could affect repository performance, software applications that implement the conceptual models, and parameter values and their associated distributions that form inputs to the software applications.

After agency discussions and the submittal of additional information by DOE, EPA determined the CCA to be complete in May 1997. EPA later required a verification of the calculations performed for the CCA, the PAVT. In its review of the CCA, the EPA identified a subset of the CCA parameters whose values and distributions were in question (EPA, 1998). EPA then required DOE to use the revised parameters in a new PA calculation (the PAVT calculation) that subsequently became part of the WIPP's regulatory basis.

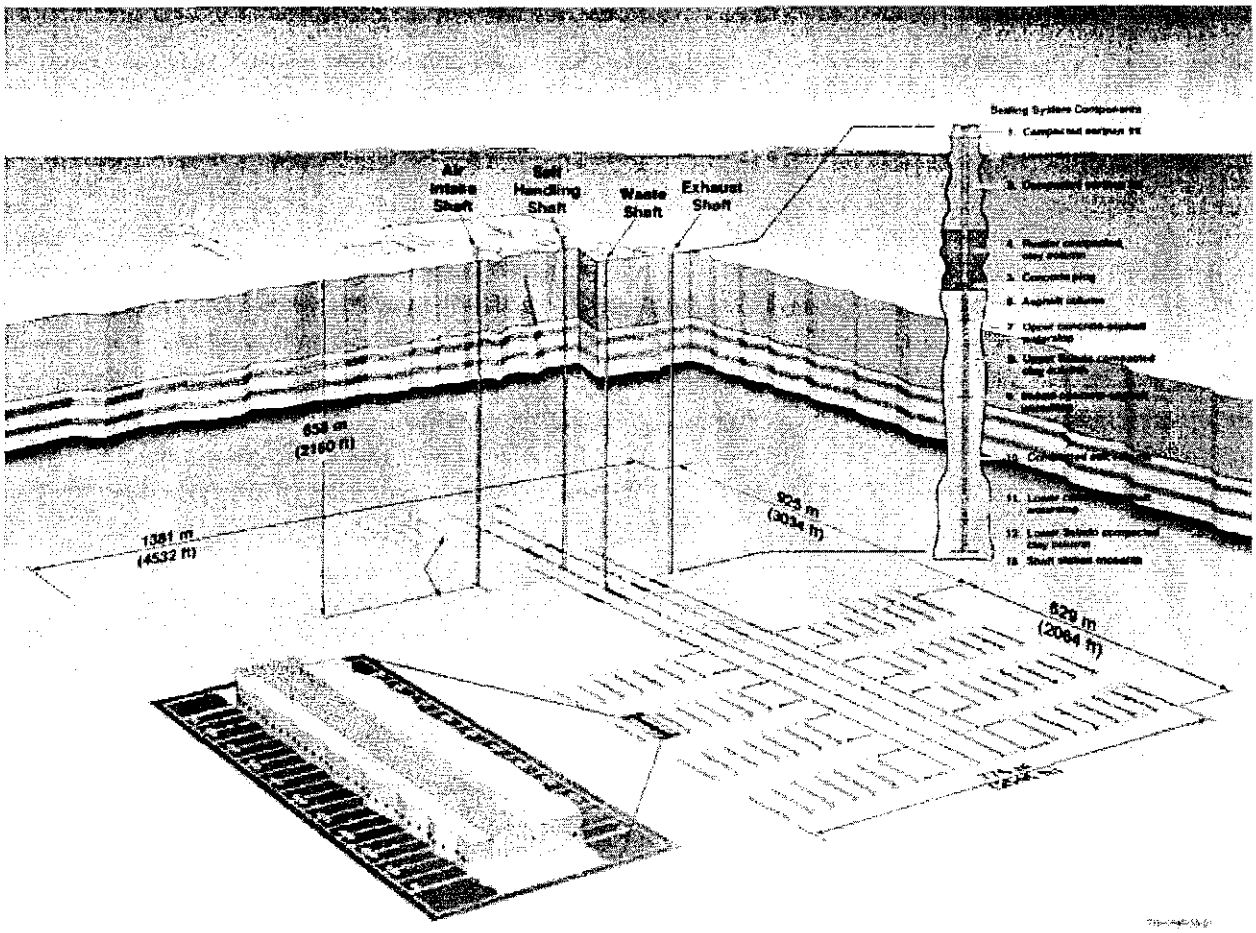

Figure 1. The WIPP Repository Layout

In May 1998, after undergoing a rulemaking, the EPA certified that the WIPP would comply with the radioactive waste disposal regulations of 40 CFR Part 191. The first shipment of TRU waste arrived at the WIPP for disposal in April 1999.

1.2 MOTIVATION FOR THE TBM

Since completion of the CCA SNL's understanding of the physical and chemical processes that control releases to the environment has improved. SNL has identified several errors in the CCA and PAVT Calculations that have been corrected, evaluated, and found to have minimal impact on risk. Furthermore, in EPA's certification, the agency mandated use of a specific panel closure that is inconsistent with the panel closure modeled in the CCA calculation.

- As SNL's ability to assess WIPP's performance evolves or WIPP operations change, it is incumbent upon SNL to update upon its PA tools to support DOE in its future compliance certification efforts. The TBM consolidates the improvements and corrections in conceptual models and parameters in order to advance the WIPP's performance assessment baseline. This report focuses on the effects of these changes on the brine and gas flow (BRAGFLO) model in the PA.

1.3 REPORT ORGANIZATION

This report first outlines PA methods in general and as applied to the WIPP. The improvements and corrections to the conceptual models and parameters are described, and the results of the peer review are summarized. The report compares the BRAGFLO calculations for the TBM to those obtained in the PAVT to identify the effect on repository performance resulting from the changes, and finally presents the conclusions of this analysis.

2. WIPP PERFORMANCE ASSESSMENT METHOD

The WIPP PA is a series of computer simulations that describe the natural and engineered components of the disposal system (e.g., site characteristics, waste forms, waste quantities, and engineered features) in a manner that reflects the behaviors and interactions among these components (DOE, 1996). The computer simulations are developed from conceptual models that represent the physical and chemical attributes of the repository. The conceptual models are expressed as mathematical relationships, which are translated into computer code and solved with iterative numerical models. The results of the simulations quanitify the potential releases of radioactive materials from the disposal system to the accessible environment over the 10,000-year regulatory period.

Scenario Conceptualization

Scenario S1 represents the undisturbed conditions.

Scenario S3 represents an intrusion event where a borehole penetrates the repository and a Castile brine reservoir 1,000 years after repository closure.

Scenario S5 represents an intrusion event where a borehole penetrates the repository but not a Castile brine reservoir 1,000 years after repository closure.

2.1 PERFORMANCE ASSESSMENT SCENARIOS

Scenarios are representations of the evolution of the disposal system and are composed of specific combinations of features, events, and processes. The PA process formulates scenarios by considering the natural and man-made processes and events that could affect the disposal system, as well as probable release mechanisms from the disposal system. Cumulative radionuclide releases from the disposal system are calculated for each scenario and are combined with the probability of each scenario's occurrence to construct distributions of releases. The WIPP PA considered scenarios for undisturbed performance and disturbed performance. Thus, potential releases from both natural processes (e.g., via dissolution) and human-initiated activities (e.g., via drilling intrusions) that would occur were assessed. In the WIPP PA there are six scenarios defined (S1 through S6).

Undisturbed performance (Scenario S1) is defined in 40 CFR § 191.12 to mean "the predicted behavior of a disposal system, including consideration of the uncertainties in predicted behavior, if the disposal system is not disturbed by human intrusion or the occurrence of unlikely natural events." Conceptually, there are several pathways for radionuclide transport within the undisturbed disposal system that may result in releases to the accessible environment. These conceptual pathways are shown in Figure 2. Contaminated brine may migrate away from the waste-disposal panels if pressure within the panels is elevated by the generation of gas from corrosion or microbial degradation. Radionuclide transport may occur laterally, through the anhydrite marker beds toward the subsurface boundary of the accessible environment in the Salado, or through access drifts or anhydrite marker beds (primarily Marker Bed [MB] 139) to the base of the shafts. In the latter case, if the pressure gradient between the panels and overlying strata is sufficient, then contaminated brine may migrate up the shaft seals. As a result, radionuclides may be transported directly to the ground surface, or they may be transported laterally away from the shafts, through permeable strata such as the Culebra, toward the subsurface boundary of the accessible environment.

Disturbed performance scenarios (S2-S6) represent deep drilling events that intersect the waste disposal region. While mining scenarios are also disturbed performance scenarios, the deep drilling events are the only disturbed scenarios that can potentially affect repository brine and gas flow. The conceptual pathways releases due to a deep drilling event are shown in Figure 3. Releases to the accessible environment may occur at the time of the drilling event through cuttings, cavings, direct brine release (DBR), and spallings. Cuttings are the materials cut by the drill bit as it passes through the waste Cavings are the materials that may be eroded from the borehole walls by the drilling fluid. Spallings are the materials that may be transported up the borehole by venting gas if there is sufficient pressure in the waste disposal panel.. Shortly after the drilling event, contaminated brine may flow up the borehole and reach the surface, depending on fluid pressure within the waste panels. Finally, the borehole may alter the flow of brine and gas in and around the repository and thus affect releases by transport mechanisms.

Five distinct disturbed scenarios that impact release from the repository are defined for the WIPP PA. Four of these involve a single drilling intrusion that occurs at either 350 or 1,000 years after repository closure. There are two types of drilling intrusions that are considered: 1) a borehole is drilled through a single waste panel and intersects a pressurized brine pocket located approximately 250 meters below the repository, and 2) a borehole is drilled into the repository but does not intersect a brine pocket. One

multiple intrusion scenario is considered. The six scenarios used in the BRAGFLO calculations at WIPP are listed below.

S1 Undisturbed scenario
S2 Single drilling intrusion that intersects repository and brine pocket at 350 years
S3 Single drilling intrusion that intersects repository and brine pocket at 1,000 years
S4 Single drilling intrusion that intersects repository only at 350 years
S5 Single drilling intrusion that intersects repository only at 1,000 years
S6 Multiple intrusion: drilling intrusion that intersects repository and brine pocket at 1,000 years followed by a second intrusion that intersects the repository only at 2,000 years.

2.2 SCENARIO IMPLEMENTATION

The WIPP PA system currently relies on eight primary computer models: BRAGFLO, NUTS, PANEL, CUTTINGS_S, SECOFL2D, SECOTP2D, BRAGFLO_DBR, and CCDFGF. Figure 4 illustrates the WIPP PA in a simplified format.

Many parameters that are inputs to these models are uncertain. To account for this uncertainty, the PA system samples from a distribution for each uncertain parameter. A set of input values, one for each uncertain parameter, is called a vector. In each scenario, the models are run once for each vector, generating a single outcome. For each model, the set of outcomes for all vectors constitutes a distribution of outcomes for that model and scenario class. The PA system then generates a set of possible futures for the repository and uses the distribution of outcomes from each model to construct a distribution of releases.

2.2.1

The results from the BRAGFLO code are the focus of this report. The BrineAndGasFlow (BRAGFLO) model simulates the interaction of brine, gas and the response of the surrounding host rock during undisturbed conditions and intrusions scenarios. It simulates two-phase, three-dimensional, isothermal fluid flow in porous media using a finite-difference numerical solution scheme. BRAGFLO includes corrosion and biodegradation gas-generation sub-models that simulate the waste's iron and cellulose decomposition effects. The model is linked to input utility codes.

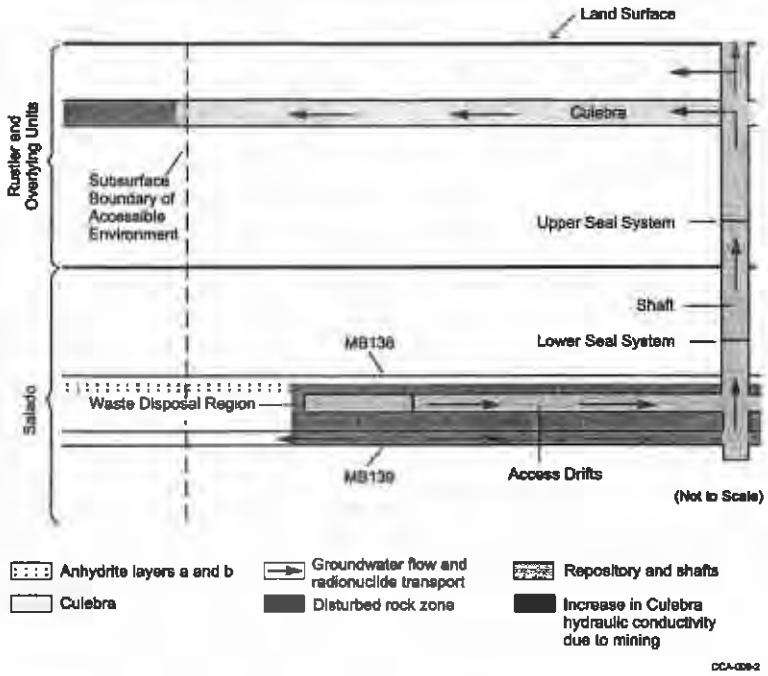

Figure 2. Conceptual Pathways for Undisturbed Performance

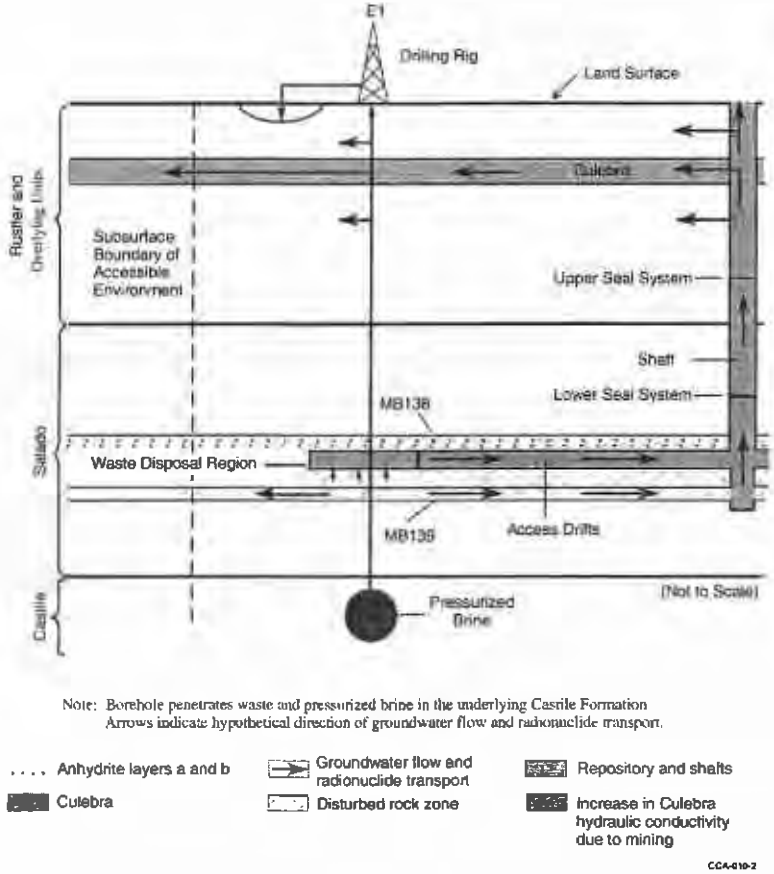

Figure 3. Conceptual Pathways for Disturbed Performance Due to Deep Drilling

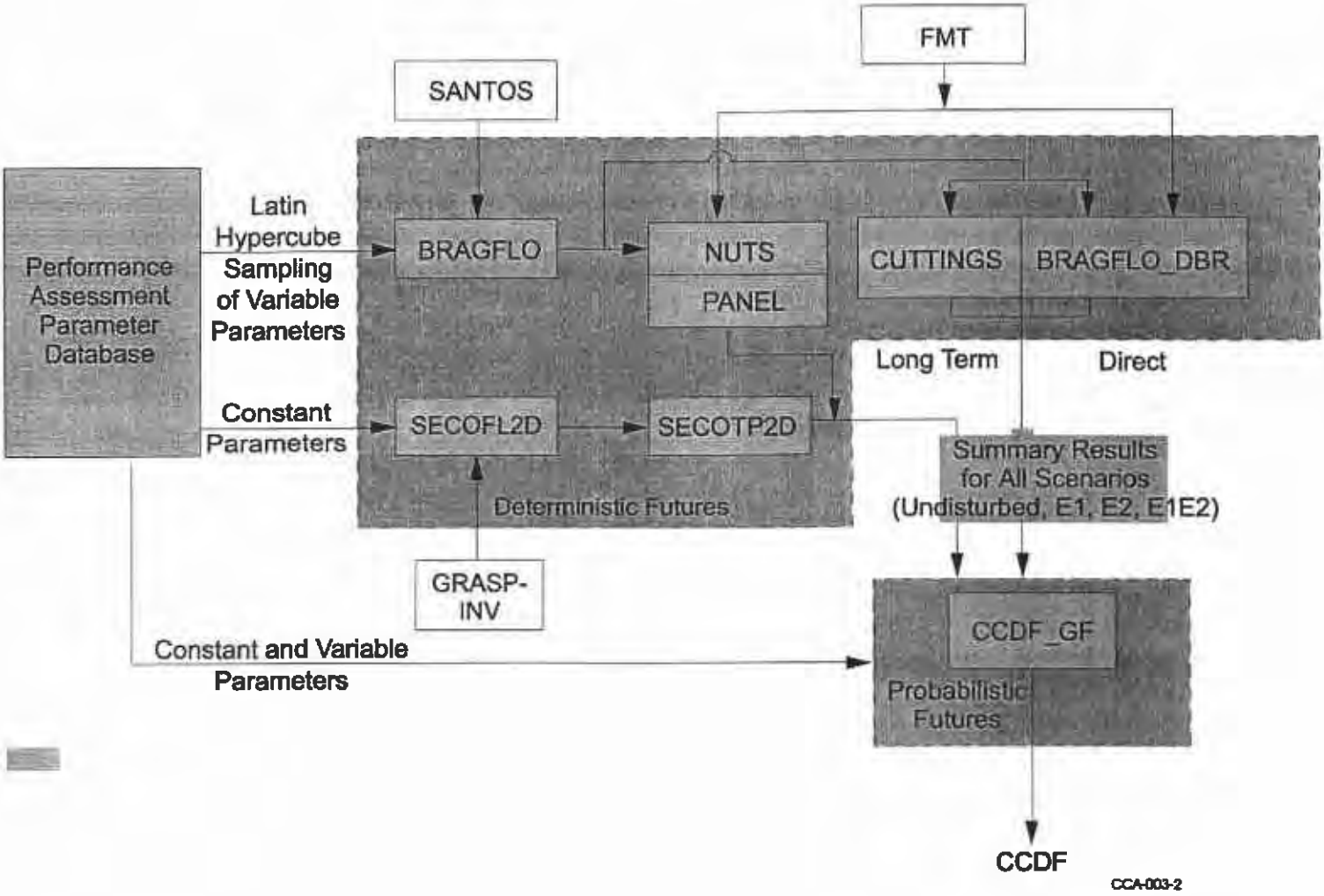

Figure 4. Simplified Depiction of WIPP Performance Assessment Process

3. CHANGES MADE FOR THE TECHNICAL BASELINE MIGRATION

Since completion of the CCA and EPA's certification of the WIPP SNL's conceptual understanding of the physical and chemical processes that control releases to the environment has improved, errors have been identified in the baseline calculation that require correction, and a specific panel closure design (Option D) that was not modeled in the CCA has been specified by the EPA (40 CFR Part 194). These three developments have precipitated changes in the WIPP PA system which are manifested in a changed computational grid and changed material properties used in BRAGFLO. The following discussion addresses the changes in the BRAGFLO computational grid (Section 3.1) and the changes to parameters used by BRAGFLO (Section 3.2). A final section (Section 3.3) summarizes the conclusions of the Salado Flow peer review.

3.1 BRAGFLO COMPUTATIONAL GRID

The BRAGFLO code uses a finite-difference numerical scheme to simulate brine and gas flows and interactions within and around the repository. The finite-difference scheme employs a computational grid that defines the length, width, and height of grid elements that are configured to represent important repository features like the waste panels and panel closures, and the surrounding geologic units.

The primary assumption underlying the formulation of the BRAGFLO computational grid is that spatial processes in the vicinity of the repository can be adequately represented in a 2-dimensional domain. The BRAGFLO simulations are executed with a vertical 2-dimensional grid that comprises a cross-section on a north-south axis (the X axis of the grid) directly through the repository. The vertical dimension of the repository corresponds to the Y axis of the grid. Flows convergent to and divergent from the waste regions are accommodated in a grid flaring scheme in which the depth of grid elements perpendicular to the X-Y plane (the Z axis of the grid) are increased with horizontal distance from the waste regions. This flaring is a mathematically rigorous technique for capturing flow in radical geometry.

3.1.1 Baseline Computational Grid

The CCA and PAVT calculations used the 33 × 31 element grid shown in Figure 5. The dimensions of each grid element are shown in Appendix A. Horizontal grid spacing in the excavated region was determined largely by the dimensions of repository features (e.g. the shaft and intrusion borehole). Horizontal spacing to the north and south of the excavated region started at 10 m and increased by a factor of 2-5 out to 20 km beyond the Land Withdrawal Boundary (LWB). Vertical spacing at the repository level was determined by the dimensions of the excavated regions and marker beds. In the upper Salado, vertical spacing was set by the thickness of shaft seal materials. For units above the Salado, vertical spacing was controlled by the thickness of

The Baseline Computational Grid

The baseline BRAGFLO grid has 1023 elements. Grid flaring is used to represent convergent and divergent fluid flow patterns in a 2-D geometry. The waste areas are divided into two regions: a single panel and a 9-panel "rest of repository." Two generic panel closures are represented. The four shafts are represented by a composite shaft explicitly included in the grid.

each major geologic formation.

In the CCA and PAVT calculations, the repository regions that contain waste were divided into two sub-regions, a single panel at the south end of the waste region and a "rest of repository" region, comprising the other nine waste panels. The single panel represents the volume of a typical panel and is used to calculate the consequences from various intrusion scenarios. It is located in the southern or "down-dip" portion of the repository because this was shown to result in slightly larger release consequences and it is awkward to vary the location of an intruded panel in an efficient manner for PA production runs. This geometry allowed for a detailed representation of an intrusion borehole penetrating a single panel. All excavated regions in the grid were bordered on the top and bottom by the disturbed rock zone (DRZ). The single waste panel was bordered by intact Salado on the south side, and by a 40m long panel closure on the north side. The rest of repository lay immediately north of the 40m panel closure, and had an 80m panel closure forming its northern boundary. Each panel closure was represented by a single column of three grid cells with a constant permeability of $10^{-15}m^2$. North of the 80 m panel closure was the operations region and then the experimental region.

The four shafts, air intake shaft, salt handling shaft, waste shaft, and exhaust shaft, were combined into a single shaft positioned between the operations area and experimental area in the computational grid. This single shaft is positioned at the smallest distance between a shaft and the waste disposal regions (i.e., the location of the waste handling shaft). To represent aging of selected shaft materials, material properties were changed five times during the 10,000-year simulationsand BRAGFLO calculations were restarted.

Effects of flow in the third (out-of-plane) dimension were approximated with a flaring scheme that simulated convergent or divergent flow to the north and south of the repository. Two scales of flaring were included: local-scale flaring around the intrusion borehole and shaft; and regional-scale flaring around a point near the north end of the rest of the repository. Flaring simplifies calculation by representing three-dimensional phenomena within a two-dimensional grid. Results from the simplified 2-D model were compared to three-dimensional model simulations and found to be acceptable because the computed releases to the accessible environment for both representations were nearly equivalent (Vaughn, 1996). The comparison concluded that the two-dimensional model was sufficient for calculating releases.

Simulations of various intrusion scenarios were achieved for the CCA and PAVT by using three different maps of material properties: one for undisturbed conditions; one for the intrusion event in which a borehole penetrates the repository and a Castile brine reservoir (Scenario S3); and one for the intrusion event in which a borehole penetrates the repository but not a Castile brine reservoir (Scenario S5) (see also Figures 2 and 3). For example, at the time of a drilling intrusion into the repository, the borehole grid block properties were changed to those consistent with a borehole and plug system. Using this strategy, all scenarios could be represented with the same computational grid.

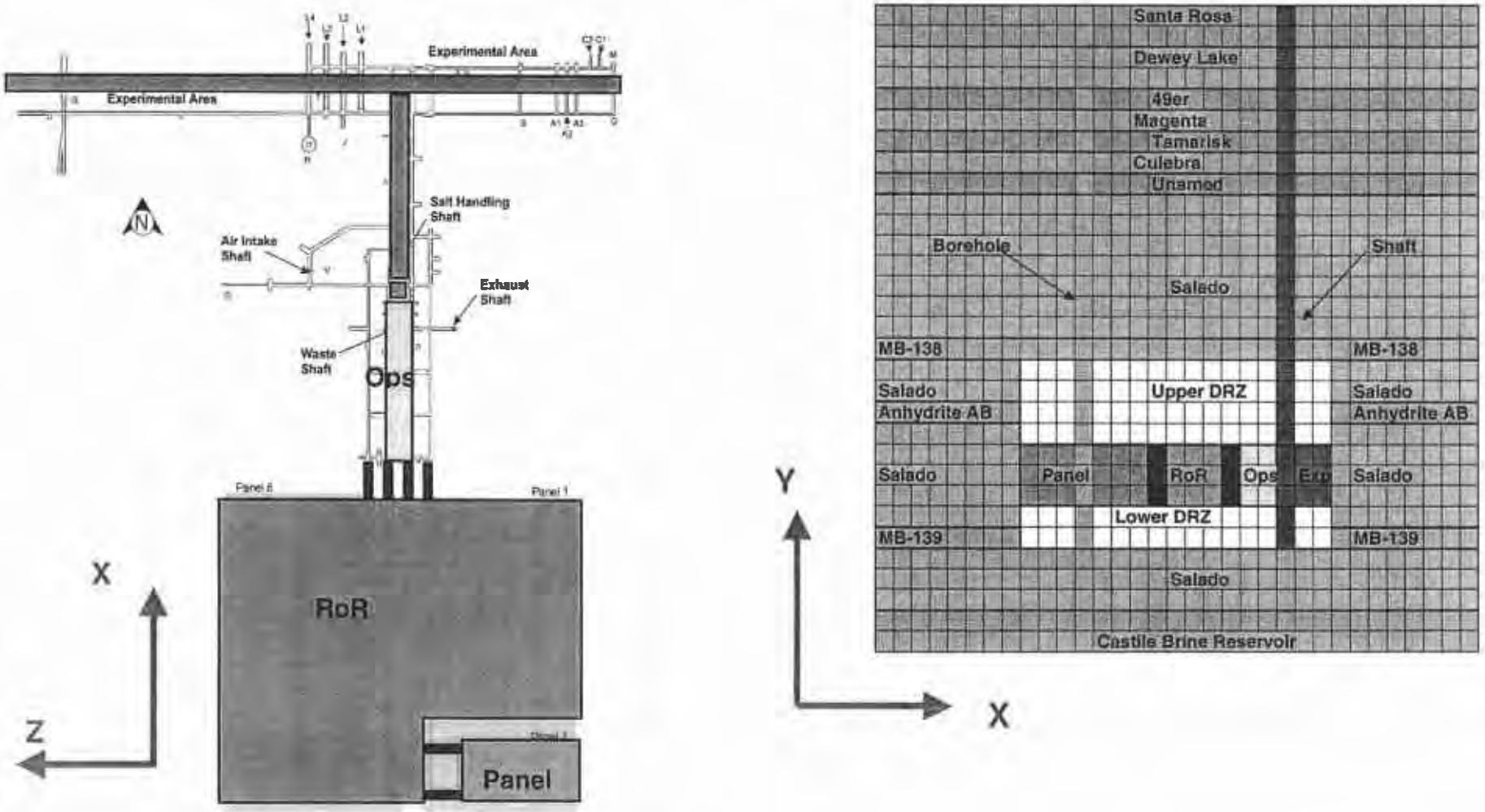

Figure 5. Baseline Grid Conceptualization

3.1.2 TBM Computational Grid

Changes to the BRAGFLO computational grid include: (1) refinements of the number and dimensions of grid cells to increase numerical accuracy, (2) correction of the flaring scheme for varying the Z-dimension of cells, (3) removal of the shaft seal system from the model domain, and (4) implementation of the Option D panel closures. The TBM computational grid is shown in Figure 6. The dimensions of the computational grid are shown in Appendix A.

The TBM Computational Grid

The TBM grid has 2244 elements. Grid cell spacing has been refined to increase numerical accuracy. Grid flaring has been modified to place the center of flaring at the center of the waste. The shaft has been removed from the grid. The waste areas are represented by three regions. Four Option D panel closures are included. Each closure extends into the surrounding DRZ and is represented with materials consistent with its design.

3.1.2.1 Grid Cell Refinements

Adequate grid refinement is critical to numerical accuracy in a finite difference approximation. A finite difference solution is correct to the first and second order only when grid spacing is regular. For irregular grids, a finite difference solution is only correct to the first order. The BRAGFLO grid is "irregular" meaning that the dimensions of grid cells change depending on location. Grid cell dimensions in the baseline grid increase in the north-south direction by a factor of about 5 with distance away from the repository. Grid cell dimensions in the baseline grid increase in the vertical direction by a factor of up to 10 with distance from the repository. These refinement factors are considerably larger than the recommended maximum value of 1.5 (Anderson and Woessner, 1992), With the shaft system removed from the computational grid, more resolution can be placed in the repository and surrounding host rock without negatively impacting computational efficiency.

Adequate grid refinement is especially important for accurately representing transient processes such as drilling intrusions and chemical transport that rely on adequate second order accuracy. The TBM grid addresses this issue by using a refinement factor of 1.45 outside the repository. 1.45 was chosen because it is smaller thatn the recommended maximum of 1.5. In addition the TBM grid fixes a vertical refinement problem near Marker Bed 139, which in the baseline grid has a refinement factor of 10. The TBM reduces this factor by an order of magnitude. One effect of these changes will be to reduce numerical dispersion in the transport calculations made in NUTS.

3.1.2.2 Correction to Grid Flaring

Computational Grid Changes

Additional changes to the grid include correcting the grid flaring, increasing the grid refinement from a very coarse grid to a level generally considered adequate by numerical modeling and engineering standards.

While reviewing the CCA and PAVT calculations SNL identified an error in the baseline grid related to flaring. The CCA incorrectly states that the grid flaring is centered at the borehole located in the intruded panel. This assertion was true for the grid used in the 1992 WIPP PA (WIPP, 1992-93). Between the 1992 PA and the CCA calculation, the location of the intruded panel and rest of repository blocks were switched from their positions in the 1992 grid. However, the flaring was not re-calculated after

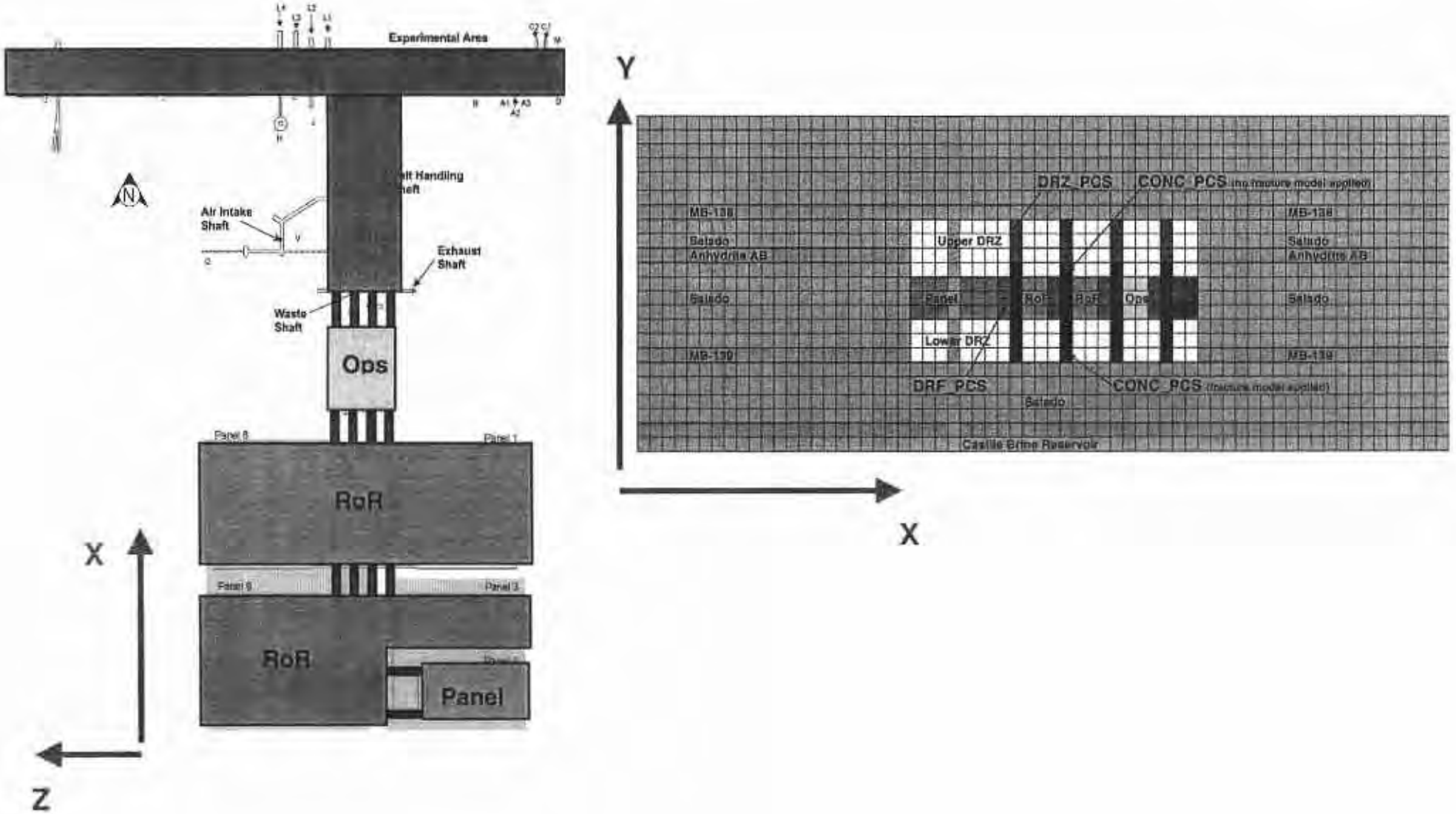

Figure 6. TBM Grid Conceptualization

the switch. Consequently, in the CCA the center of flaring was actually a point near the northern end of the rest of repository.

The location of the center of flaring determines the volume of accessible rock surrounding the repository at any given distance from that center. By moving the intruded panel (and borehole) to the southern end of the repository without recalculating the flaring, the intruded panel came into contact with the volume of rock that previously surrounded the rest of repository, which is nine times bigger than the intruded panel. In a similar way, the volume of rock surrounding the experimental area was smaller than it should have been since it was based on a center of flaring located at the northern end of the waste region instead of at the borehole.

This error has several consequences. First, brine exiting the repository out the southern marker beds has to flow through more rock than is representative and thus transport away from the repository may be underestimated. Second, brine inflow from the southern marker beds to the intruded panel is overestimated while the flow from the north into the experimental area is underestimated. In addition, brine inflow to the rest of repository is reduced since it is no longer adjacent to the Marker Beds. In fact, this effect is quite apparent in the PAVT results that show that the intruded panel is significantly more saturated than the rest of repository for all undisturbed vectors. This result is not consistent with SNL's current understanding of the disposal system, which anticipates no significant differences between waste panels during undisturbed conditions. The TBM grid corrects the CCA and PAVT implementation of flaring by recalculating the flaring centered on the center of the waste filled regions.

3.1.2.3 Elimination of the Shaft

The baseline grid included a composite shaft representing the combination of the four repository shafts and their associated surrounding DRZ. Deterministic numerical modeling of the shaft seal design demonstrated that the shaft seal was exceedingly effective in preventing flow up the shaft (DOE, 1996, Appendix SEAL). In addition, all PA calculations have indicated negligible flow up the shaft, and in no vector was the shaft seal system a pathway for releases (Helton et al., 1998; MacKinnon and Freeze, 1997). For these reasons, the TBM screens out this release pathway and removes the shaft from the computational grid.

Implementation of Option D Panel Closures

Greater detail was needed to represent the Option D design, which has two main components, a concrete monolith keyed into the DRZ and an explosion wall separated from the monolith by empty drift. These features have significantly different properties and thus needed to be discretized separately in the grid.

Because the Option D panel closures are designed to be effective at preventing the flow of brine and gas between panels, it was necessary to increase the detail within the repository so that there would be sufficient segmentation to evaluate the effect of the panel closures on neighboring regions in the repository.

Removal of the shaft from the grid is beneficial to the numerical stability of the model and simplifies model set-up and debugging. The shaft's presence had an unrealistic influence on units above the repository by blocking horizontal flow between regions separated by the shaft; in reality, these regions communicate around the shaft materials. Removal of the shaft reduces this flow restriction. With

the shaft system removed from the computational grid, more resolution can be placed in the repository and surrounding host rock without negatively impacting computational efficiency.

3.1.2.4 Implementation of Option D Panel Closures

In the CCA, DOE presented four options for panel closure designs, labeled Options A through D. Upon reviewing the options, EPA mandated the implementation of Option D (Figure 7), which is designed to provide the least fluid flow between panels. The compliance baseline calculations from the CCA and PAVT do not explicitly model the Option D configuration, however. Changes in material properties of the panel closure and neighboring DRZ, as well as refinement of grid geometry were deemed necessary by SNL in order to capture the effects of the Option D closure system on repository processes.

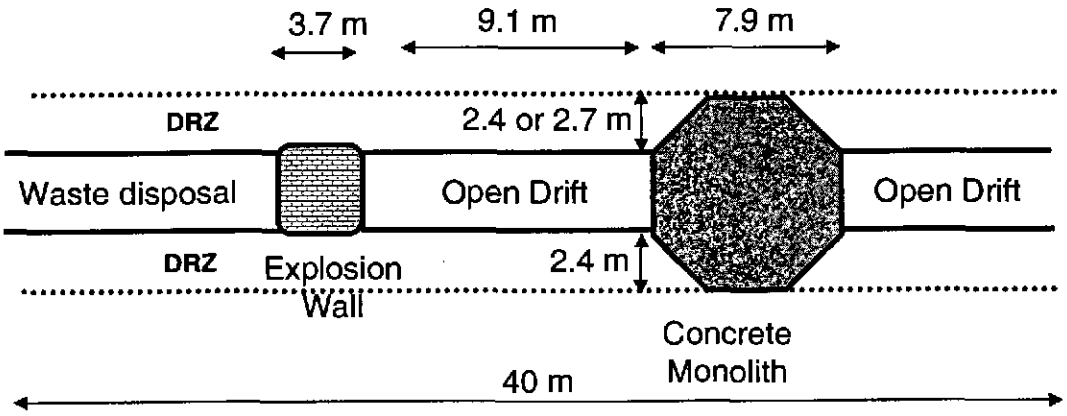

Figure 7. Side View of Option D Panel Closure

The TBM explicitly represents the Option D panel closures in the computational grid. Figures 8 and 9 compare the panel closure implementation in the CCA/PAVT and TBM grids and show several important differences. First, the TBM grid extends the concrete into the upper and lower DRZ, as called for in the Option D design (Figure 7). Furthermore, while the baseline model approach lumped the panel closure into one column of three cells with uniform properties, the TBM divides the panel closure and surrounding materials into a system of four materials in 13 grid cells including:

1. Six cells of panel closure concrete represented by the material CONC_PCS (shown in red in Figure 8)
2. Three cells of healed DRZ above the panel closure system (PCS) represented by the material DRZ_PCS (Shown in light blue in Figure 8)
3. Three cells of empty drift and explosion wall represented by the material DRF_PCS (Shown in teal in Figure 8)
4. One cell of panel closure concrete that is embedded in MB 139 represented by the material CPCS_F (Shown in pink in Figure 8).

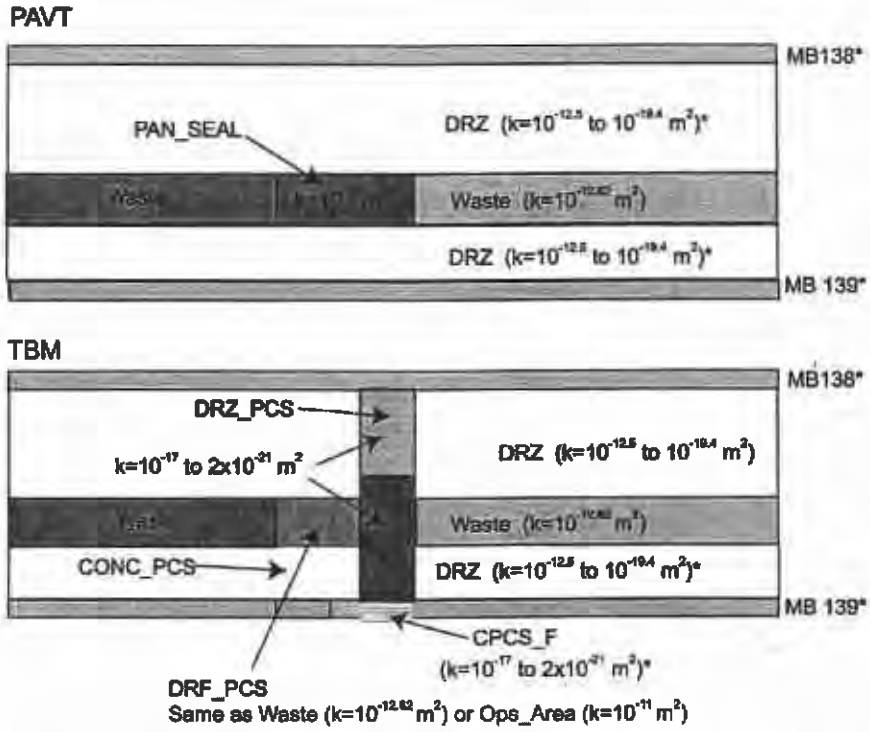

Figure 8. Panel Closures in PAVT and TBM

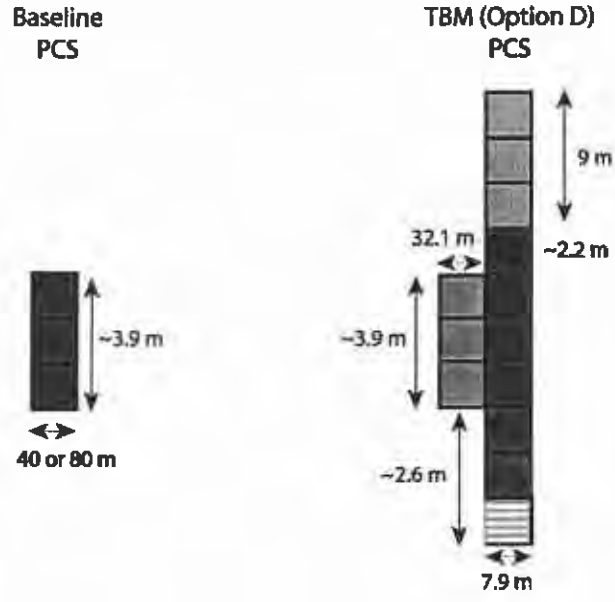

Figure 9. Panel Closure Grid Cell Diagram for PAVT and TBM

Unlike the baseline panel closure representation where significant flow occur through and around panel closures permitting strong inter-repository communication, the Option D panel closures are designed to impede such flows. It is therefore necessary to include greater segmentation within the repository such that the serial effects of these panel closures can be adequately simulated. Consequently, the TBM grid divides the rest of repository block into two separate blocks: the southern and northern rest of repository blocks. For the TBM, four sets of panel closures were included in the model domain (Figure 6). These panel closures lie in between the following grid regions: the single intruded waste panel, southern rest of repository, northern rest of repository, operations area, and experimental area. The inclusion of four panel closures as compared to the CCA/PAVT grid's two is considered necessary to evaluate the effects of Option D type panel closures.

One example when greater segmentation is warranted is immediately following a drilling intrusion. In the baseline grid, the intruded panel is separated from a single rest of repository block representing nine panels with no panel closures separating panels within the rest of repository from each other. This representation is not considered adequate in light of improved panel closure representations if the panel closures are assumed to be relatively tight barriers. Since only one panel closure lies between the intruded panel and 90% of the waste region, this representation overestimates the extent to which a single intrusion can depressurize other parts of the repository. The TBM grid places more panel closures between blocks representing waste-filled regions and thus provides a more accurate and conservative representation of the effect of multiple drilling intrusions. In the TBM grid an intrusion into one panel is less likely to influence other parts of the repository that may be separated by as many as four sets of panel closures.

3.2 PARAMETERS USED BY BRAGFLO

As part of their review of the CCA, the EPA reviewed the parameters used in the PA, the probability distributions for the sampled parameters and DOE's sensitivity analysis. The EPA also performed a sensitivity analysis on some parameters to determine if uncertainties in the parameter values would have a significant impact on the PA. They concluded that 24 parameters could significantly affect the results of the PA (EPA, 1998). EPA then required DOE to use the revised parameters in a new PA calculation (the PAVT calculation) that subsequently became part of the WIPP's regulatory basis. The TBM PA calculations use the parameter set from the PAVT which is documented in SNL (2002).

In addition, since EPA's certification of the WIPP repository, SNL has performed its own review of the parameters and has made corrections to parameter values where errors were found (Tisinger, 2001). The TBM PA calculations also incorporate the corrections documented in Tisinger 2001.

Now in support of the TBM, several BRAGFLO materials and their property values have been added or updated. Those materials are shown in Figure 7 and include:

1. DRZ_1: material representing the DRZ above and below the repository excluding the DRZ above the PCS (Section 3.2.1)
2. DRZ_PCS: material representing the DRZ above the PCS (Section 3.2.2)
3. CONC_PCS: material representing panel closure concrete (Section 3.2.3)

4. DRF_PCS: material representing the empty drift and explosion wall (Section 3.2.4) This is a derived parameter and does not appear in the parameter database.
5. CPCS_F: material representing panel closure concrete that is embedded in MB 139 (Section 3.2.5). This is a derived parameter and does not appear in the parameter database.

The TBM also includes a correction to the molecular weight of cellulose which is discussed in Section 3.2.6.

3.2.1 Disturbed Rock Zone Above and Below the Repository

Disturbed Rock Zone Changes

The emplacement of the rigid, Option D concrete monolith will cause the surrounding DRZ to heal. This effect was included in the material map for the DRZ above the monolith. In addition, because the monolith will excavate Marker Bed 139, a mechanism was included to simulate the possible flow around the panel closure through the marker bed.

The DRZ is the rock surrounding the excavated areas such as waste panels, empty drifts, and shafts that is altered by the process of mining, filling, and ultimately closing the repository. In the DRZ near the repository, permeability and porosity are expected initially to increase in both Salado halite and anhydrite marker beds. While the increase in permeability and porosity in the Salado halite is expected to reverse itself over time due to salt creep, the increase in permeability and porosity in the anhydrite marker beds is not expected to be completely reversible, even with creep closure of the disposal rooms. This residual increase in DRZ permeability increases the ability of fluid to flow from the anhydrite marker beds to the waste disposal region. Also, the increase in DRZ porosity provides a volume in which fluid can be retained so that it does not contact waste. Additional pore volume may also slow actinide transport.

3.2.1.1 Baseline Disturbed Rock Zone

At the time of certification, PA approximated the effects of the DRZ in a fashion which tends to overestimated fluid flow to and from the repository. The PA modeled a DRZ that extended above and below the repository from the base of MB 138 to MB 139 and that did not vary over time. For the CCA the DRZ was assigned a constant permeability of 1×10^{-15} m^2. The PAVT represented the log of the DRZ permeability as a sampled variable with a range between -19.4 and -12.5 and a uniform distribution. In addition, the PAVT applied the pressure-induced fracture model (designed for the anhydrite marker beds) to the DRZ both above and below the repository thus ensuring that fluids could access the marker beds in the PA realizations with high repository pressures and low DRZ sampled permeabilities.

3.2.1.2 TBM Disturbed Rock Zone

In the TBM conceptualization of the DRZ, the permeability and porosity in the DRZ are represented as they were for the PAVT. However, because there is a 12 m section of Salado halite between the repository and MB 138, SNL has determined that the anhydrite fracture model should not be applied to the DRZ above the repository.

Within the lower DRZ the fracture model has been retained from the PAVT. There is only a 2 m section of Salado halite between the repository floor and MB 139. As rooms close the floor heaves and fractures, and in the presence of higher gas pressures, fractures are not expected to heal thereby maintaining a hydraulic connection to MB 139. For this reason, the pressure dependent anhydrite fracture model is applied only to the DRZ *below* the repository.

3.2.2 Panel Closure Concrete

The Option D panel closure design requires the use of a salt-saturated concrete, identified as SMC, as is required for the shaft seal system. The design of the shaft seal system and the properties of SMC are described in Hurtado et al. (1997). The TBM BRAGFLO grid incorporates a new material, CONC_PCS, which is assigned the material properties of undegraded SMC and is used to represent the concrete monolith of the Option D panel closure system.(Stein, 2002b)

The SMC properties assumed for the shaft differ slightly from those assumed for the option D panel closures. The CCA assumed that cementitious materials used in the shaft seal system would degrade after 400 years. This assumption may overestimate flow throught the shaft althought little was observed in the CCA and PAVT and gave greater confidence to the redundant, multi-barrier design of the shaft seal system. It is not at all clear that a similar assumption would be conservative for the Option D panel closures. Thompson and Hansen (1996) estimated that only minor degradation would be expected for the concrete members of the panel closure concrete during the regulatory period. They determined that potential flow through the concrete closure would be nearly two orders of magnitude too small to cause any significant degradation of the concrete component. Consequently, the TBM assigns to CONC_PCS the properties of the CCA material CONC_T1, representing undegraded SMC. Appendix B lists the properties assigned to CONC_PCS.

3.2.3 Disturbed Rock Zone Above the Panel Closure

The design of Option D panel closures requires the removal of the DRZ above and below the panel entry drifts. The depth of cut below the floor will mine out MB 139. Loose salt in the roof also will be taken down just prior to construction of the concrete monolith. After construction the salt surrounding the monolith will be subjected to compressive stresses, which will facilitate the rapid healing of disturbed zones. The rounded configuration of monolith creates a situation very favorable for concrete: high compressive stresses and low stress differences. In turn, the compressive stresses developed within the salt will quickly heal any damage caused by construction excavation, thereby eliminating the DRZ along the length of the panel closure. The permeability of the salt immediately above and below the rigid concrete monolith component of Option D will approach the intrinsic permeability of the Salado halite.

To capture the healed DRZ above the monoliths, the TBM uses a new material, DRZ_PCS, in the BRAGFLO grid. The property values assigned to DRZ_PCS are the same as those values used for a similar DRZ-related material (DRZ_1), except for the properties PRMX_LOG, PRMY_LOG, and PRMZ_LOG, the logarithm of permeability in the X, Y, and Z directions, respectively. These permeability values are assigned the same distributions used for the new material CONC_PCS. In this instance, the values are based on the nature of the model set-up, and not directly on

experimental data (although the general range of the distribution agrees with experimental observations of healed salt).

The use of these permeabilities ensures that fluid flow is equally probable through or around the Option D panel closures and best represents the uncertainty that exists in the performance of the panel closure system. Appendix C shows the properties for DRZ_PCS.

3.2.4 Empty Drift And Explosion Wall Materials

DRF_PCS is the material representing the empty drift and explosion wall. This is a derived parameter and does not appear in the parameter database. This material has properties equivalent to the material representing the waste panel (except it is not filled with waste) and is used for the three panel closures that are adjacent to waste regions. The creep closure model is applied to this material to be consistent with the neighboring materials. The non-concrete portion of the northernmost panel closure between the operations area and the experimental area is assigned properties equivalent to the operations area. This is done so that the creep closure model is applied consistently to different regions in the grid (the waste regions have the creep closure model applied whereas the operations area is modeled as pre-closed and assigned an initial low porosity for all times).

3.2.5 Panel Closure Concrete Embedded in MB 139

CPCS_F is the material representing the portion of panel closure concrete that is embedded in MB 139. This is a derived parameter and does not appear in the parameter database. At low pressures, CPCS_F has the same properties as CONC_PCS. At high pressures, CPCS_F is allowed to fracture similar to the anhydrite Marker Bed 139 located at the same level.

The application of the fracture model simulates a fluid pathway around the panel closure in the event that fracture pressures are reached (Figure 10). Such a pathway is reasonable because floor heave will cause fracturing of the lower DRZ, establishing a hydraulic path to Marker Bed 139. Flow around panel closures through MB 139 is a possibility if pressures exceed fracture initiation levels. In these cases, a two-dimensional grid doesn't allow such flows to be modeled directly in all dimensions. Instead the effect of such flow is simulated by allowing the lowermost cell of the concrete monolith to fracture as in MB 139. In this way significant flow around the panel closure is simulated only when pressures are quite high. The application of the fracture model to this material is reasonable since the concrete permeability range is very close to the range used for the anhydrite marker beds.

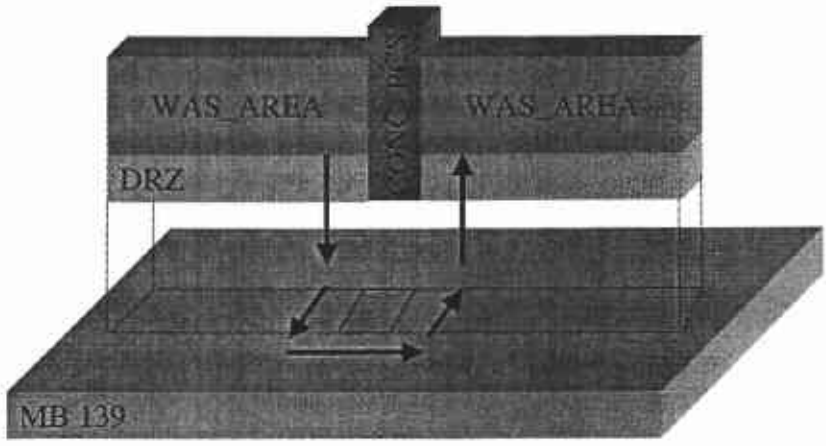

Figure 10. Flow Pathway Around Option D Closure

3.2.6 Molecular Weight of Cellulose

One error correction that has been made since Tisinger 2001 is to the molecular weight of cellulosic materials in the BRAGFLO code. In order to calculate gas generation by microbial degradation, the BRAGFLO code uses a single molecular weight for cellulosic material,. However, the TRU waste inventory includes a variety of cellulosic materials, which are represented by a single material and molecular weight in BRAGFLO.

Molecular Weight of Cellulose

The molecular weight of cellulose was corrected in the TBM calculation to reflect the formulation, $C_6H_{10}O_5$ as described in the CCA. This correction has direct and predictable effects on gas generation in the BRAGFLO simulations.

Within BRAGFLO, the correction to the molecular weight of cellulose results in slightly more gas produced from biodegradation. More gas may result in slightly higher pressures for those vectors with biodegradation.

At the time of certification, it was decided that the most appropriate representation for cellulosic materials that are present in TRU waste was a uniform, cellulosic material in the form of $C_6H_{10}O_5$. However the certification calculations erroneously used of the molecular weight of CH_2O. The TBM corrects this error in the BRAGFLO code. Specifically, the carbon-normalized molecular weight of cellulose in TBM was lowered from 30.026×10^{-3} kg/mol for CH_2O to 27.023×10^{-3} kg/mol for $C_6H_{10}O_5$.

This correction has two direct effects on BRAGFLO calculations that include biodegradation (50% of vectors). First, in BRAGFLO the mass of cellulose is converted to moles of cellulose by dividing by the molecular weight. Therefore, a reduction in the molecular weight corresponds to an increase in the total number of moles of carbon available for gas production, and thus, more total gas can be produced.

Second, the biodegradation rate used by BRAGFLO is calculated using the molecular weight of cellulose. This is because the sampled rate is in units of [moles Carbon/m^3-sec]. BRAGFLO works in units of mass and therefore multiplies the sampled rate by the molecular weight to obtain a rate in units of [kg Carbon/m^3-sec]. This unit conversion results in a reduction in the mass generation rate of gas when the molecular weight is decreased. The implication of these effects for WIPP PA calculations is the potential for slightly higher pressures in those vectors that include biodegradation.

3.3 PEER REVIEW OF CHANGES MADE FOR TBM

The changes that have been made to PA in support of the TBM cannot be described exclusively in terms of any one conceptual model or phenomenological process. They have bearing on several phenomenological processes and three WIPP conceptual models: (1) disposal system geometry, (2) repository fluid flow, and (3) the disturbed rock zone. The disposal system geometry conceptual model describes how the various components of the WIPP repository (waste panels, panel closures, shaft seals, operations and experimental areas) are represented in the computational grid. The repository fluid flow conceptual model is concerned with (1) fluid (brine and gas) flow and distribution in the waste, (2) fluid flow to and from the Salado Formation, and (3) fluid flow between the repository and intrusion boreholes (DOE, 1996). The disturbed rock zone conceptual model describes the hydraulic and physical parameters used to represent the zone around excavated areas such as waste panels, empty drifts, and shafts that are altered by the process of mining, filling, and ultimately closing a repository. Changes to the BRAGFLO computational grid and material properties affect all three of these conceptual models.

Because the changes made in support of the TBM affect conceptual models, they had to be peer reviewed. §194.27 Peer Review states:

> (a) Any compliance application shall include documentation of peer review that has been conducted, in a manner required by this section, for:
>
> a. Conceptual models selected and developed by the Department;
>
> b. Waste characterization analyses as required in §194.24(b); and
>
> c. Engineered barrier evaluation as required in §194.44.
>
> (b) Peer review processes required in paragraph (a) of this section, and conducted subsequent to the promulgation of this part, shall be conducted in a manner that is compatible with NUREG-1297, "Peer Review for High-Level Nuclear Waste Repositories," published February 1988. (Incorporation by reference as specified in §194.5.)

A peer review of the changes included in the TBM calculations was held between April 30 and May 3, 2002 in Carlsbad, NM. The panel identified three major points in their conclusions. They are included here verbatim from the Executive Summary of the report (Caporuscio et al., 2002):

"1) The changes to the three conceptual models appear generally sound in their structure, reasonableness, and relationship to the original models.

2) The proposed implementation of the three changed models appears reasonable; however impacts of the changes cannot be assessed at this time. Although the data presented depicts selected gas pressure and brine saturations cases, a total system PA is needed to show a complete comparison of the prior CCA results to the new results.

3) Implementation of the three changed models and their interactions with other models cannot be assessed at this time because determination of "adequacy in application" and "accuracy of calculations" requires a total system PA."

The peer review panel provided their "conditional" acceptance of the changes incorporated in the TBM calculations and requested that a full PA be run to assess the impact on the CCDF plots of the changes. Following the complete TBM PA, the panel will be called back to review the final results and make their assessment of the adequacy of the changes being proposed.

4. COMPARISON OF BRAGFLO RESULTS

Calculation Cases

TBI: BRAGFLO was run with the new grid incorporating the PAVT PCS and without fracturing in the upper DRZ.

TBM: BRAGFLO was run with the new grid incorporating the Option D PCS, no fracturing in the upper DRZ, and the corrected molecular weight.

This chapter compares results of BRAGFLO calculations to identify the effects of the changes outlined previously. First, the calculation cases are defined, and the methods used to compare results from calculation cases are outlined. The comparison examined brine flow into the repository, brine saturation and pressure in the repository, and brine flow from the repository. Finally, sensitivity analyses for the TBM and the PAVT calculations are compared. In order to identify the effects on BRAGFLO results of individual changes to the models, the analysis considered three calculation cases: the PAVT, the Technical Baseline Intermediate (TBI), and the TBM cases. The TBI case incorporated only two of the changes to the models, namely, the revised computational grid and the removal of the fracture model from the upper DRZ; the TBM case included all of the changes described in Chapter 3 of this report. The TBI case allows the analysis to establish cause and effect relationships between particular changes to the models and the corresponding responses of the output variables. Comparing of PAVT and TBI results reveals the effects on BRAGFLO of the grid refinements and corrections and of the change to the fracture model; comparison of the TBI and TBM cases shows the effects of Option D panel closures and the correction to the molecular weight of cellulose. The analysis shows that the Option D panel closures greatly affect the results of BRAGFLO, while the effects of the other changes are relatively minor.

4.1 DEFINING THE INTERMEDIATE CASE

The intermediate case implemented a set of changes that demonstrated only minor effects on the output variables. These changes included removal of the shaft, refinement of the grid, revision of the grid flaring algorithm, and removal of fracturing the upper DRZ. Changes separating the TBI from the full TBM were more substantive. These included correcting the molecular weight of cellulosics, and implementing the Option D panel closure system.

The TBI case was defined by analysis of a single vector, as outlined in Appendix D. The single vector analysis compared three output variables (brine saturation, gas generation, and pressure) for just one selected vector over five cases distinguished by a single model change. By this technique, changes in output variables could be interpreted as a response to a specific model change. The single vector analysis allowed the model changes to be identified as having significant, or insignificant, impact on output. The model features determined to have insignificant impact on output were grouped to define the TBI case. The TBI represents a deviation from the analysis outlined in SNL AP-075. It was added to the scope of the work for AP-075 for the reasons described above. In other words, BRAGFLO was run first with the new grid incorporating the PAVT PCS. Next, BRAGFLO was run with the new grid incorporating the PAVT PCS but without fracturing in the upper DRZ. Then BRAGFLO was run with the new grid, incorporating the PAVT PCS, no fracturing in the upper DRZ, and the new molecular weight of cellulose. Finally,

BRAGFLO was run with the new grid incorporating the option D PCS, no fracturing in the upper DRZ, and the new molecular weight of cellulose.

4.2 METHOD OF COMPARISON

The analysis selected a small number of BRAGFLO output variables for comparison between the calculation cases. A full replicate of 100 vectors was calculated for each case, and the output variables were compared between cases. To allow a vector-by-vector comparison between calculation cases, all cases used the same sampling of the uncertain input parameters.

The analysis used two principal techniques to compare results between cases: horsetail plots, showing the results of a single output variable for all 100 vectors in a case; and scatter plots, which compare the results of a single output variable between cases at a specific point in time. This section lists the BRAGFLO output variables that were compared between calculation cases, and describes horsetail and scatterplots.

4.2.1 Variables Chosen for Analysis

Previous PA calculations for the WIPP (CCA and PAVT) indicate that direct releases from drilling intrusions (cuttings, cavings, spallings, and direct brine release) account for nearly all the radionuclide releases from the WIPP repository. Direct releases are determined in part by repository pressure and brine saturation at the time of intrusion. High pressures increase direct releases by increasing spallings and direct brine releases, whereas high saturations increase direct brine releases. Consequently, this analysis seeks to identify the effects of the changes made to BRAGFLO on pressure and saturation. Other important output variables, such as brine flow out of the repository and gas generation, are examined for completeness.

Variables Chosen for Analysis

Total brine present in the repository, brine flow between the repository and the marker beds, brine flow between the repository and the DRZ, and brine flow in the borehole.

Brine saturations in the intruded panel, the rest of repository, and the experimental area

Pressure in the intruded panel, the rest of repository, and the experimental area.

However, to explain why pressure and saturation results are affected by the changes in the model, it is necessary to examine other BRAGFLO output variables, such as brine flow in and around the repository. Many processes modeled in BRAGFLO are coupled, and therefore, changes in one process can affect several other procceses in turn. For instance the long-term pressure in the repository is primarily the result of gas generation reactions. These reactions require that brine is present and therefore are controlled by the saturation in the waste regions. High pressures in the repository can slow the inflow of brine from the marker beds which affects saturation and thus can decrease gas generation. Dynamic feedback mechanisms such as this complicate the analysis since they make it difficult to draw definitive relationships between output variables for all vectors.

Table 1 lists and defines the specific BRAGFLO output variables that are examined in this analysis.

Table 1. TBM BRAGFLO Variables Selected for Comparison to PAVT

BNBHDNUZ	Brine Flow Down The Borehole At The Top Of The Upper Disturbed Rock Zone [m^3]
BNBHLDRZ	Brine Flow Up The Borehole At The Bottom Of The Lower Disturbed Rock Zone [m^3]
BNBHUDRZ	Brine Flow Up The Borehole At The Top Of The Upper Disturbed Rock Zone [m^3]
BRNREPTC	Cumulative Brine Flow Into The Waste Regions [m^3]
BRNVOL_A	Total Brine Volume In Excavated Areas [m^3]
CELL_KG	Remaining Mass Of Cellulose [kg]
EXP_PRES	Volume-Averaged Pressure In The Experimental Area [Pa]
FE_KG	Remaining Mass Of Steel [kg]
GAS_MOLE	Total Moles Of Gas Generated [moles]
REP_POR	Volume-Averaged Porosity In The Rest Of Repository
REP_PRES	Volume-Averaged Pressure In The Rest Of Repository [Pa]
REP_SATB	Volume-Averaged Brine Saturation In The Rest Of Repository
WAS_POR	Volume-Averaged Porosity In The Waste Panel
WAS_PRES	Volume-Averaged Pressure In The Waste Panel [Pa]
WAS_SATB	Volume-Averaged Brine Saturation In The Waste Panel

4.2.2 Horsetails

The range of responses in an output variable across a full replicate are displayed on a "horsetail" plot. In this type of plot, each vector is plotted against time as a separate curve. The set of 100 overlaid curves form the horsetail plot. The variation between curves indicate the uncertainty in the output variable arising from the uncertainty in the input parameters. Horsetail plots reveal patterns of behavior in the output variables.

4.2.3 Scatter Plots

This analysis employs scatter plots to compare the results from a single output variable among the three calculation cases. In the scatter plots, individual calculations (TBI and TBM) are plotted against the PAVT results on a vector-by-vector basis for a snapshot in time. Each symbol on the scatter plot represents the value of an output variable at a given time for an individual vector. If the PAVT result for that vector is the same as the TBI and/or TBM result, the symbol will lie on the diagonal line (with a slope of 1) that divides the plot in half. If this equivalence holds true for all the vectors the scatter plot will show one hundred symbols per calculation that all fall on the 1 to 1 line. If the results are nearly equivalent but not systematically different, there will be scatter around the 1 to 1 line. If there is a systematic difference, symbols on the scatter plot will fall on one or another side of the 1 to 1 line depending on which calculation systematically produces results that are greater in value. If the PAVT results and the individual case results are significantly different, the scatter plot will show little or no linear relationship.

4.3 BRINE FLOW TOWARDS REPOSITORY

Brine entering waste-filled regions in the repository causes gas generation reactions to proceed and repository pressures to increase. Gas is generated in the waste regions both by corrosion of steel and by microbial action. Experimental evidence indicates that the corrosion of ferrous metals does not occur under humid conditions, therefore the only contributions to the total corrosion reaction is from the fraction of the pore space that is inundated. Brine is consumed during the corrosion reaction.Microbial degradation of plastics, rubbers and cellulose occurs under both humid and inundated conditions at a rate scaled by the brine saturation in the waste, but does not consume brine in the reaction. Hence, the total amount of brine flowing into the waste is a significant variable that affects brine saturation, gas generation, pressure and in turn repository performance.

This section describes the effects on brine flow into the waste regions of the changes implemented into the TBM and TBI calculations. The analysis illustrates in general how brine flow patterns are affected by the changes in the TBM calculations in the S1, S3, and S5 scenarios. This analysis considers brine flow only to the detail needed to understand changes to brine saturations and pressures. Thus, a thorough description and explanation of brine flow patterns within and near the repository for each vector is not necessary for this analysis.

Brine Flow Towards Repository

The accurate representation of brine flow toward the waste is important in PA because brine is required for gas generation reactions to proceed. The TBI results indicate that modifications and corrections to the grid spacing and flaring modestly affect the rate of brine inflow. However the TBM results demonstrate that the Option D panel closures have greater effect on the amount of brine that can access the waste regions. The Option D panel closures impede the gravity driven flow of brine from the northern experimental area into the waste areas. This results in drier conditions in the waste regions and wetter conditions in the experimental areas than for the PAVT.

These differences do affect pressures and saturations in the repository and will affect predicted releases. The full set of PA models needs to be run to completion before the full impact of the panel closures on repository performance can be evaluated. Estimates based on TBM BRAGFLO results indicate that a significant increase in releases is not expected. However, the relative importance of specific release mechanisms may change significantly.

4.3.1 Sources of Brine

Brine flows into the waste-filled regions from four principal sources: the DRZ above the excavated regions; the anhydrite marker beds; downhill from the northern excavated areas, and in disturbed scenarios, through the borehole upward from the castile brine pocket when present or downward from the culebra and supra-Culebra formations. Brine flow from the Salado halite is negligible compared to these other sources.

The upper DRZ is the primary source of brine flowing into the waste regions during the first few hundred years. Initially brine moves toward the repository because a significant pressure gradient exists between the excavated areas, which begin at atmospheric pressure, and the surrounding regions at lithostatic pressure. The flow of brine from this source is controlled, in part, by the permeability of the DRZ. For vectors in which the DRZ permeability is low, little brine flows from

the DRZ into the waste panel. For vectors in which the DRZ permeability is high, large volumes of brine flow from the DRZ into the waste panel within the first few decades after repository closure.

Brine also flows from the anhydrite marker beds into the surrounding DRZ and thence into the repository. Brine in Marker Bed 138 and Anhydrite Bed A/B flows into the upper DRZ; brine in Marker Bed 139 flows into the lower DRZ. This analysis focuses on flow from marker beds located to the south of the repository, since flow from the northern marker beds generally enters the northern excavated regions before flowing downhill to the waste-filled regions. Marker bed flow occurs throughout the simulation at a rate determined by the permeability of the marker bed and the hydraulic gradient caused by the difference in pressure. As pressures equilibrate the hydraulic gradient decreases, and flow slows correspondingly.

Brine in the northern excavated areas flows downhill to the south and may enter the waste regions. This flow pathway is frequently called "gravity-driven flow" because it is due to the 1° southerly dip of the Salado formation and repository horizon. This pathway is especially apparent in calculations that implement the PAVT panel closures (the PAVT and TBI) since the PAVT panel closures do not impede this gravity-driven flow, especially in the lower DRZ. In contrast, the Option D panel closures implemented in the TBM present a significant barrier to brine flow in the drift and DRZ, essentially removing the gravity driven component of brine flow.

In the S3 intruded scenario, a borehole penetrates through the waste panel into a brine reservoir in the Castile formation. Brine may flow into the repository either up the borehole from the brine reservoir or down the borehole from the Culebra. Brine may also flow up the borehole from the repository to the Culebra or towards the surface. In the S5 intruded scenario, the borehole stops at the repository. Brine may flow down the borehole from the Culebra to the repository, or up the borehole from the repository toward the surface.

4.3.2 Brine Flow Into Waste-Filled Regions for the TBI Calculation

Brine flow into the waste-filled regions was compared between the PAVT and the TBI for a full replicate of 100 vectors. The TBI is the intermediate case where BRAGFLO was run with the new grid incorporating the PAVT panel closures and without fracturing in the upper DRZ. Comparison of TBI and PAVT results identifies the effects of changing to the new grid and removing the upper DRZ fracturing. The analysis shows that these two changes do not significantly affect brineflow into the waste-filled regions. In the PAVT grid, the waste-filled regions are the Waste Panel and the Rest of Repository; in the TBM grid, the waste-filled regions include the Waste Panel, the South Rest of Repository and the North Rest of Repository.

4.3.2.1 Undisturbed Scenario (S1)

Total brine entering the waste-filled regions varies over four orders of magnitude across the 100 vectors. Despite this variability, some patterns are observable in the data that are common to both the PAVT and the TBI. Figure 11 shows total brine flow into the waste regions for all 100 vectors for the TBI. Approximately one third of the total brine flow into the waste regions is from DRZ "rain" during the first 50 years. The DRZ "rain" roughly doubles the total brine volume present in the waste regions when compared to the brine volume present initially. Approximately one quarter

of the total brine flow into the waste regions occurs between 50 and 1,000 years with the remaining brine entering the waste regions between 1,000 and 10,000. The mechanisms for brine in-flow over the long-term (from 50 years out to 10,000 years) are marker bed flow and gravity-driven flow. The outlying curve is Vector 24. It has one of the highest values of halite (and DRZ) porosity and one of the highest values of DRZ permeability. These two parameters mean that there is a lot of brine in the DRZ and it can flow easily to the waste regions.

Figures 12, 13 and 14 compare brine inflow volumes at 50, 1,000 and 10,000 years. In most vectors where there is a large volume of brine entering the waste regions, brine inflow volumes are slightly higher in the TBI than in the PAVT. The slightly greater inflow for the TBI is due to the change in grid refinement near the repository and in the lower DRZ, and the corrected grid flaring that results in larger brine flows into the northern excavated regions and thence downhill to the waste regions. The differences, however, are not large enough and are not present in enough vectors to be significant.

Figure 14 shows two vectors (28 and 58) that have less total brine flow into the waste regions in the TBI than in the PAVT. For these two vectors in the PAVT, the upper DRZ fractured and greatly increased in permeability after about 2,000 years. In the TBI the fracture model is not applied to the upper DRZ. Consequently, the upper DRZ permeability remains relatively low for these two vectors in the TBI, resulting in less total brine inflow.

4.3.2.2 Disturbed Scenarios (S3 and S5)

The two disturbed scenarios model drilling intrusions. The S3 scenario assumes a borehole that penetrates through the waste panel into a pressurized brine reservoir below the repository. During an S3 intrusion brine can flow from the brine pocket and enter the repository, as well as down from the Culebra and supra-Culebra formations. This analysis examines the amount of brine flowing up the borehole that crosses the boundary between the Salado and the lower DRZ. Flow is monitored at the bottom of the lower DRZ, from the Castille brine pocket, because brine may flow laterally from this location through the DRZ when DRZ permeability is high.

Figure 15 shows cumulative brine flow from the brine pocket into the intruded panel over time for all 100 vectors in Scenario S3. Figure 16 compares cumulative brine flow from the brine pocket into the intruded panel after 10,000 years for the PAVT and the TBI.

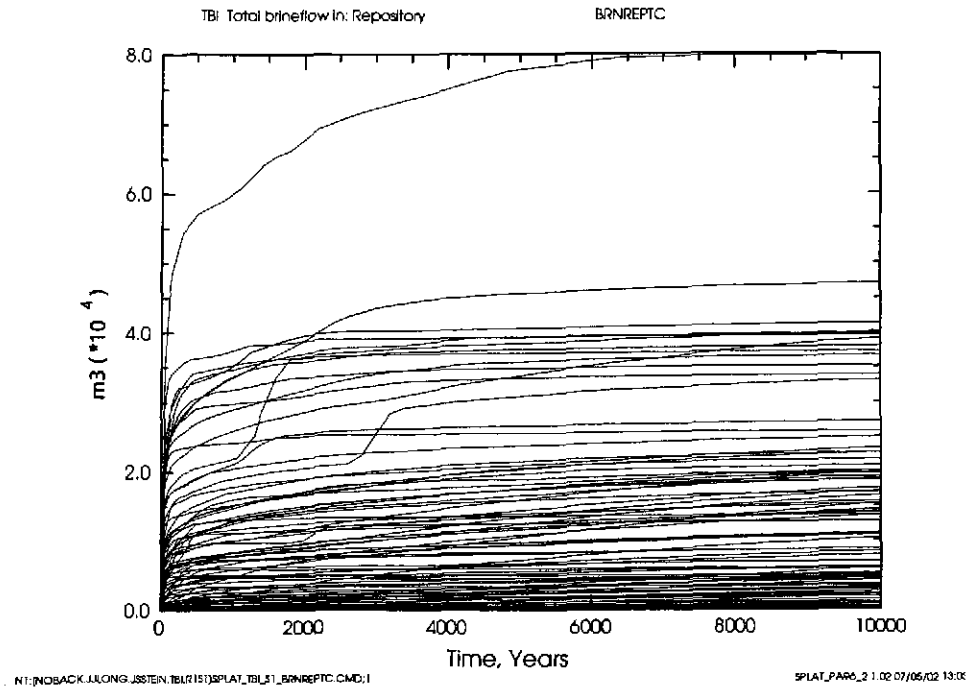

Figure 11. Undisturbed Scenario (S1); Cumulative Brine Flow Into the Waste Regions [BRNREPTC]; TBI

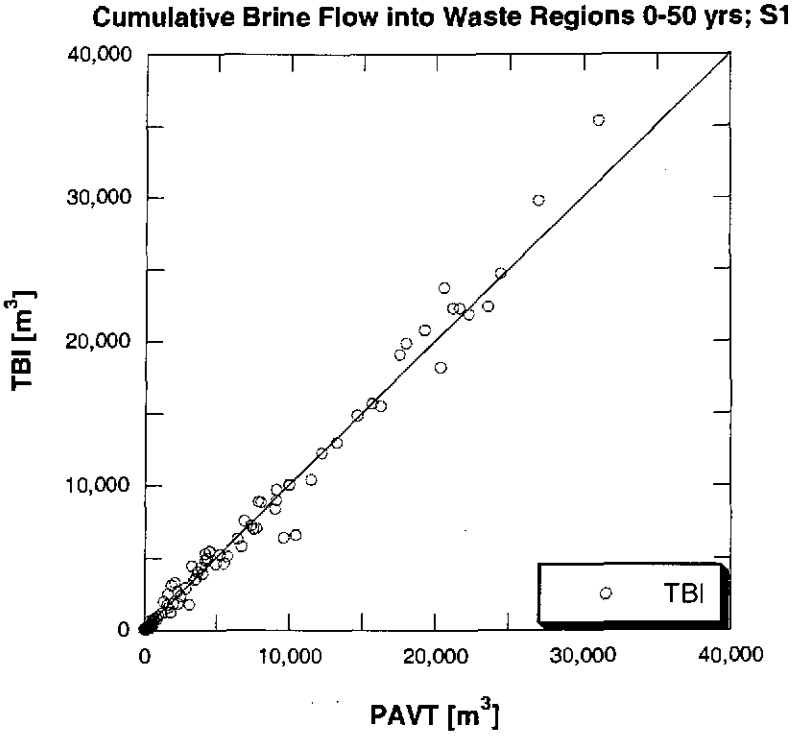

Figure 12. Undisturbed Scenario (S1); Cumulative Brine Flow Into the Waste Regions [BRNREPTC]; Scatter Plot TBI versus PAVT; 50 Years After Repository Closure

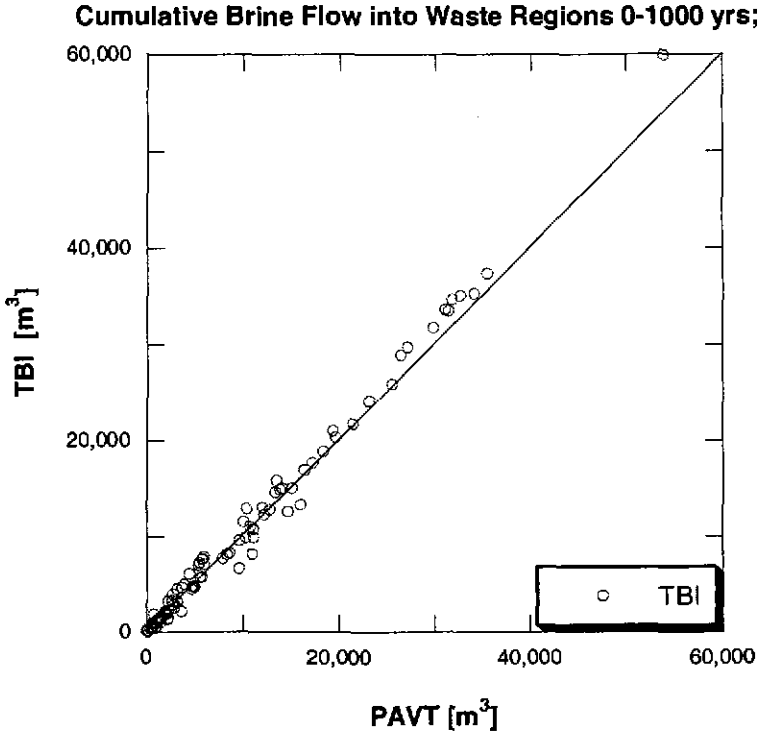

Figure 13. Undisturbed Scenario (S1); Cumulative Brine Flow Into the Waste Regions [BRNREPTC]; Scatter Plot; TBI versus PAVT; 1,000 Years After Repository Closure

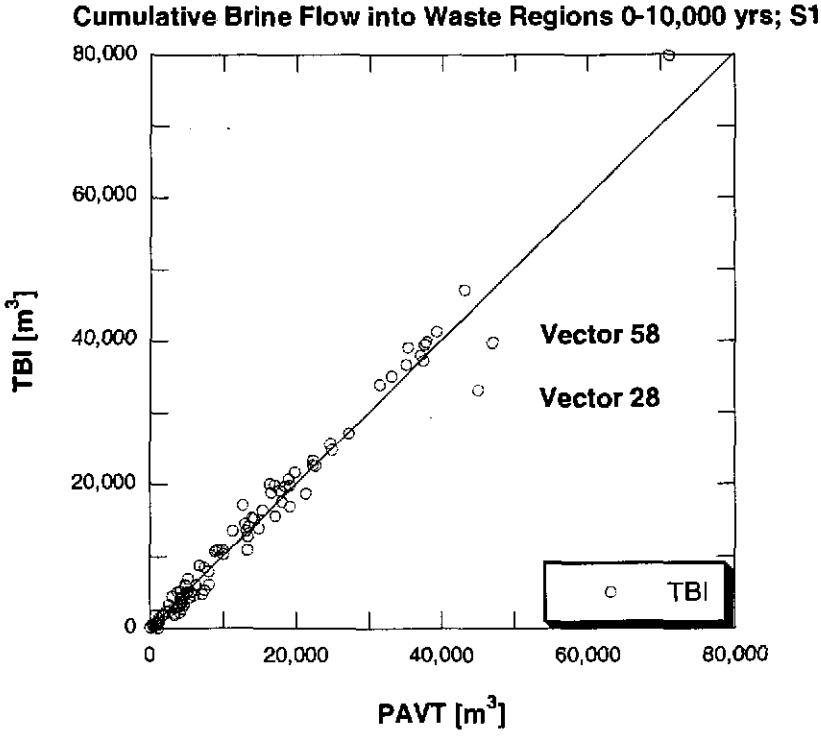

Figure 14. Undisturbed Scenario (S1); Cumulative Brine Flow Into the Waste Regions [BRNREPTC]; Scatter Plot; TBI versus PAVT; 10,000 Years After Repository Closure

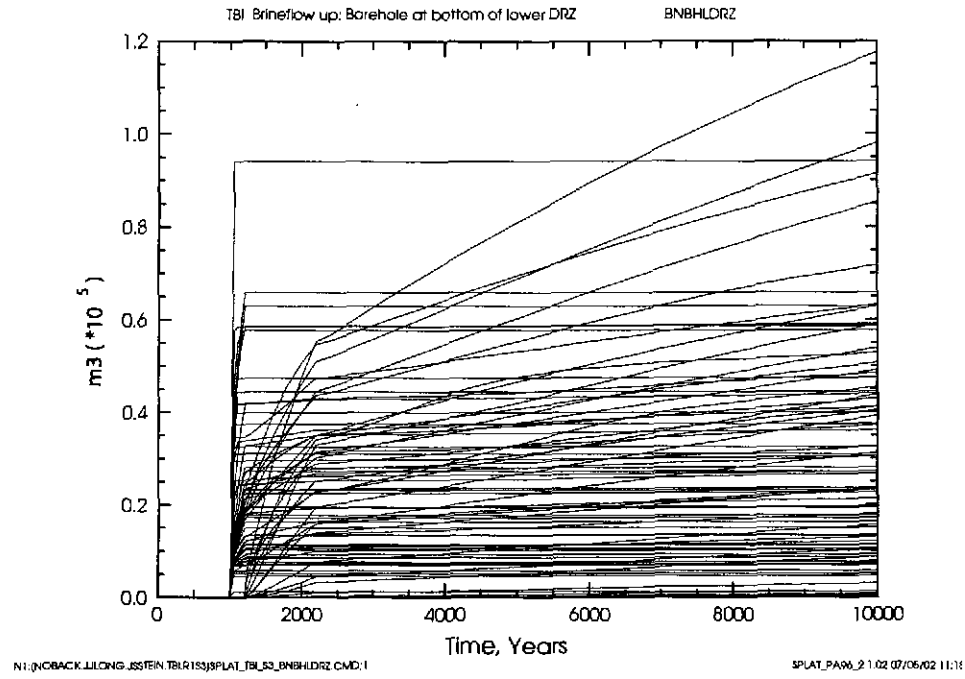

Figure 15. Disturbed Scenario (S3); Cumulative Brine Flow in Borehole From Brine Pocket Into Intruded Panel at Bottom of Lower DRZ [BNBHLDRZ]; TBI

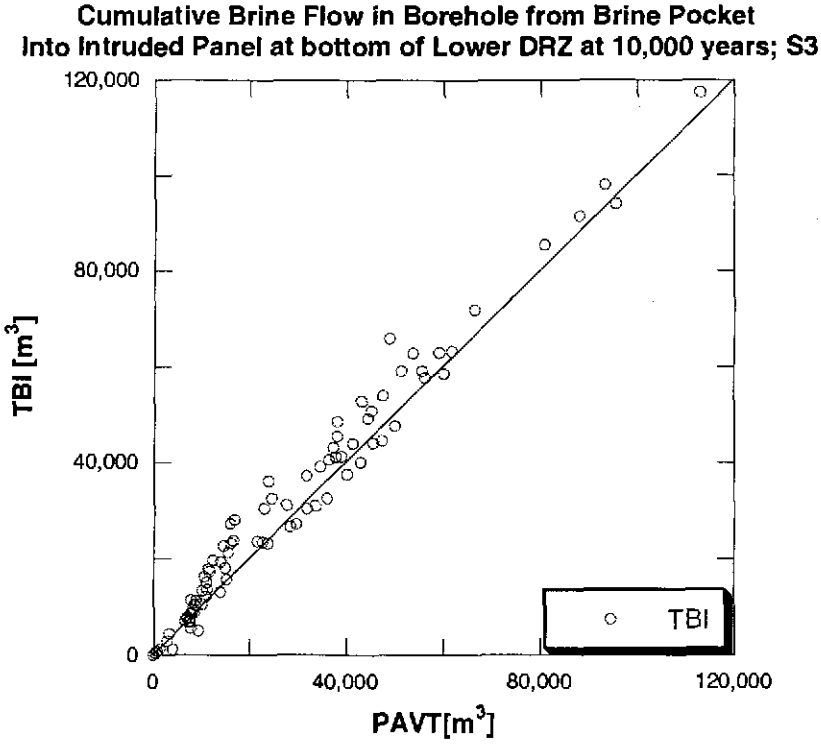

Figure 16. Disturbed Scenario (S3); Cumulative Brine Flow in Borehole From Brine Pocket Into Intruded Panel at Bottom of Lower DRZ [BNBHLDRZ]; Scatter Plot; TBI versus PAVT; 10,000 Years After Repository Closure

Brine flow up the borehole from the Castile brine pocket tends to be slightly greater in the TBI than in the PAVT. This small difference is due to the changes in the grid refinement and flaring.

In the S5 scenario, the borehole does not extend below the repository. During an S5 intrusion we examine brine flow down the borehole at the boundary between the Salado and the upper DRZ.

Figure 17 shows cumulative brine flow down the borehole to the top of the upper DRZ after 10,000 years for all 100 vectors in Scenario S5. Figure 18 compares cumulative brine flow down the borehole after 10,000 years between the PAVT and the TBI. Most vectors show little to no brine flow down the borehole. Vectors with significant flow exhibit quite a bit of variation between the PAVT and TBI. These differences illustrate that highly transient processes with large hydraulic gradients like drilling intrusions are particularly sensitive to changes in the grid refinement, particularly when the important features such as the borehole are represented crudely. Considering the differences between the two grids, it is not surprising that flows following a drilling intrusion would differ. Calculations addressing the impact of these differences on release are ongoing and will be published in a follow-up to this report.

4.3.3 Brine Flow Into the Waste Regions in the TBM Calculation

Brine flow into the waste-filled regions was compared between the PAVT, the TBI and the TBM for a full replicate of 100 vectors. Brine flow up the borehole toward the surface is examined in Section 4.6. The previous comparison with the TBI identified the effects on brine flow of the new grid and the removal of the fracture model from the upper DRZ. Comparison between the TBI and the TBM identifies the effects on brine flow of the Option D panel closures and the correction to the molecular weight of cellulose. The PAVT results are shown for completeness. The following discussion deals first with the undisturbed scenario (S1), then the two disturbed scenarios (S3 and S5).

4.3.3.1 Undisturbed Scenario (S1)

Figure 19 shows brine flow into the waste regions over time for all 100 vectors in the TBM. Figures 20, 21, and 22 compare brine flow into the waste regions at 50, 1,000 and 10,000 years for the PAVT, the TBI and the TBM. Figures 21 and 22 show that after 1,000 years the total brine flow into the waste regions is depressed in the TBM. The reduction is due to the Option D panel closures, which block gravity-driven brine flow and which elevate pressures in the waste regions (see Section 4.5); the elevated pressures in turn impede brine flow from the upper DRZ and marker beds.

The Option D panel closures effectively block gravity-driven brine flow from the northern operations and experimental areas. The Option D panel closures extend down to Marker Bed 139 at the bottom of the lower DRZ, removing any highly permeable path for brine flow between panels. A simple calculation using Darcy's Law yields a rough estimate of the total flow that can occur through the baseline panel closures due to the 1° dip. The calculation assumes the head difference across the panel closure arises only from the difference in elevation due to the 1° dip, and that panel closures are fully saturated with brine. The 1° dip results in a hydraulic gradient of $tan(1°) = 0.0175$. With a panel closure cross-sectional area equal to 40 x 4 m = 160 m^2 and permeability of

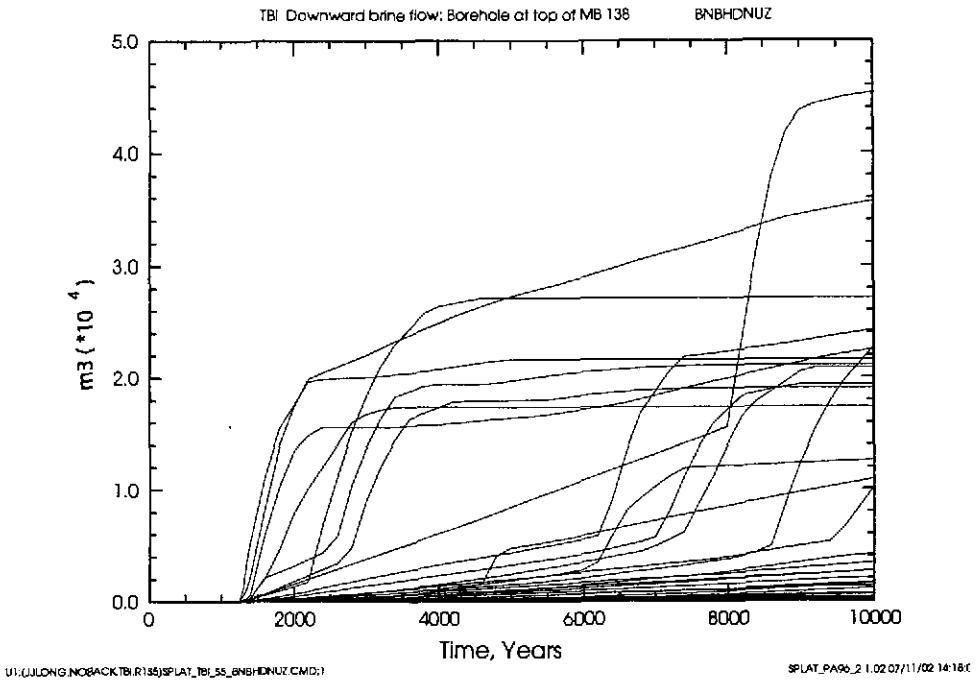

Figure 17. Disturbed Scenario (S5); Cumulative Brine Flow Down Borehole at Top of Upper DRZ [BNBHDNUZ]; TBI

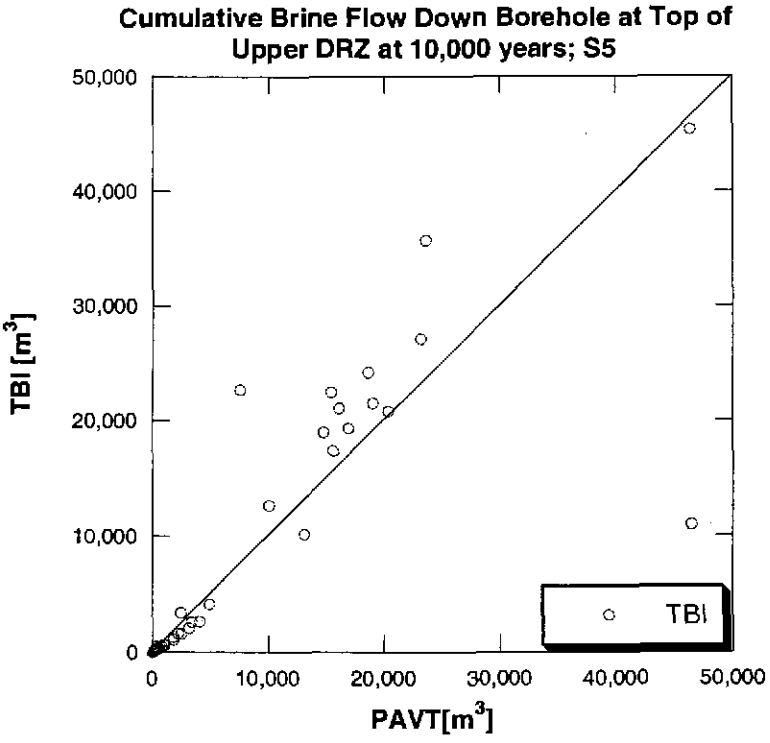

Figure 18. Disturbed Scenario (S5); Cumulative Brine Flow Down Borehole at Top of Upper DRZ [BNBHDNUZ]; Scatter Plot; TBI versus PAVT; 10,000 Years After Repository Closure

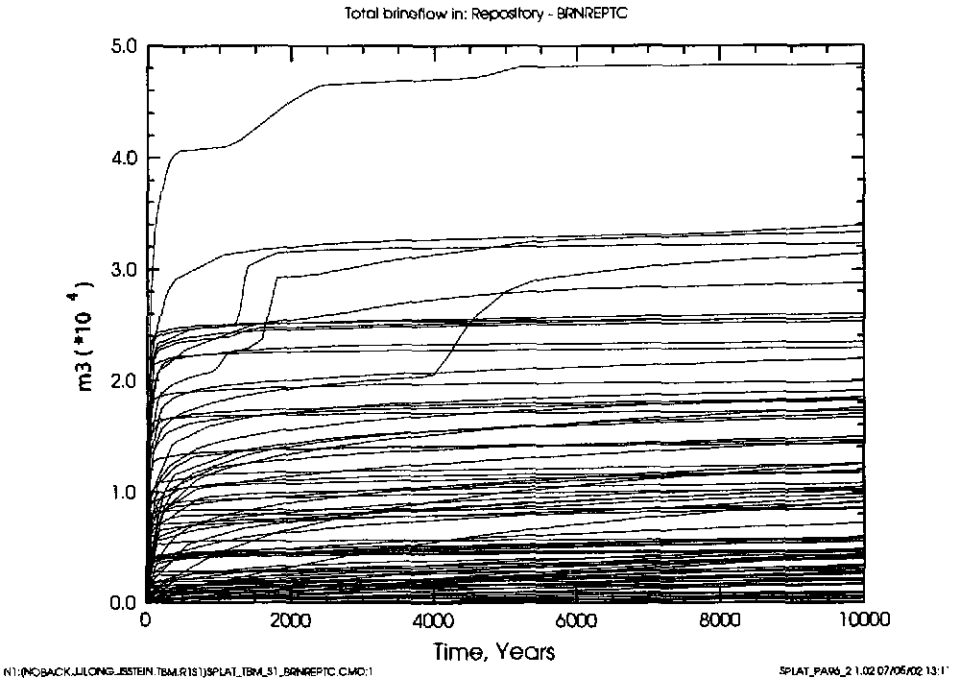

Figure 19. Undisturbed Scenario (S1); Cumulative Brine Flow Into the Waste Regions [BRNREPTC]; TBM

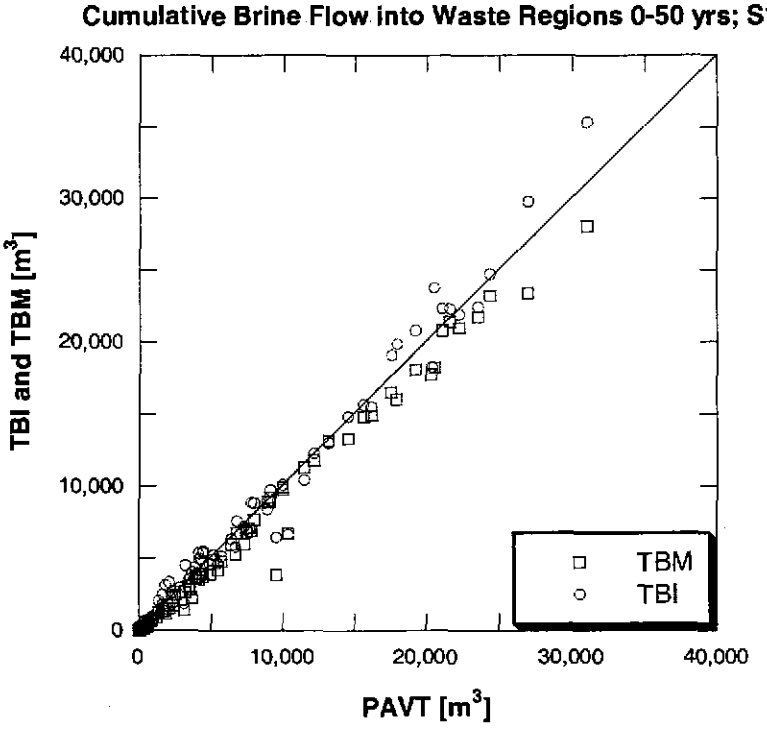

Figure 20. Undisturbed Scenario (S1); Cumulative Brine Flow Into the Waste Regions [BRNREPTC]; Scatter Plot; TBM and TBI versus PAVT; 50 Years After Repository Closure

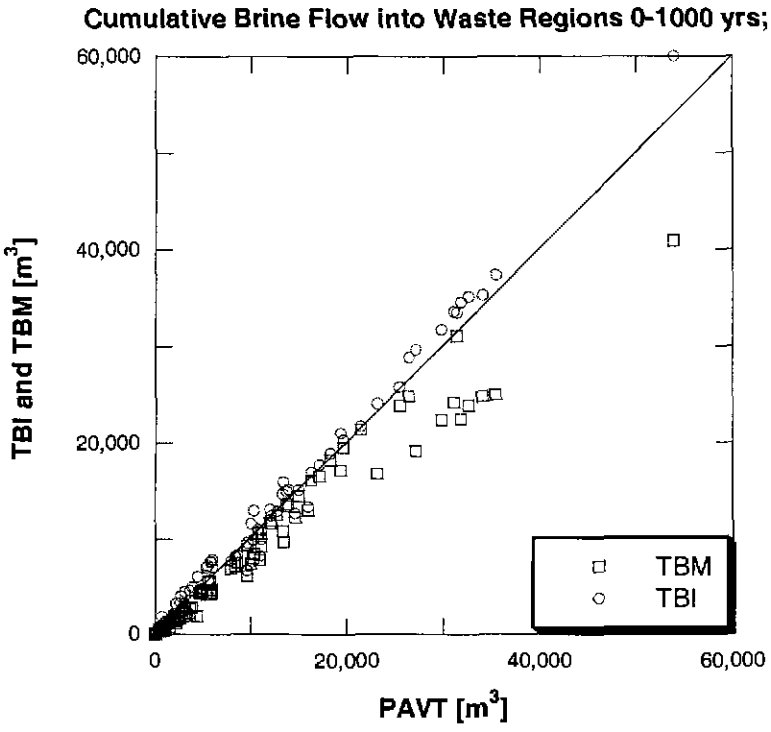

Figure 21. Undisturbed Scenario (S1); Cumulative Brine Flow Into the Waste Regions [BRNREPTC]; Scatter Plot; TBM and TBI versus PAVT; 1,000 Years After Repository Closure

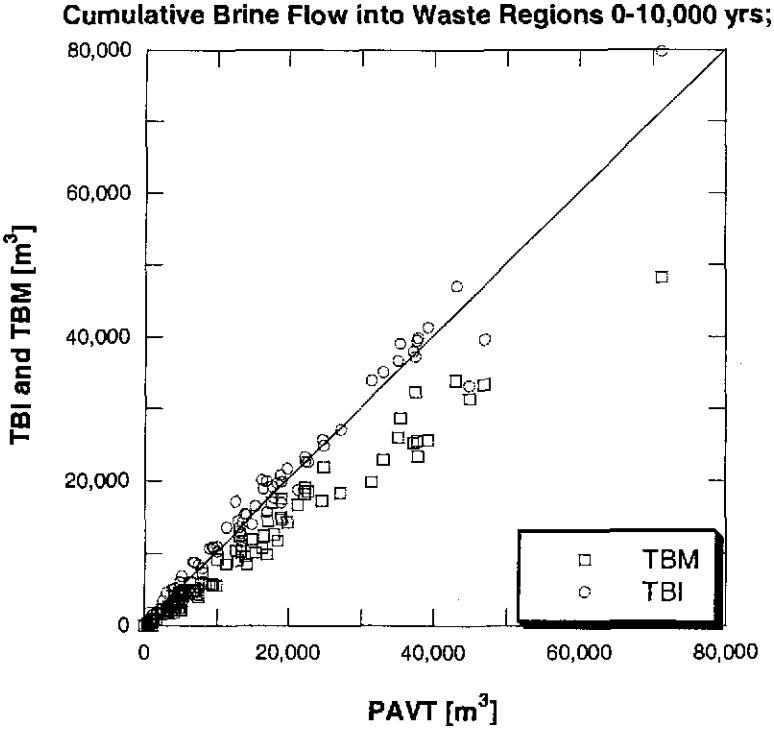

Figure 22. Undisturbed Scenario (S1); Cumulative Brine Flow Into the Waste Regions [BRNREPTC]; Scatter Plot; TBM and TBI versus PAVT; 10,000 Years After Repository Closure

10^{-15} m^2, which are representative of the PAVT panel closure, Darcy's Law predicts an integrated flux of ~500 m^3 over 1000 years. Over 10,000 years, this adds up to 5,000m3 of brine. Since the average cumulative brine inflow into the waste regions for the PAVT over 10,000 years is less than 13,000m3. Actual brine fluxes through the panel closures in the PAVT and TBI are likely to be limited by actual brine inflow to the northern areas. The Option D panel closure permeability is several orders of magnitude less than that of the PAVT panel closures, thus by Darcy's Law, the flux will also be reduced by several orders of magnitude. This simple calculation illustrates why gravity-driven brine flow is significant in the PAVT and TBI but is greatly reduced in the TBM due the Option D panel closures.

As will be shown later in this report, the Option D panel closures delay the movement of gas to the north, elevating pressures in the waste regions relative to the PAVT and TBI during the first several thousand years. These elevated pressures effectively reduce the hydraulic gradient for flow toward the repository resulting in lower flow rates during this period. Once pressures have equilibrated throughout the repository, inflow rates through the marker beds accelerate to roughly the same rates as in the TBI.

A comparison of mean brine flow out of Marker Bed 139 toward the south end of the repository shows the following results and illustrates the effect of higher pressures on brine flow. Between 1,000 and 2,000 years the total brine flow was about 17% greater in the TBI than TBM. This is due to the higher pressures in the TBM during this period. Between 9,000 years and 10,000 the pattern is reversed with approximately 16% less inflow in the TBI than the TBM. This occurs for two reasons. First, because flow is impeded early in the TBM, pressures in the marker beds do not assume repository valves as fast as they do in the TBI. Second, repository pressures at 10,000 years in the TBM are slightly lower on average than in the TBI, which in turn slightly increases brine flow. The slightly lower pressures at later times may result from the overall lower brine saturations in the waste regions in the TBM, which may in turn result in less steel corrosion over 10,000 years and consequently less gas. Steel corrosion in the TBM is on average 3.6% less than in the TBI after 10,000 years. Such interplay between coupled processes illustrates why it is difficult to determine definitive cause and effect relationships in a complex model such as the WIPP BRAGFLO simulations.

4.3.3.2 Disturbed Scenario (S3)

The S3 disturbed scenario models a drilling intrusion where the borehole penetrates through a waste panel into a pressurized brine reservoir below the repository. Figure 23 shows flow from the brine pocket into the intruded panel over time for all 100 vectors in the S3 scenario. The drilling intrusion takes place at 1,000 years. At the time of intrusion, borehole plugs effectively prevent brine from flowing through the borehole to the repository. These borehole plugs are assumed effective for 200 years, at which time the plug degrades and is replaced by a silty material. After degradation, the boreholes are highly permeable to gas and brine, and can allow significant flow to or from the repository.

Figure 24 compares flow from the brine pocket into the intruded panel at 10,000 years for the PAVT, the TBI, and the TBM for the S3 scenario. Brine flow up the borehole from the Castile is significantly less in the TBM and PAVT. The brine flow up the borehole from the castile brine

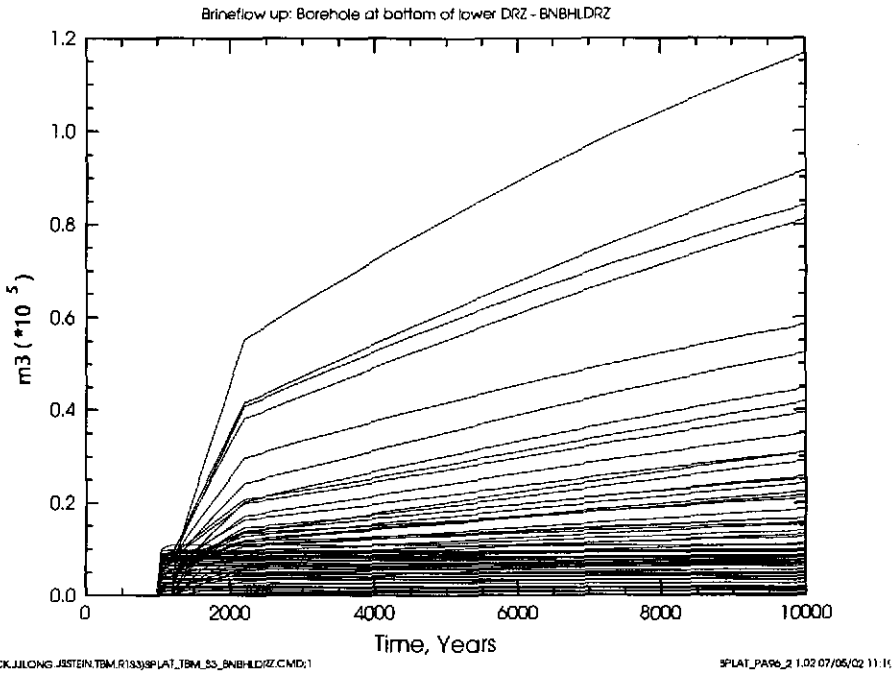

Figure 23. Disturbed Scenario (S3); Cumulative Brine Flow in Borehole from Brine Pocket Into Intruded Panel at Bottom of Lower DRZ [BNBHLDRZ]; TBM

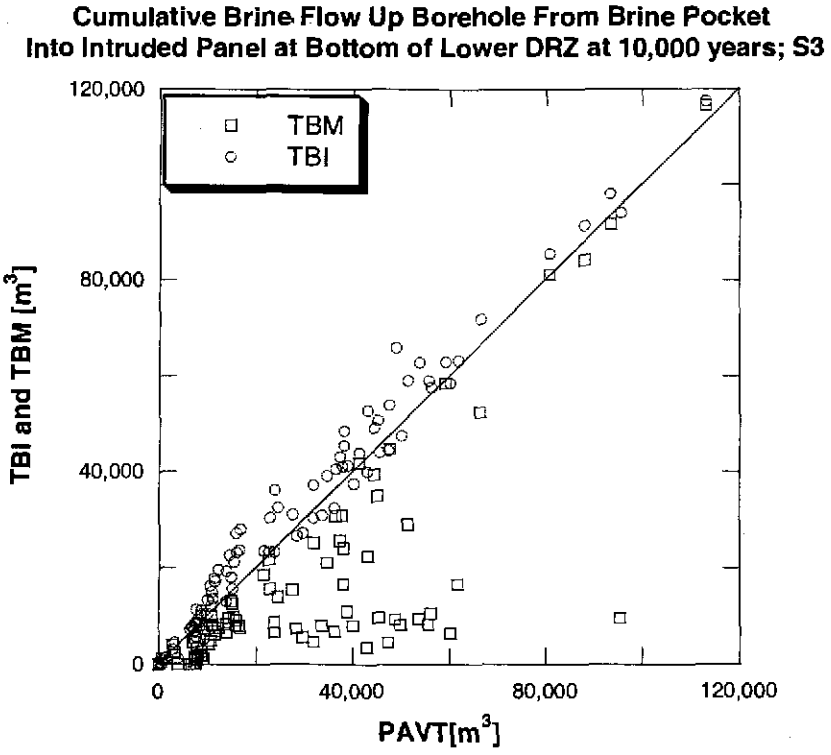

Figure 24. Disturbed Scenario (S3); Cumulative Brine Flow in Borehole from Brine Pocket Into Intruded Panel at Bottom of Lower DRZ [BNBHLDRZ]; Scatter Plot; TBM and TBI versus PAVT; 10,000 Years After Repository Closure

pocket is slightly greater in the TBI compared to that in the PAVT. The reduction in brine inflow in the TBM compared to that in the BAVT and TBI is due to the Option D panel closures, which interfere with the movement of brine and gas within regions of the repository.

4.3.3.3 Disturbed Scenario (S5)

The S5 disturbed scenario models a drilling intrusion where the borehole penetrates through the waste panel but not into a pressurized brine reservoir below the repository. Figure 25 shows the brine flow down the borehole for all 100 vectors in the S5 scenario. As in the S3 scenario, the drilling intrusion takes place at 1,000 years and the borehole is effectively plugged for the next 200 years. At 1,200 years, the plugs degrade and the borehole becomes highly permeable to gas and brine, and can allow significant flow to or from the repository.

Figure 26 compares cummulative brine flow from the intruded panel to the surface at 10,000 years for the PAVT, TBI, and TBM for the S5 scenario. As in the S3 scenario, brine flow in the borehole towards the repository is significantly less in the TBM than in the TBI or PAVT. The reduction in brine inflow is due to the Option D panel closures, which interfere with the movement of brine and gas within regions of the repository

4.3.4 Total Brine Volume in the Excavated Areas in the TBM Calculation

Since brine flow to the repository is reduced in the waste-filled regions in the TBM, it is natural to ask whether total brine volume in all excavated areas is also reduced in the TBM. Figures 27 and 28 compare the total brine volume in the excavated areas at 1,000 and 10,000 years for the PAVT, TBI, and TBM for the S1 scenario. The figures show that total brine volume in the repository is not reduced in the TBM as compared to the TBI or PAVT for this scenario. Rather, at 10,000 years total brine volume in the repository is slightly greater in the TBM than in the other calculations. In the TBM, less brine is consumed in steel corrosion in the waste-filled regions than in the TBI or PAVT. As this report will show, brine saturations in the experimental area are significantly higher in the TBM than in the TBI. Thus, in the undisturbed scenario, similar amounts of brine flow into the repository in all calculations, but in the TBM, the Option D panel closures prevent the brine from flowing downhill to the waste-filled regions where it can be consumed.

Figures 29 and 30 show the total brine volume in the excavated areas for the S3 and S5 scenarios at 10,000 years. In the S3 scenario, there is significantly less brine in the excavated areas in the TBM than in the PAVT or TBI. This difference is caused by the Option D panel closures. In the PAVT and TBI, brine from the Castile enters the waste panel and is able to flow laterally into the rest of the repository. In the TBM, the Option D panel closures prevent this lateral flow and result in less total brine in the excavated areas. In the S5 scenario, the total brine volume in the excavated areas for the TBM and TBI generally matches the PAVT, with some scatter. This indicates that the Option D panel closures do not significantly affect total brine volume in the excavated areas for this scenario.

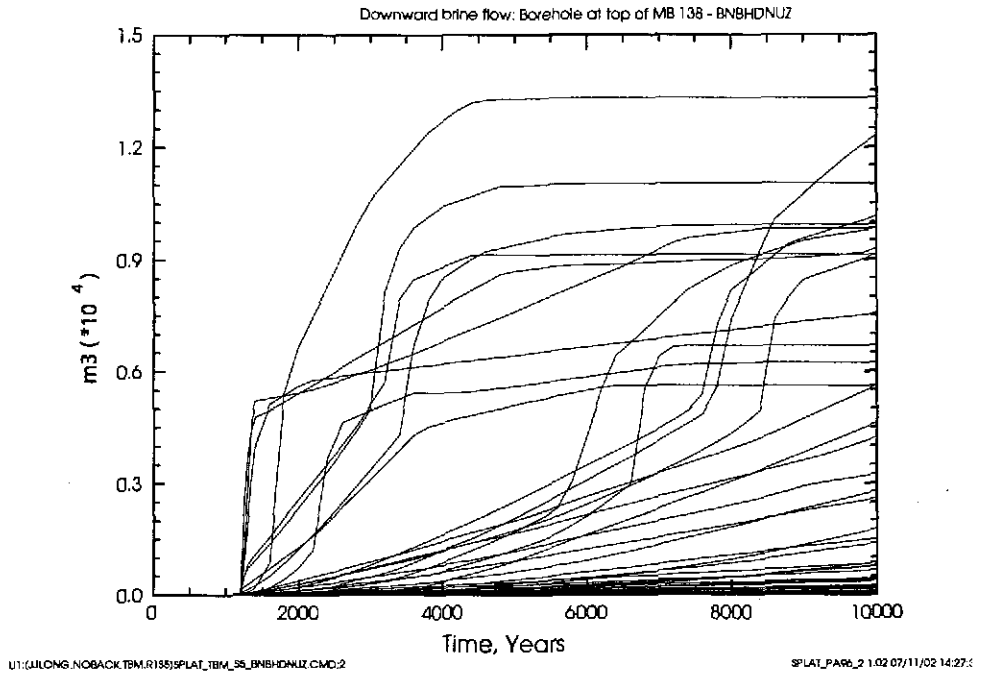

Figure 25. Disturbed Scenario (S5); Cumulative Brine Flow Down Borehole at Top of Upper DRZ [BNBHDNUZ]; TBM

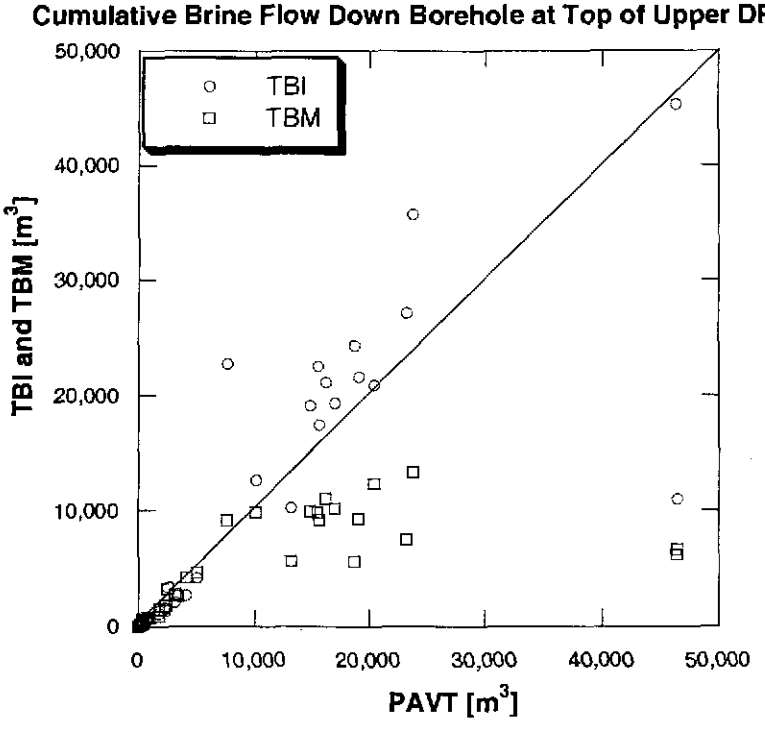

Figure 26. Disturbed Scenario (S5); Cumulative Brine Flow Down Borehole at Top of Upper DRZ [BNBHDNUZ]; Scatter Plot; TBM and TBI versus PAVT

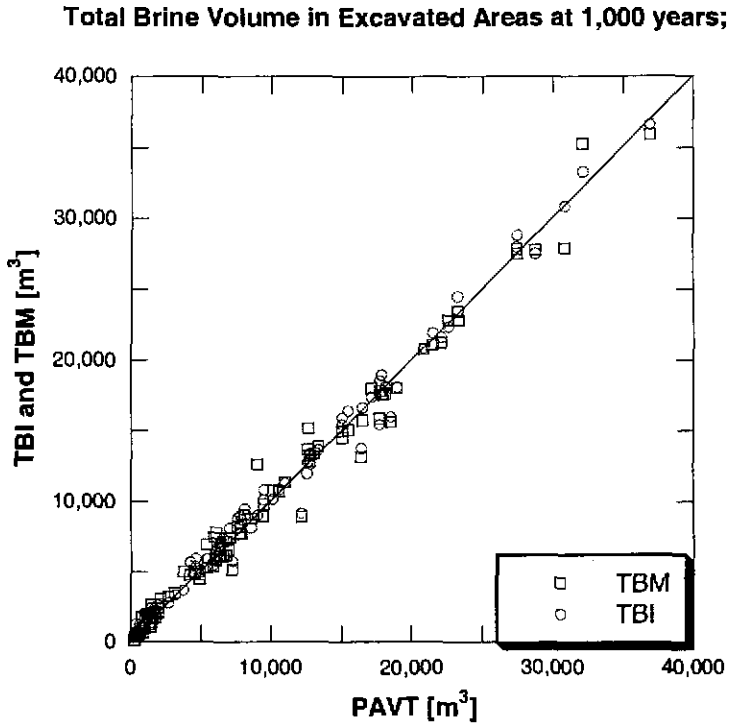

Figure 27. Undisturbed Scenario (S1); Total Brine Volume in Excavated Areas at 1,000 years [BRNVOL_A]; Scatter Plot; TBM and TBI versus PAVT

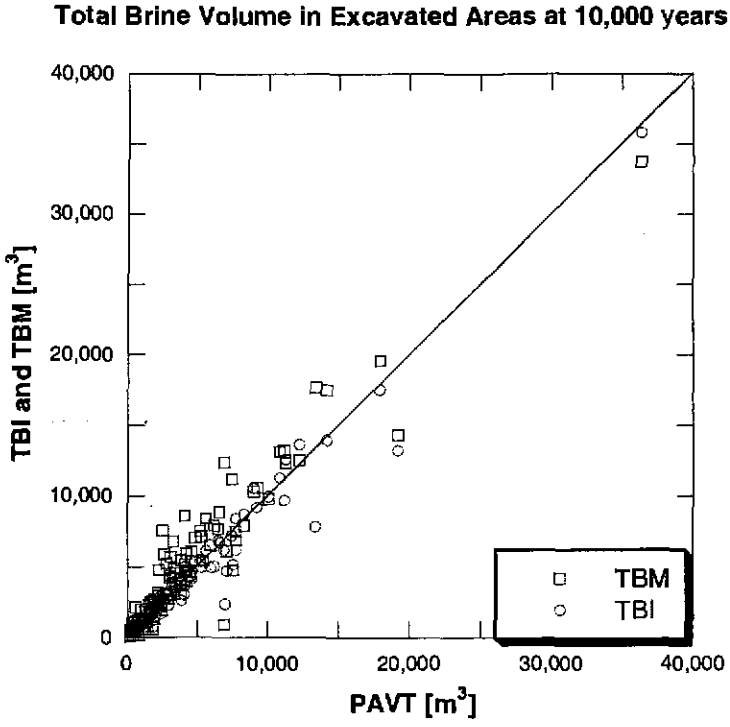

Figure 28. Undisturbed Scenario (S1); Total Brine Volume in Excavated Areas at 10,000 years [BRNVOL_A]; Scatter Plot; TBM and TBI versus PAVT

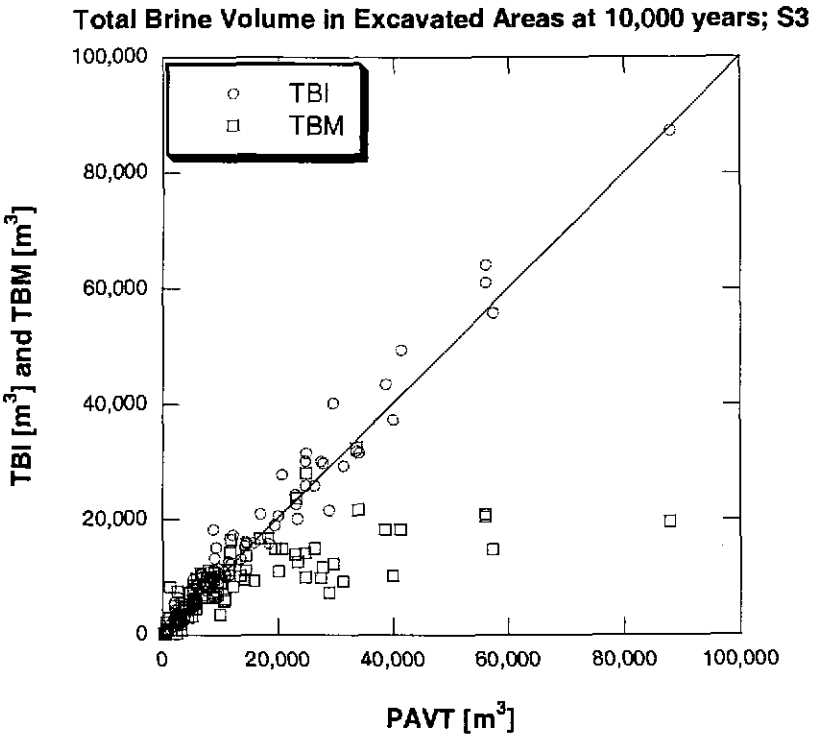

Figure 29. Undisturbed Scenario (S3); Total Brine Volume in Excavated Areas at 10,000 years [BRNVOL_A]; Scatter Plot; TBM and TBI versus PAVT

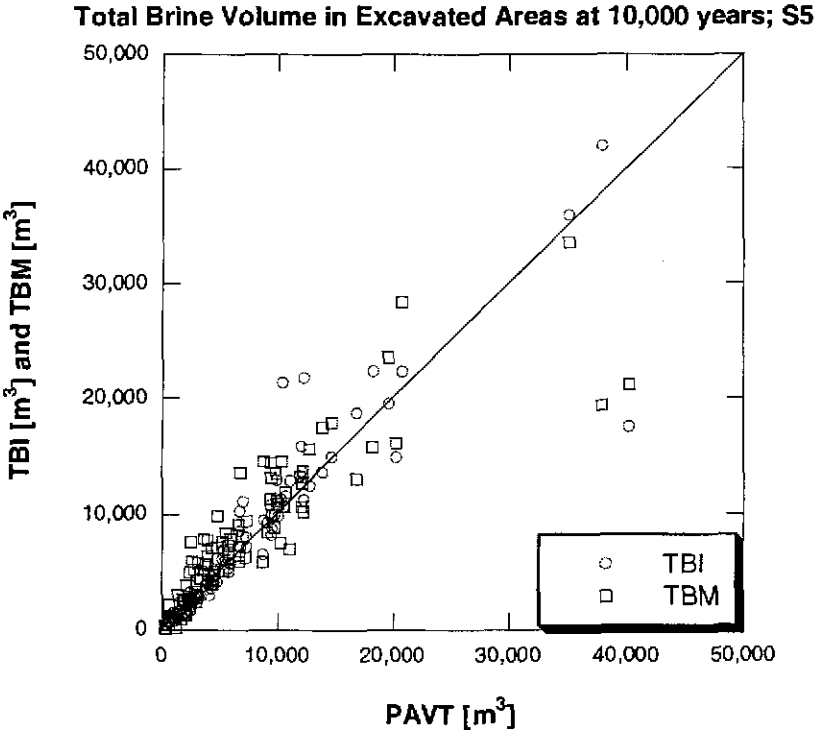

Figure 30. Undisturbed Scenario (S5); Total Brine Volume in Excavated Areas at 10,000 years [BRNVOL_A]; Scatter Plot; TBM and TBI versus PAVT

4.4 BRINE SATURATION

Brine Saturation

Brine saturation is calculated as the quotient of the volume of brine divided by the total pore volume. It is influenced by the rate of brine inflow, the rate of consumption due to gas generation reactions, and the creep closure rate which affects the total pore volume. The TBI results indicate that modifications and corrections to the grid spacing and flaring slightly affect the brine saturations. However, the Option D panel closures, implemented in the TBM, significantly reduce the brine saturations in the single waste panel as compared to the PAVT. This reduction is due to the reduced gravity-driven flow of brine through the panel closures from the northern areas. In the PAVT this gravity flow resulted in significantly higher saturations in the southern waste panel than in the rest of repository. The saturations in these regions in the TBM are more consistent across the waste regions for each vector. Following a brine pocket intrusion, only the saturation in the intruded panel increases in the TBM. In the PAVT, the generic panel closures did not stop brine from invading the entire repository and increasing saturations across the excavated areas.

BRAGFLO calculates brine saturation in the waste regions as a function of time. Brine saturation is used internally to estimate gas generation and externally as an initial condition in the models of direct brine release and of Salado transport, and thus is a significant output from BRAGFLO.

Brine saturation is calculated as the quotient of the volume of brine divided by the total pore volume. Both brine volume and total pore volume vary with time, the latter changing in response to the pressure-dependent model of creep closure of the waste regions and through rock compressibility or fracturing in the host rock. The preceding section outlined a comparison of the volumes of brine flowing into the waste-filled regions of the repository. The comparison showed that total brine volume in the excavated areas remains similar for all three calculations (PAVT, TBI, and TBM), although the distribution of that brine differs when the performance of option D panel closures are simulated. In the TBI, the changes to the grid and the fracturing of the upper DRZ have only minor effects on brine flow into the waste regions. However, as shown in the TBM, the Option D panel closures cause a significant reduction in brine volume in the waste regions. Thus, the TBM is expected to show brine saturations in the waste regions lower than those in the TBI or PAVT. In order to confirm that brine saturations are lower because of the panel closures' effects on brine flow into the waste regions, this analysis must also examine pore volume in the waste regions.

This section presents the changes in volume-averaged brine saturation due to the changes made in BRAGFLO. First, pore volume in the waste regions is examined. Next, the effects on brine saturation of the changes to BRAGFLO are presented.

4.4.1 Pore Volume

Figure 31 shows the mean value of porosity in the waste panel over all 100 vectors in the undisturbed scenario. During the first thousand years, porosity decreases dramatically due to creep closure of the waste regions. In this transient period porosity may be as much as twice as large in the TBM as in the PAVT. After about 1,000 years, porosity reaches a minimum value and then slowly increases for the remaining 9,000 years. The increase in porosity is due to gas generation, which increases pressure and thus slowly opens pore volume.After the transient effects during the first 1,000 years, there is no effect on porosity of the change to the new grid, as shown by the curve for TBI coinciding with the curve for the PAVT in Figure 31. The TBM maintains slightly higher

porosity than the TBI for the next few thousand years. This increase in porosity results from higher pressures in the waste panel in the TBM than in the TBI; the Option D panel closures cause the higher pressures, a fact which will be demonstrated in Section 4.7. As a consequence of the higher pressures, creep closure slows, resulting in higher porosity. However, over the long-term the TBM pressure equilibrate, causing the waste panel to close as in the TBI and PAVT, achieving the same porosity. Figure 32 shows that the same phenomenon takes place in the rest of the repository region, which for the TBI and TBM is the average over the north and south rest of repository regions.

We conclude that pore volume changes are negligible in the TBI, while in the TBM, there is a slight increase in pore volume for the first few thousand years. Given equal amounts of brine present, higher pore volume results in lower saturations. However, after the first 1,000 years the difference in pore volume is small, thus, differences in saturation more probably arise from differences in brine volume present in the waste.

4.4.2 Brine Saturation Results for the TBI Calculation

Brine saturation in the repository was compared between the PAVT and the TBI for a full replicate of 100 vectors. The TBI is the intermediate case where BRAGFLO was run with the new grid incorporating the PAVT panel closures and without fracturing in the upper DRZ. This comparison identifies the effects of changing to the new grid and removing the upper DRZ fracturing on brine saturation in the repository. In the TBM grid, volume-averaged brine saturation is calculated for the combined South Rest of Repository and North Rest of Repository in order to compare to brine saturations in the Rest of Repository in the PAVT grid.

Since pore volume in the TBI closely matches that in the PAVT, any changes in brine saturation in the TBI are due to the changes to brine flow caused by the new grid and by removal of the fracture model from the upper DRZ. Section 4.5 of this report showed that the changes in brine flow toward the repository and brine consumption by corrosion in the TBI are primarily due to the new grid and not to the removal of fracturing from the upper DRZ. Hence, any systematic change in brine saturation is due to the new grid.

The following discussion deals first with the undisturbed scenario (S1), then the two disturbed scenarios (S3 and S5). Brine saturation in the waste panel is examined since this variable is significant in determining direct brine releases from the repository. Brine saturation in the experimental area is presented to show the effects of changing to the new grid and of the Option D panel closures.

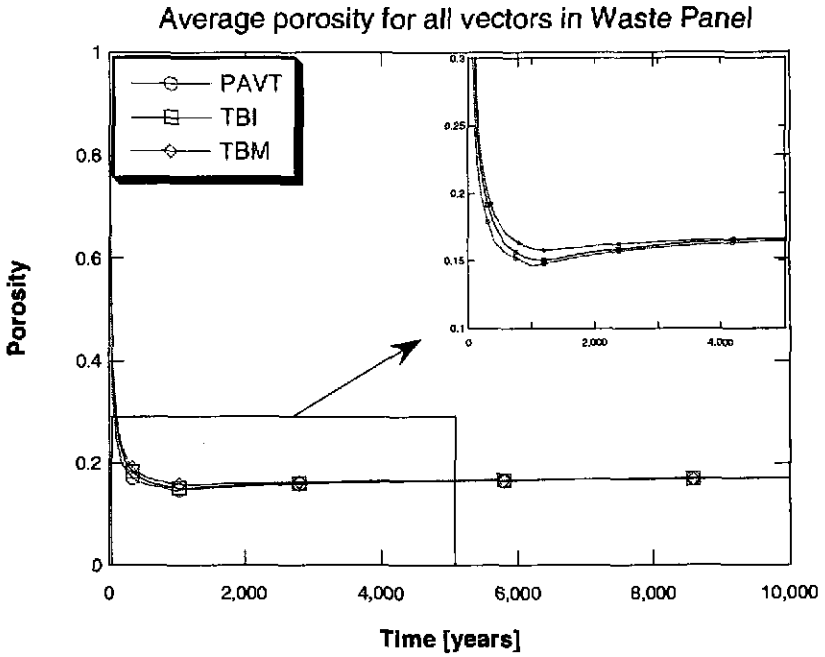

Figure 31 . Undisturbed Scenario (S1); Average of Porosity in the Waste Panel [WAS_POR]

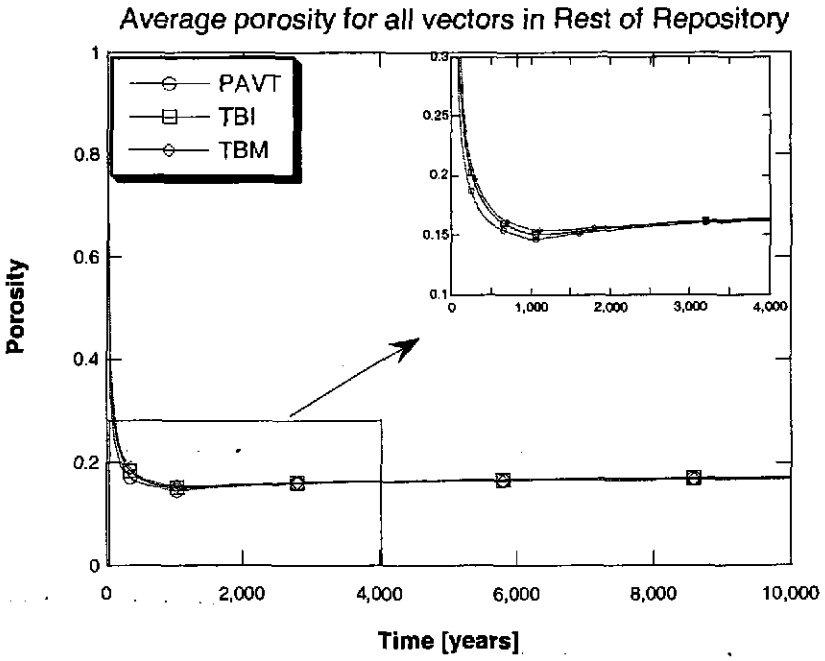

Figure 32. Undisturbed Scenario (S1); Average of Porosity in the Rest of Repository [REP_POR]

4.4.2.1 Undisturbed Scenario (S1)

Figures 33 and 34 show brine saturation in the waste panel and the experimental area over time for all 100 vectors in the undisturbed case. As these figures show, in some vectors brine saturations exhibit wide variations over time. The variation in brine saturation in Figures 33 and 34 result from the combination of brine consumption by corrosion, the dynamic coupling of gas generation, creep closure and brine inflow, and the uncertainty in parameters such as residual brine saturations and the steel corrosion rate. This time-dependent variation complicates comparisons between sets of 100 vectors at a specific point in time. If the effect of a conceptual change is to slightly accelerate or delay the time-dependent variations in brine saturation for a particular vector, the effect may be exaggerated by comparing the brine saturations for that vector at a specific point in time. Therefore, one expects more variation in the scatter plot comparisons of brine saturation than are evident in the scatter plots of pressure and brine flow.

Figures 35 and 36 compare brine saturations in the waste panel at 1,000 and 10,000 years for the PAVT and TBI. Although the change to the new grid increases somewhat the total volume of brine that flows into the waste regions, brine saturations do not change significantly. Brine consumption generally prevents the brine saturation from increasing in proportion to the increase in brine inflow. The variation around equality in Figures 35 and 36 is expected due to the time-dependent variations in brine saturation.

Figures 37 and 38 compare brine saturations in the experimental area at 1,000 and 10,000 years for the PAVT and TBI. These figures show that the change to the new grid slightly increases brine saturation in the experimental area. This increase results from an increase in brine inflow that is caused by the correction made to grid flaring. This correction slightly increases the volume of the marker beds adjacent to the experimental area. The increase in saturation is observable since brine is not consumed in the experimental area as it is in the waste regions. However, even with the increase in brine saturation in the experimental area, in the undisturbed scenario, the effect on brine saturation of the new grid is minimal.

4.4.2.2 Disturbed Scenarios (S3 and S5)

The two disturbed scenarios model drilling intrusions. The S3 scenario assumes a borehole that penetrates through the waste panel into a pressurized brine reservoir below the repository. In the S5 scenario, the borehole does not penetrate a brine reservoir below the repository. Figures 39 and 40 show brine saturation in the waste panel over time for all 100 vectors in the two disturbed scenarios. As in the undisturbed case, brine saturations exhibit wide variations over time, and thus one expects some variation in the scatter plot comparisons of brine saturations at specific points in time.

Figures 41 through 44 compare brine saturations in the waste panel at 1,000 and 10,000 years for the PAVT and TBI, for both disturbed scenarios. As in the undisturbed scenario, brine saturation in the waste panel does not change significantly from the PAVT to the TBI.

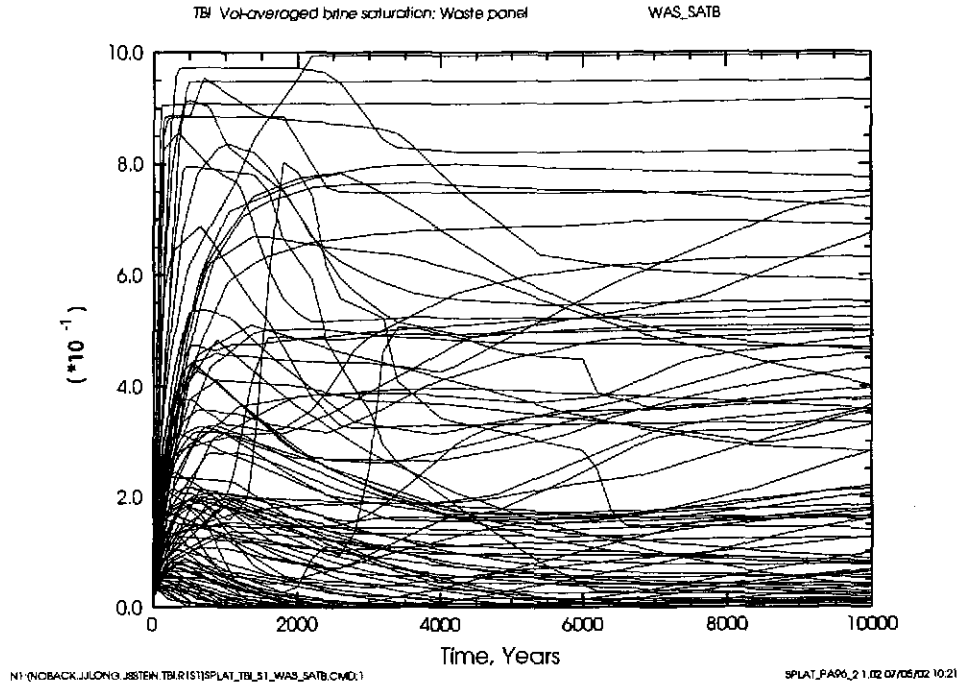

Figure 33. Undisturbed Scenario (S1); Brine Saturation in the Waste Panel [WAS_SATB]; TBI

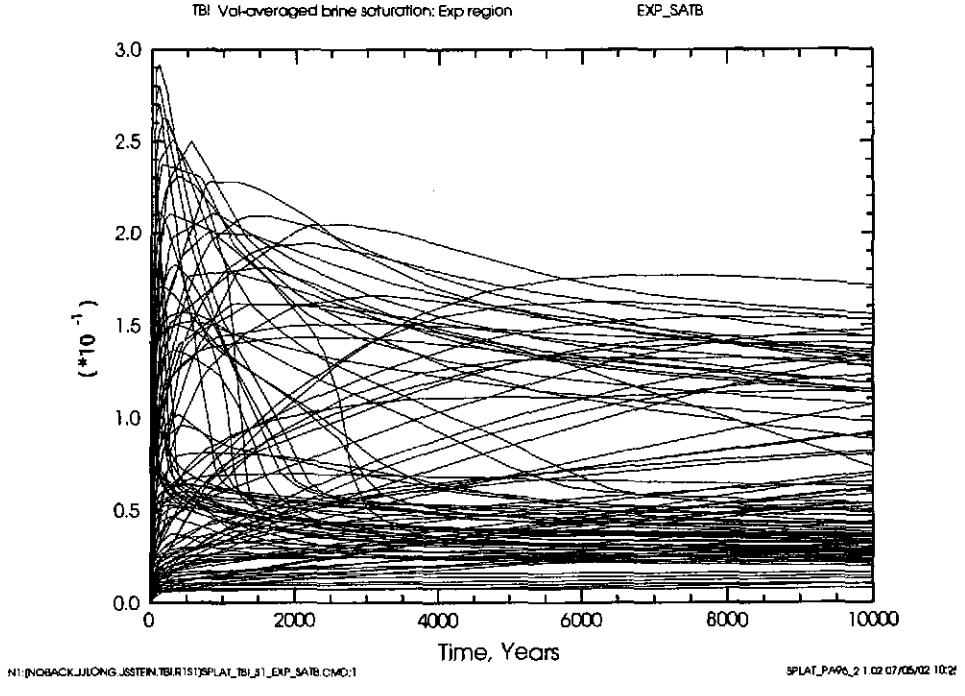

Figure 34. Undisturbed Scenario (S1); Brine Saturation in the Experimental Area [EXP_SATB]; TBI

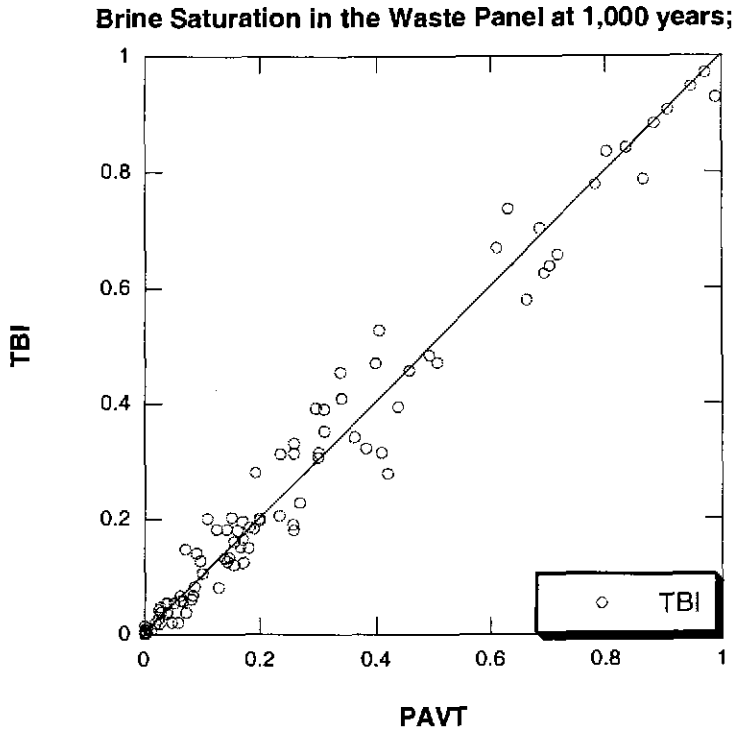

Figure 35. Undisturbed Scenario (S1); Brine Saturation in the Waste Panel at 1,000 Years [WAS_SATB]; Scatter Plot; TBI versus PAVT

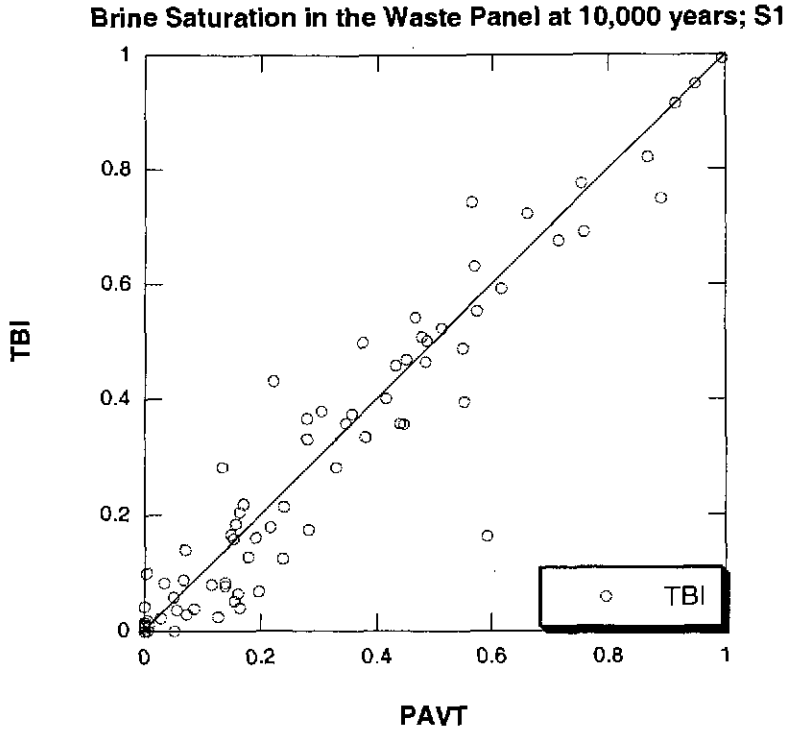

Figure 36. Undisturbed Scenario (S1); Brine Saturation in the Waste Panel at 10,000 Years [WAS_SATB]; Scatter Plot; TBI versus PAVT

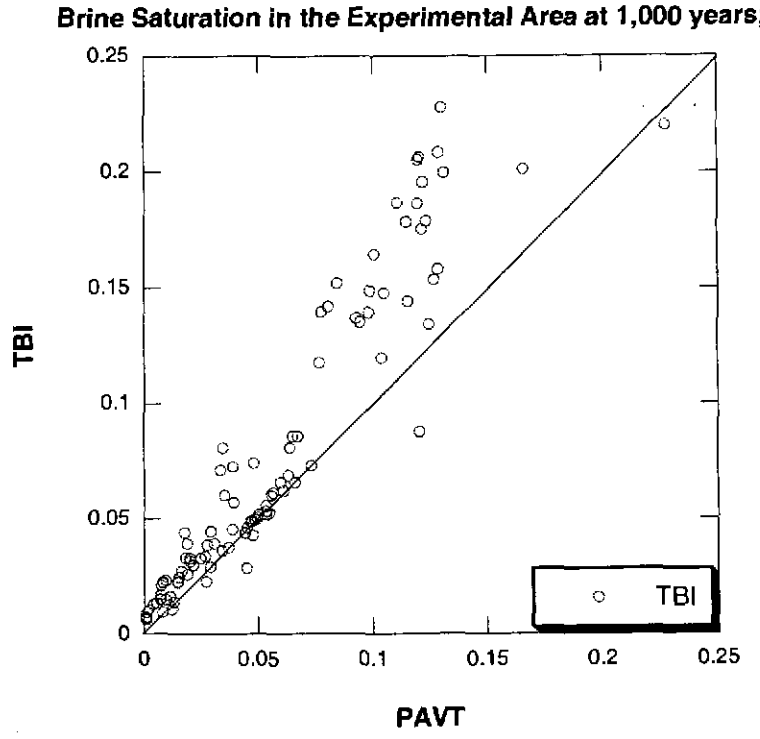

Figure 37. Undisturbed Scenario (S1); Brine Saturation in the Experimental Area at 1,000 Years [EXP_SATB]; Scatter Plot; TBI versus PAVT

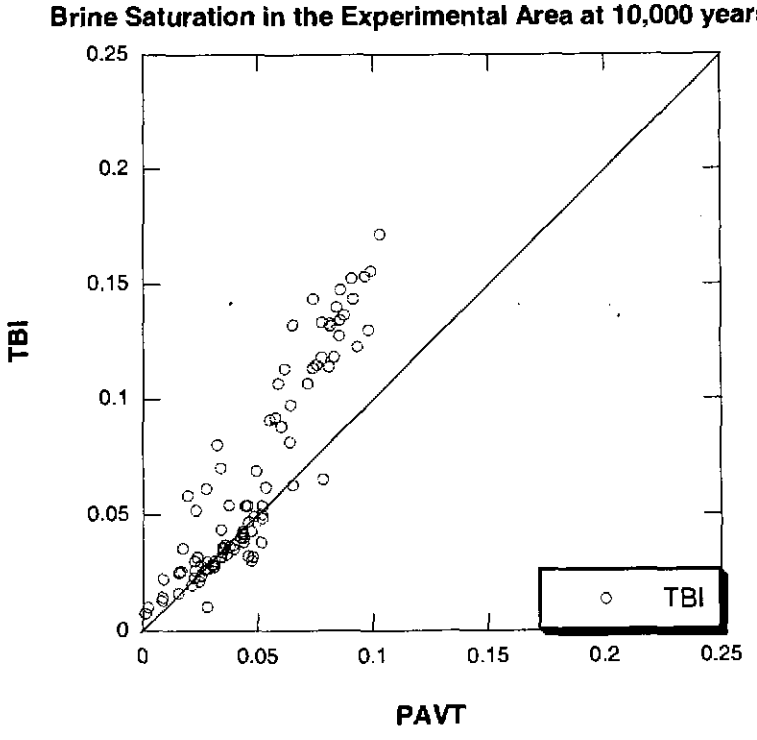

Figure 38. Undisturbed Scenario (S1); Brine Saturation in the Experimental Area at 10,000 Years [EXP_SATB]; Scatter Plot; TBI versus PAVT

Figures 45 through 48 compare brine saturations in the experimental area at 1,000 and 10,000 years for the PAVT and the TBI, for both disturbed scenarios. As in the undisturbed scenario, these figures show that the new grid's flaring algorithm slightly increases brine saturation in the experimental area. A few vectors are significantly affected by the removal of the shaft material CONC_MON, which was replaced in the new grid by a set of panel closures between the operations and experimental areas. In the PAVT, gas permeability of the material CONC_MON was unrealistically low in these two vectors, resulting in unrealistically high brine saturations in the experimental area. This problem is not present when the panel closure materials are used to separate the operations and experimental areas.

For the disturbed scenarios, one can conclude that the effect on brine saturations of the change to the new grid is minimal.

4.4.3 Brine Saturation Results for the TBM Calculation

Brine saturation in the repository was compared between the PAVT, the TBI and the TBM for a full replicate of 100 vectors. The previous comparison with the TBI identified the effects on brine saturation of the new grid and the removal of the fracture model from the upper DRZ. Comparison between the TBI and TBM identifies the effects on brine saturation of the Option D panel closures and the correction to the molecular weight of cellulose. The PAVT results are shown for completeness. In the TBM grid, volume-averaged brine saturation is calculated for the combined South Rest of Repository and North Rest of Repository in order to compare to brine saturations in the Rest of Repository in the PAVT grid.

Changes in brine saturation from the PAVT to the TBI were, in general, minimal. In the TBM, the slightly elevated pore volumes for the first few thousands years will slightly decrease brine saturations over the same time period, at a fixed brine volume. The Option D panel closures cause the increase in pore volume in the TBM because of overall higher pressures in the TBM simulations. In addition, the Option D panel closures significantly reduce brine flows into the waste regions. Consequently, reductions in brine saturation in the TBM are attributed to the Option D panel closures.

The following discussion deals first with the undisturbed scenario (S1), then the two disturbed scenarios (S3 and S5). Brine saturation in the waste panel is examined since this variable is significant in determining direct brine releases from the repository. Brine saturation in the experimental area is presented to show the effects of changing to the new grid and of the Option D panel closures.

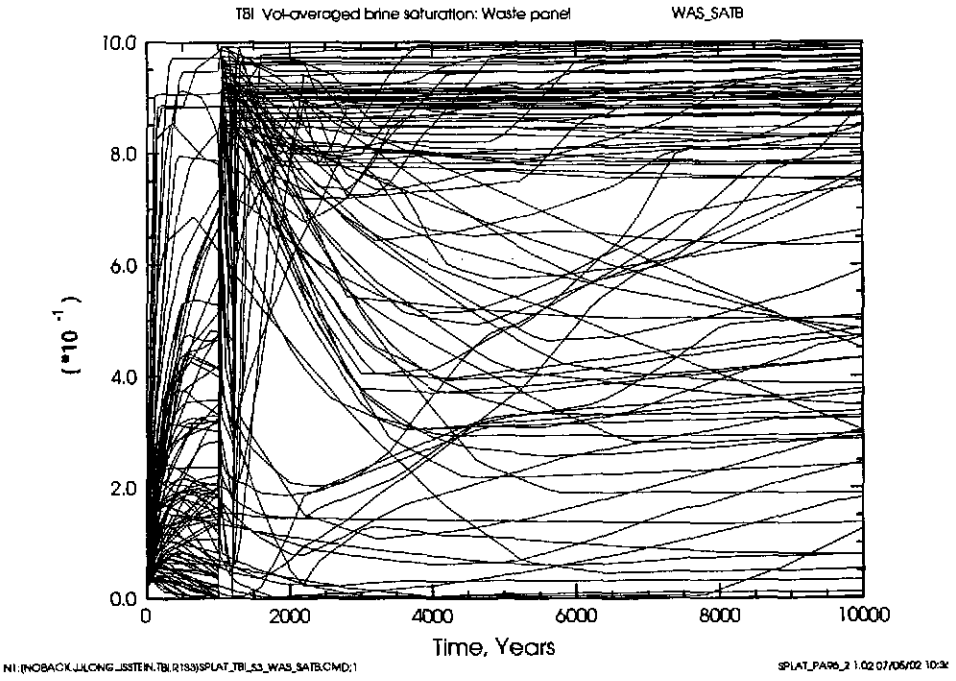

Figure 39. Disturbed Scenario (S3); Brine Saturation in the Waste Panel [WAS_SATB]; TBI

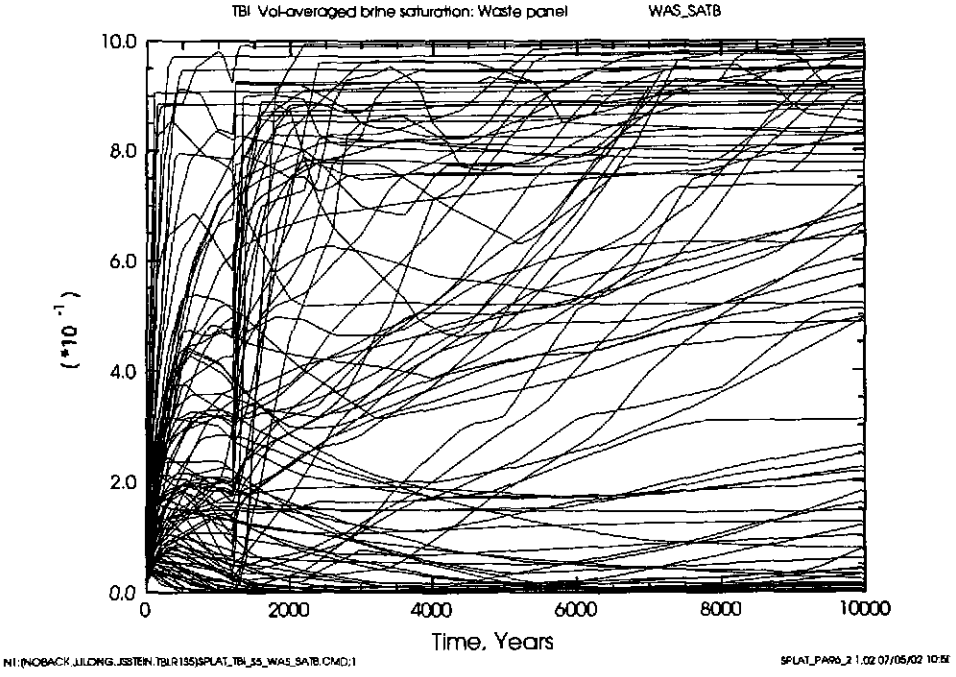

Figure 40 Disturbed Scenario (S5); Brine Saturation in the Waste Panel [WAS_SATB]; TBI

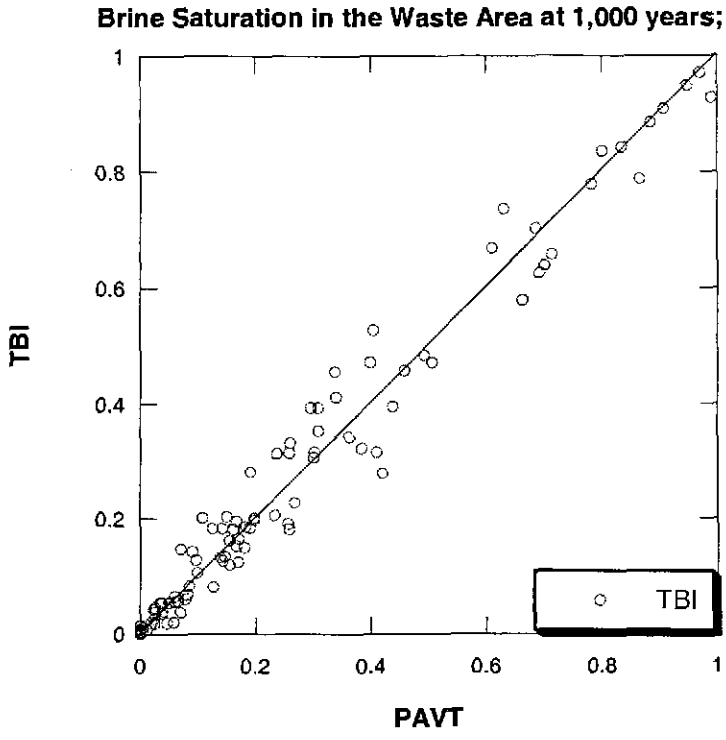

Figure 41. Disturbed Scenario (S3); Brine Saturation in the Waste Panel 1,000 Years [WAS_SATB]; Scatter Plot; TBI versus PAVT

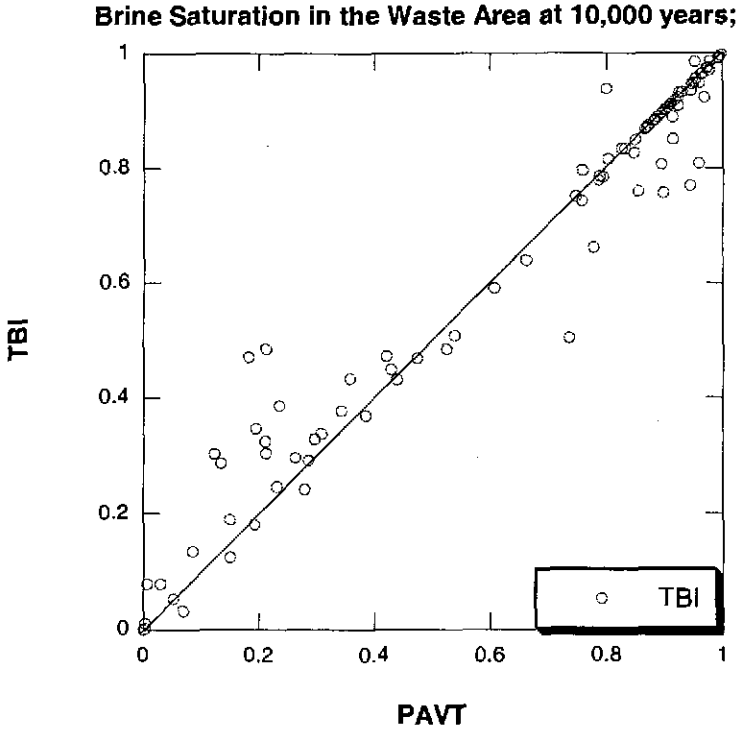

Figure 42. Disturbed Scenario (S3); Brine Saturation in the Waste Panel 10,000 Years [WAS_SATB]; Scatter Plot; TBI versus PAVT

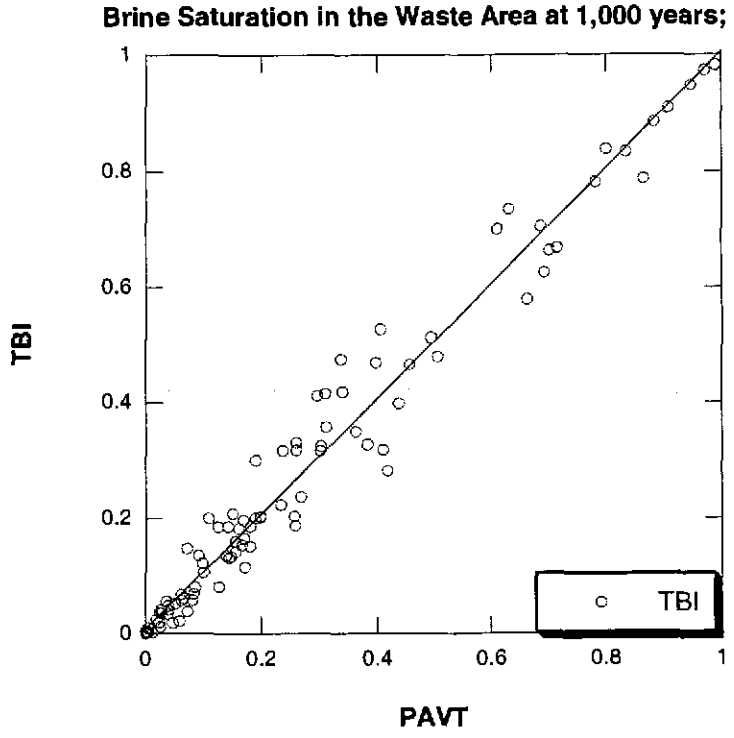

Figure 43. Disturbed Scenario (S5); Brine Saturation in the Waste Panel 1,000 Years [WAS_SATB]; Scatter Plot; TBI versus PAVT

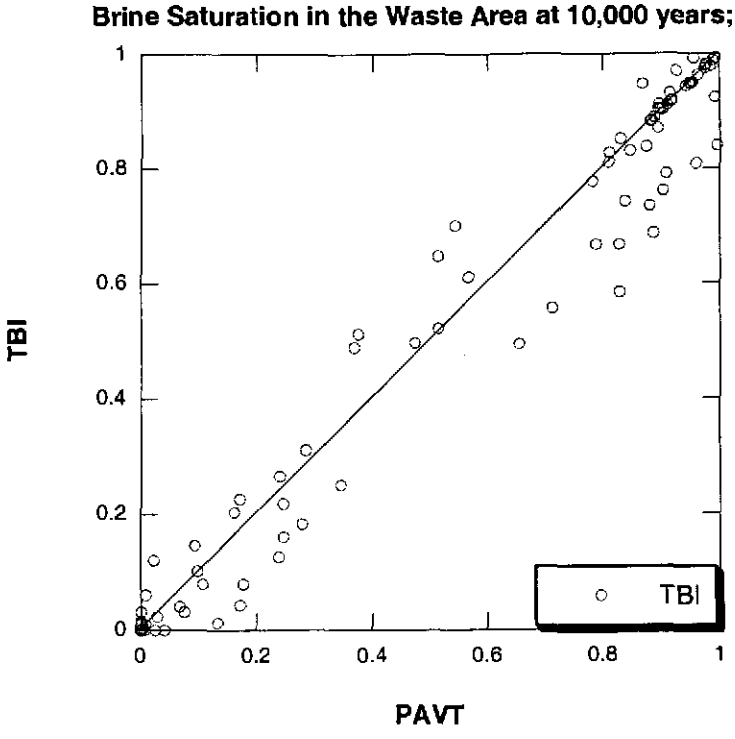

Figure 44. Disturbed Scenario (S5); Brine Saturation in the Waste Panel 10,000 Years [WAS_SATB]; Scatter Plot; TBI versus PAVT

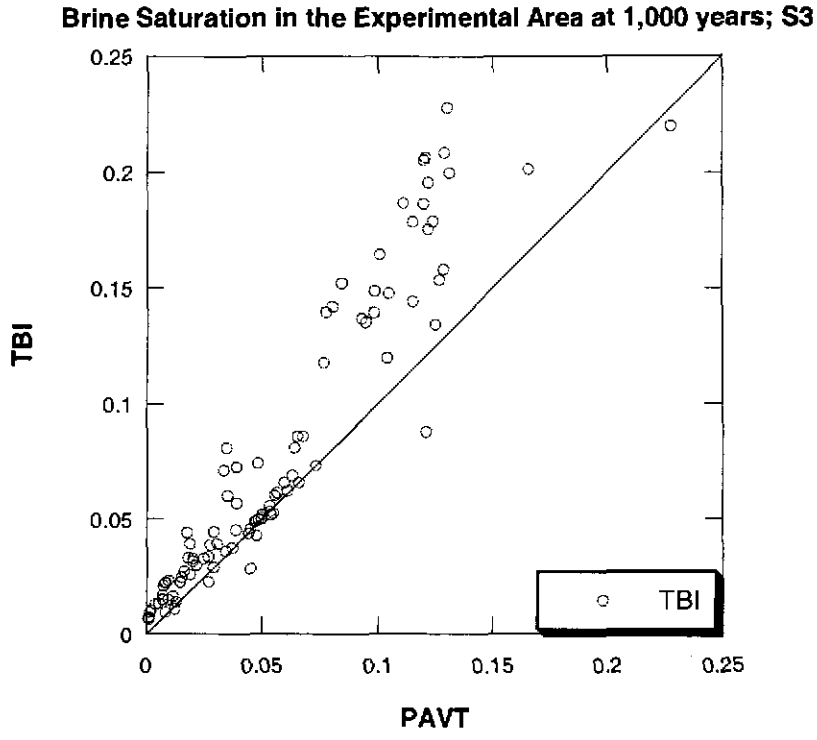

Figure 45. Disturbed Scenario (S3); Brine Saturation in the Experimental Area 1,000 Years [EXP_SATB]; Scatter Plot; TBI versus PAVT

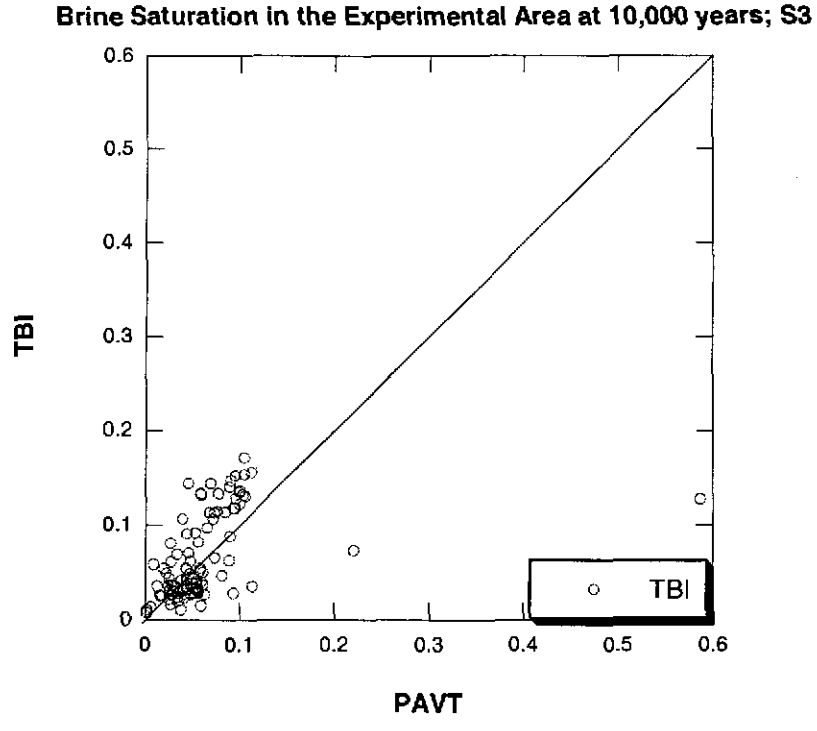

Figure 46. Disturbed Scenario (S3); Brine Saturation in the Experimental Area 10,000 Years [EXP_SATB]; Scatter Plot; TBI versus PAVT

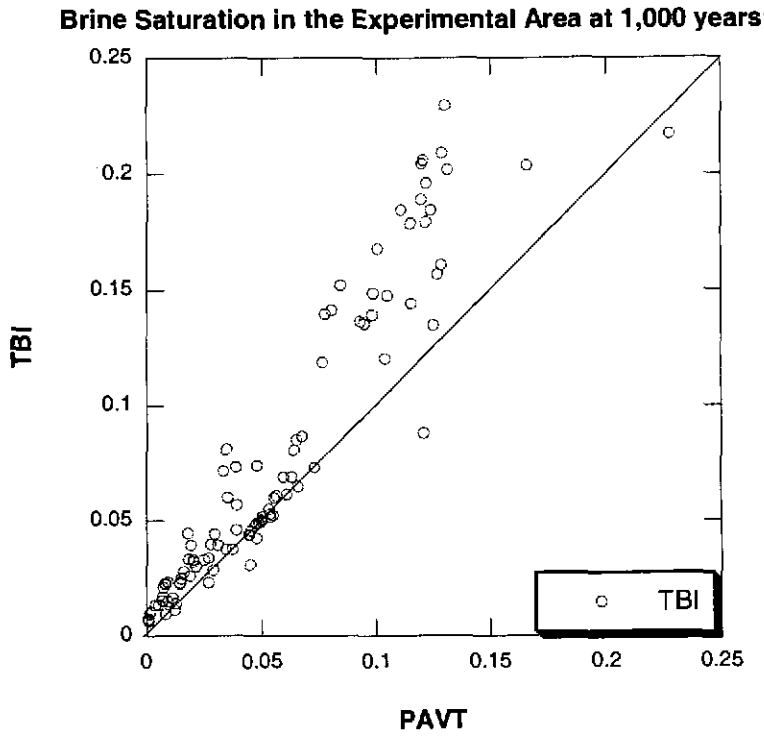

Figure 47. Disturbed Scenario (S5); Brine Saturation in the Experimental Area 1,000 Years [EXP_SATB]; Scatter Plot; TBI versus PAVT

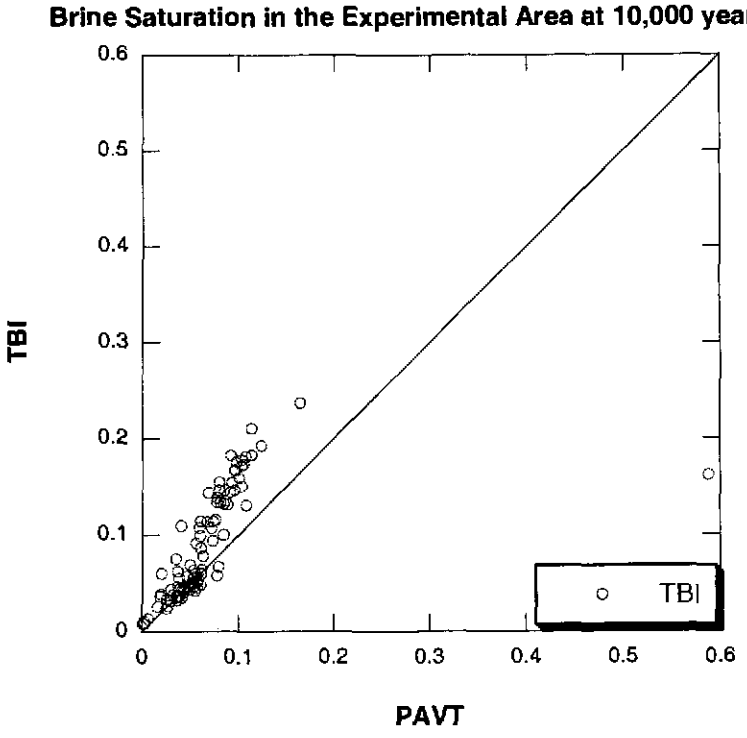

Figure 48. Disturbed Scenario (S5); Brine Saturation in the Experimental Area 10,000 Years [EXP_SATB]; Scatter Plot; TBI versus PAVT

4.4.3.1 Undisturbed Scenario (S1)

Figures 49 and 50 show brine saturation in the waste panel and the experimental area over time for all 100 vectors in the undisturbed case. As in the TBI, in some vectors brine saturations exhibit wide variations over time, thus one expects more variation in the scatter plot comparisons of brine saturation than are evident in the scatter plots of pressure. Comparing Figures 49 and 50 to the corresponding plots for the intermediate case (Figures 33 and 34), one observes that the addition of the Option D panel closures results in decreased saturation in the waste panel and increased saturation in the experimental area.

Figures 51 and 52 compare brine saturations in the waste panel at 1,000 and 10,000 years for the PAVT, the TBI and the TBM. As discussed earlier, when changing from the PAVT to the TBI, one observes no significant change in the brine saturations. However, when changing from TBI to the TBM, brine saturations in the waste panel are significantly reduced. The Option D panel closures remove all the high permeability pathways between regions in the repository grid. Consequently, brine cannot flow freely down gradient into the waste panel, which reduces the brine saturation in this region. Brine saturation is further reduced by the higher pressures in the waste panel, which increase pore volume slightly.

To verify that the reduction in saturation is caused by the panel closures and not by the correction to the molecular weight of cellulose, BRAGFLO was run with the new grid incorporating the Option D panel closures, without fracturing in the upper DRZ, and with the old molecular weight of cellulose. The calculation produced the same brine saturation in the waste panel as the TBM calculation. Hence, the differences in brine saturation between the TBM and the intermediate case are not caused by the correction to the molecular weight of cellulose.

Figures 53 and 54 compare brine saturations in the experimental area at 1,000 and 10,000 years for the PAVT, the TBI and the TBM. From the PAVT to the TBI the brine saturation in the experimental area increased slightly due to the revised grid-flaring algorithm. From the TBI to the TBM, the Option D panel closures were added. The panel closures greatly impede the flow of brine out of the experimental area downhill to the operations area, resulting in a further increase in brine saturation in the experimental area.

For the undisturbed case, the comparison of the TBI to the PAVT concluded that the effect on brine saturation of the change to the new grid is minimal. However, the Option D panel closures impede the flow of brine between regions of the excavated area, increasing saturation in the uphill regions (the experimental and operations area), and reducing saturation in the waste filled regions. The correction to the molecular weight of cellulose has no effect on brine saturation.

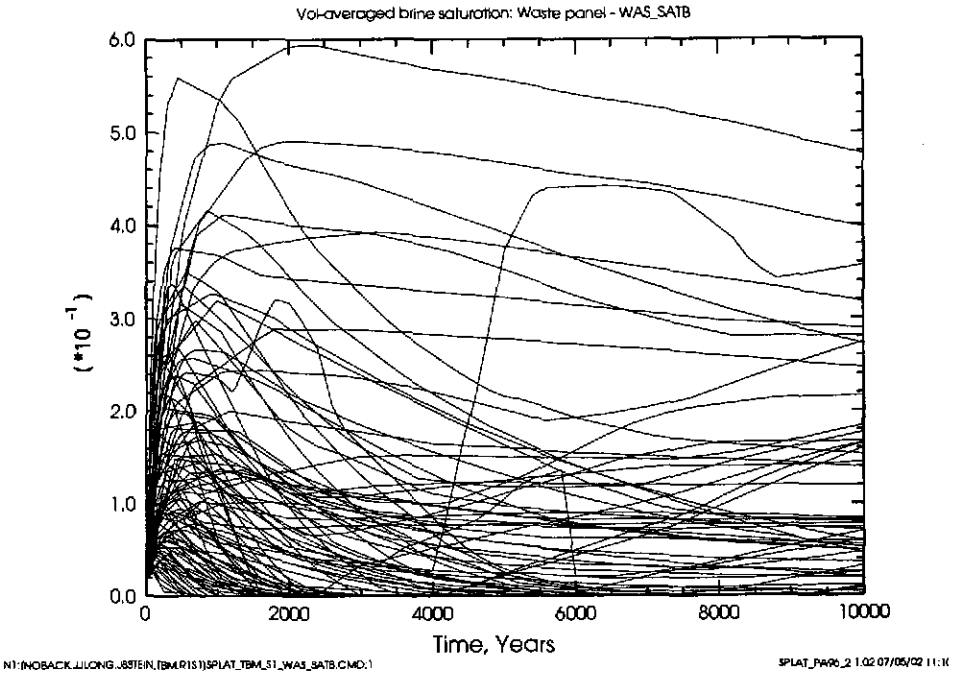

Figure 49. Undisturbed Scenario (S1); Brine Saturation in the Waste Panel [WAS_SATB]; TBM

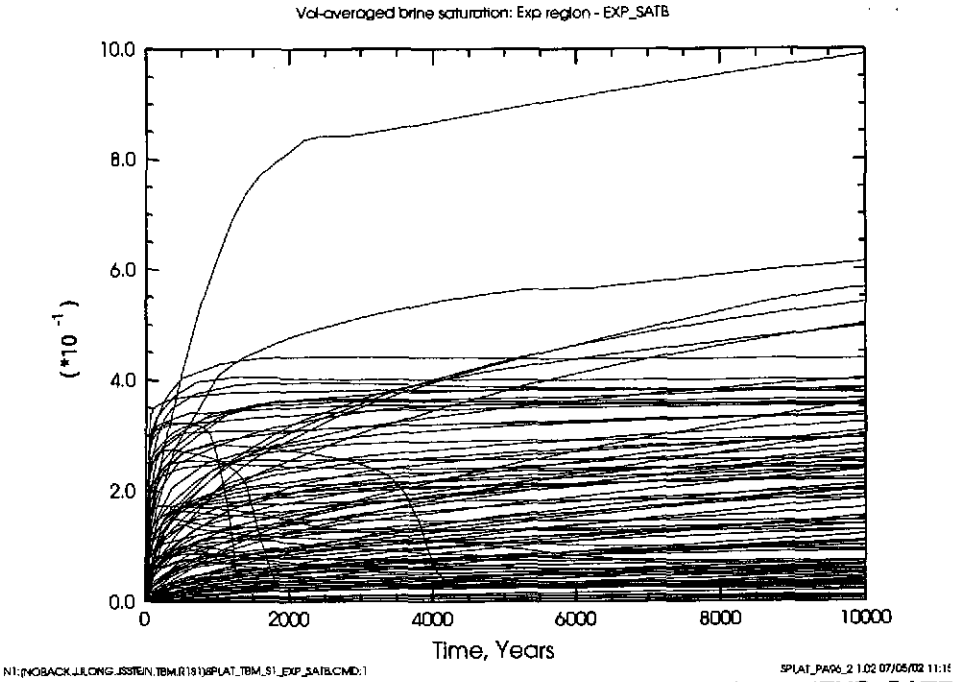

Figure 50. Undisturbed Scenario (S1); Brine Saturation in the Experimental Area [EXP_SATB]; TBM

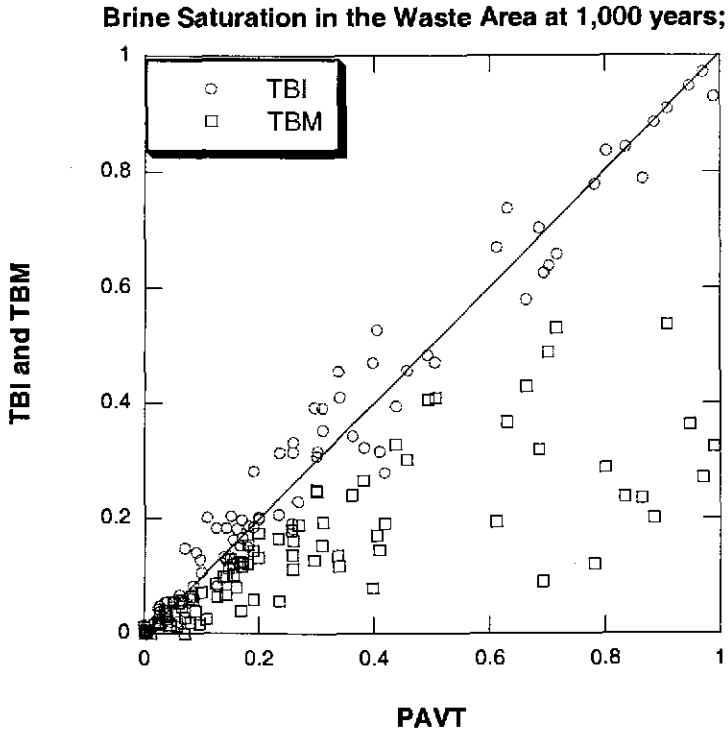

Figure 51. Undisturbed Scenario (S1); Brine Saturation in the Waste Panel at 1,000 Years [WAS_SATB]; Scatter Plot; TBM and TBI versus PAVT

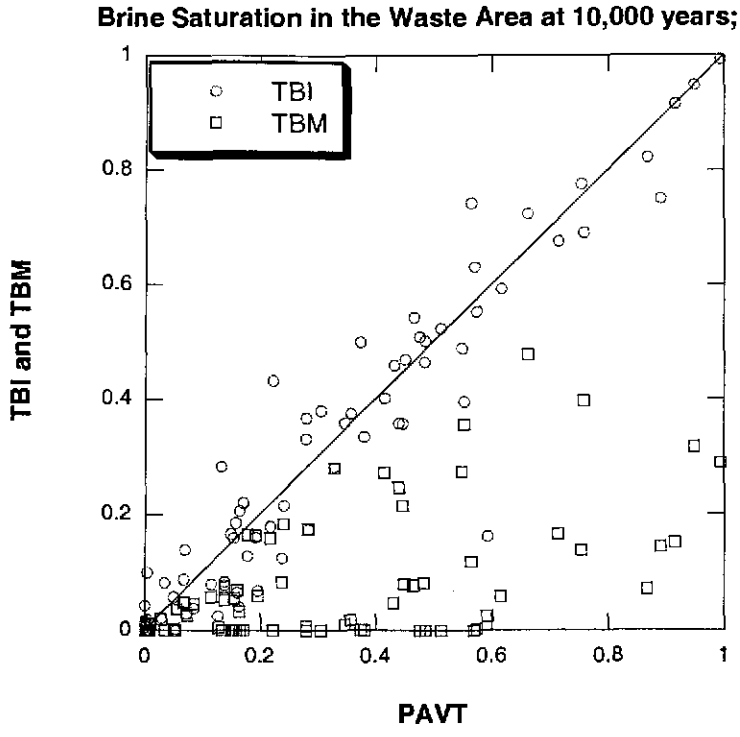

Figure 52. Undisturbed Scenario (S1); Brine Saturation in the Waste Panel at 10,000 Years [WAS_SATB]; Scatter Plot; TBM and TBI versus PAVT

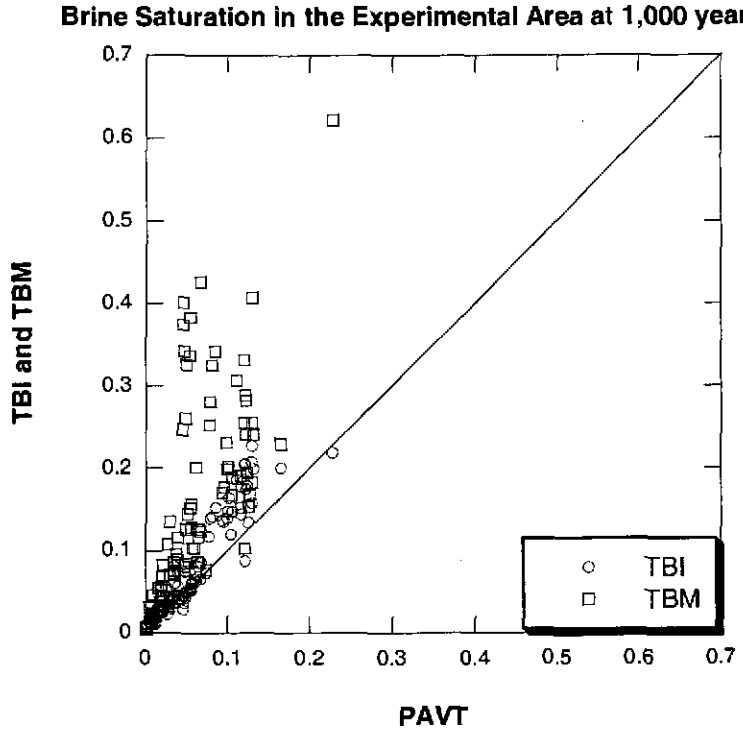

Figure 53. Undisturbed Scenario (S1); Brine Saturation in the Experimental Area at 1,000 Years [EXP_SATB]; Scatter Plot; TBM and TBI versus PAVT

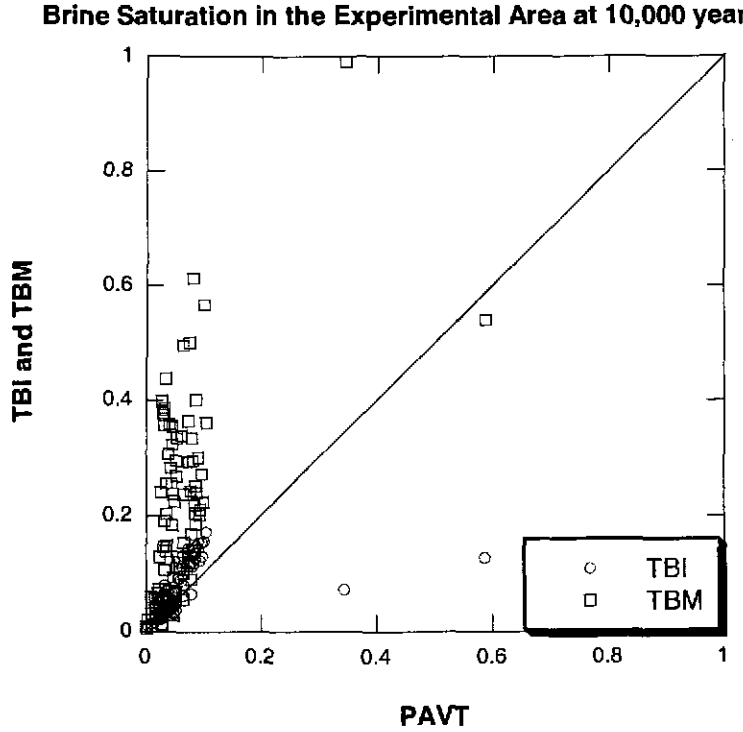

Figure 54. Undisturbed Scenario (S1); Brine Saturation in the Experimental Area at 10,000 Years [EXP_SATB]; Scatter Plot; TBM and TBI versus PAVT

4.4.3.2 Disturbed Scenario (S3)

The S3 disturbed scenario models a drilling intrusion where the borehole penetrates through a waste panel into a pressurized brine reservoir below the repository. Figure 55 shows brine saturation in the waste panel over time for all 100 vectors in the S3 scenario. The drilling intrusion takes place at 1000 years. At the time of intrusion, borehole plugs effectively prevent brine from flowing through the borehole to the repository. These plugs are assumed effective for 200 years, at which time the plug degrades and is replaced by a silty material. After degradation, the boreholes are highly permeable to gas and brine, and can allow significant flow to or from the repository. Figure 55 shows that after the plug degrades, brine saturation can change dramatically for some vectors, due to flow of brine up the borehole from the brine reservoir, or down the borehole from the Culebra.

Figures 56 and 57 compare brine saturations in the waste panel at 1,000 and 10,000 years for the PAVT, the TBI, and the TBM for the S3 scenario. At 1000 years, before the degradation of the borehole plug, the waste panel is less saturated in the TBM than in the TBI or the PAVT. This reduction in saturation is due to the panel closure's impeding the flow of brine downhill into the waste panel. However, at 10,000 years, brine saturation in the TBM is quite different than in the TBI or the PAVT. The panel closures significantly change the brine flow patterns within the repository in the disturbed case, which in turn changes the brine saturations in the waste regions.

Figures 58 and 59 compare brine saturations in the experimental area at 1,000 and 10,000 years for the PAVT, the TBI, and the TBM. As in the undisturbed scenario, these figures show that brine

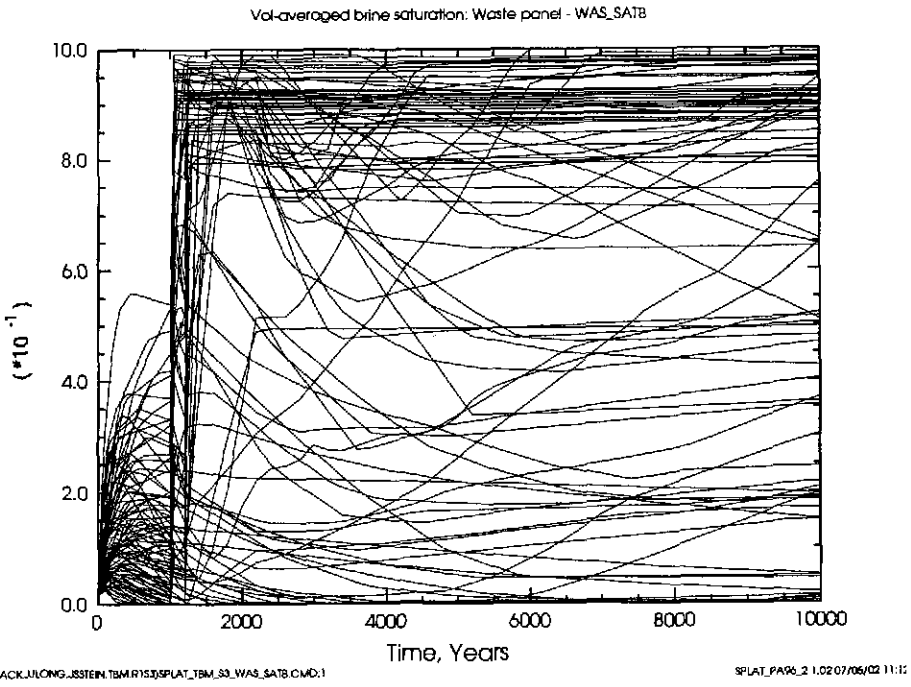

Figure 55. Disturbed Scenario (S3); Brine Saturation in the Waste Panel [WAS_SATB]; TBM

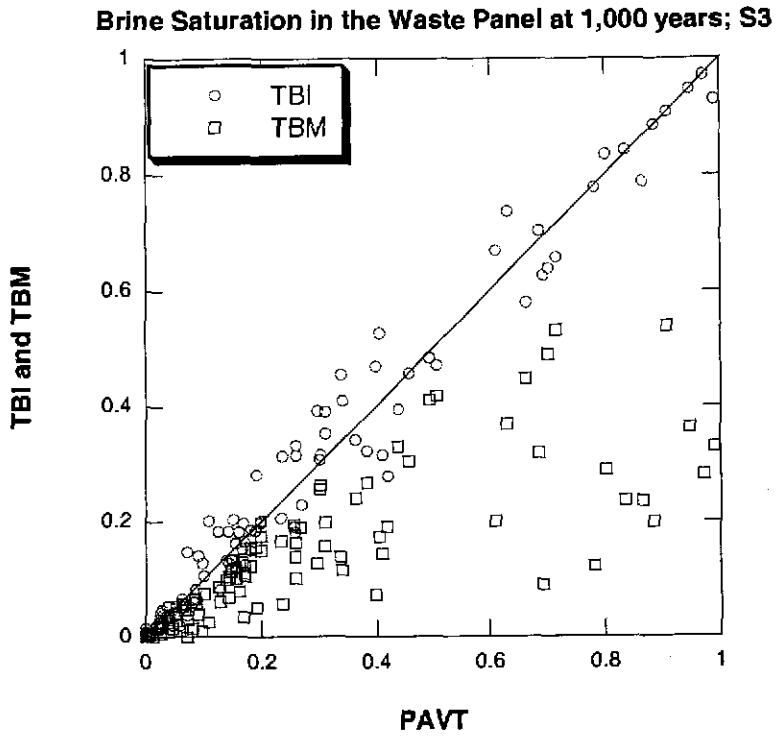

Figure 56. Disturbed Scenario (S3); Brine Saturation in the Waste Panel at 1,000 Years [WAS_SATB]; Scatter Plot; TBM and TBI versus PAVT

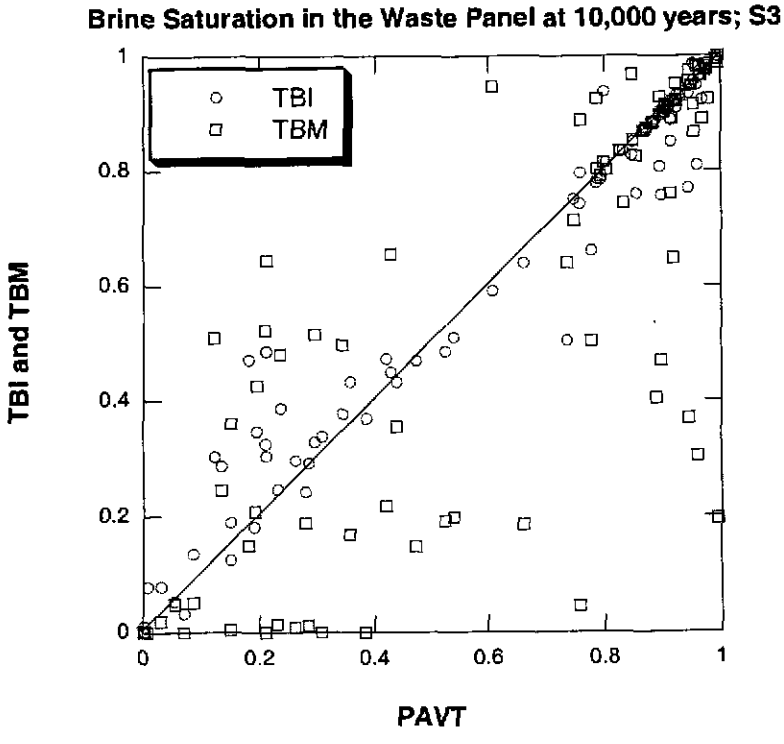

Figure 57. Disturbed Scenario (S3); Brine Saturation in the Waste Panel at 10,000 Years [WAS_SATB]; Scatter Plot; TBM and TBI versus PAVT

saturation in the experimental area increases slightly due to the corrected grid flaring, but increases significantly due to the Option D panel closures. As discussed in the analysis of brine flow, the panel closures hold brine back in the experimental area, preventing flow downhill through the panel closure and lower DRZ to the waste-filled regions. Thus, saturations in the experimental area are higher in the TBM than in the calculations without the Option D panel closures. For the S3 scenario, the comparison of the TBI to the PAVT concluded that the effect on brine saturations of the change to the new grid is minimal. However, the addition of the Option D panel closures significantly changes brine saturations, generally reducing saturation in the waste regions but increasing saturation in the other regions of the repository.

4.4.3.3 Disturbed Scenario (S5)

The S5 disturbed scenario models a drilling intrusion where the borehole penetrates through waste panel but not into a pressurized brine reservoir below the repository. Figure 60 shows brine saturation in the waste panel over time for all 100 vectors in the S5 scenario. As in the S3 scenario, the drilling intrusion takes place at 1,000 years and the borehole is effectively plugged for the next 200 years. At 1200 years, the plugs degrade and the borehole becomes highly permeable to gas and brine, and can allow significant flow to or from the repository.

Figures 61 and 62 compare brine saturations in the waste panel at 1,000 and 10,000 years for the PAVT, TBI, and TBM for the S5 scenario. In general, the waste panel is less saturated in the TBM than in the calculations without the Option D panel closures. At 1,000 years, the borehole does not yet provide a path for brine flow, hence saturation in the waste panel is equivalent to the undisturbed scenario. The panel closures impede brine flow from the north end of the repository, resulting in lower brine saturations in the waste panel. After the borehole opens, brine flows down the borehole into the waste panel, raising saturations slowly over time. However, the rate at which brine saturation increases is roughly the same for the TBM as for the TBI. As a result, brine saturations in the TBM remain lower than the TBI for the entire 10,000 year calculation time. Figure 63 shows mean saturation in the waste panel over time for the PAVT, TBI and TBM.

Figures 64 and 65 compare brine saturations in the experimental area at 1,000 and 10,000 years for the PAVT, TBI, and TBM. As in the undisturbed scenario, these figures show that brine saturation in the experimental area increases slightly due to the corrected grid flaring, but increases significantly due to the Option D panel closures. As discussed in the analysis of brine flow, the panel closures hold brine back in the experimental area, preventing flow downhill through the panel closure and lower DRZ to the waste-filled regions. Thus, saturations in the experimental area are higher in the TBM than in the calculations without the Option D panel closures.

For the S5 scenario, the comparison of the TBI to the PAVT concluded that the effect on brine saturations of the change to the new grid is minimal. However, the addition of the Option D panel closures significantly changes brine saturations, generally reducing saturation in the waste regions but increasing saturation in the other regions of the repository.

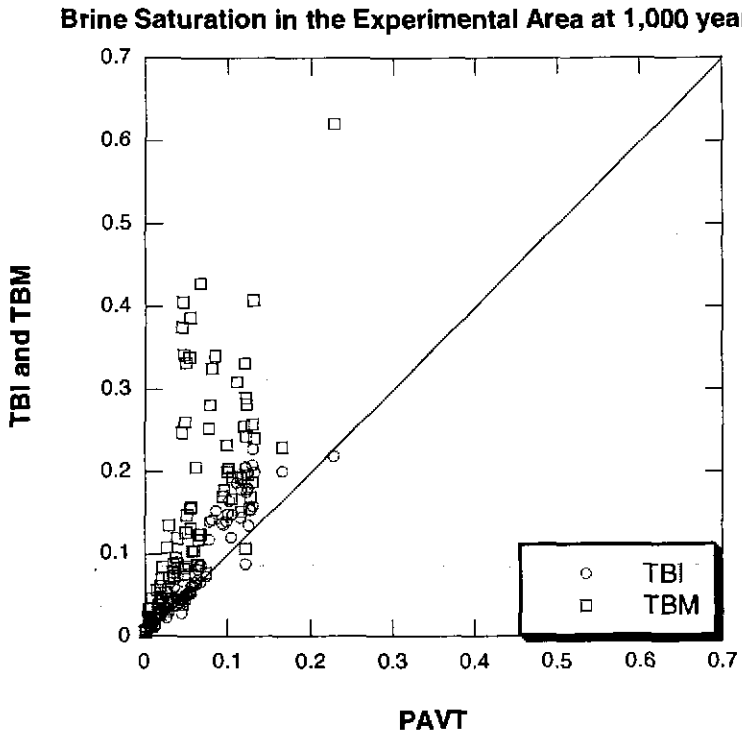

Figure 58. Disturbed Scenario (S3); Brine Saturation in the Experimental Area 1,000 Years [EXP_SATB]; Scatter Plot; TBM and TBI versus PAVT

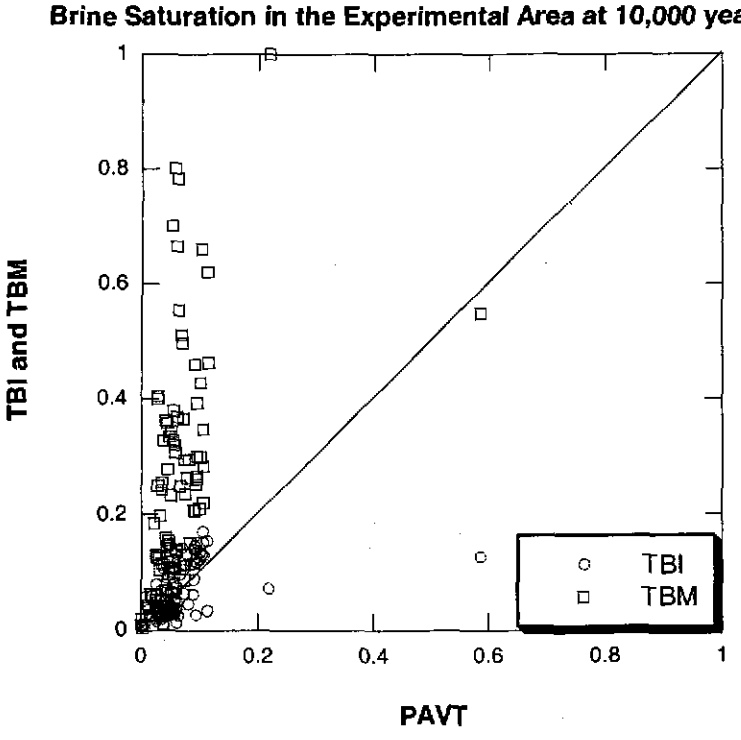

Figure 59. Disturbed Scenario (S3); Brine Saturation in the Experimental Area 10,000 Years [EXP_SATB]; Scatter Plot; TBM and TBI versus PAVT

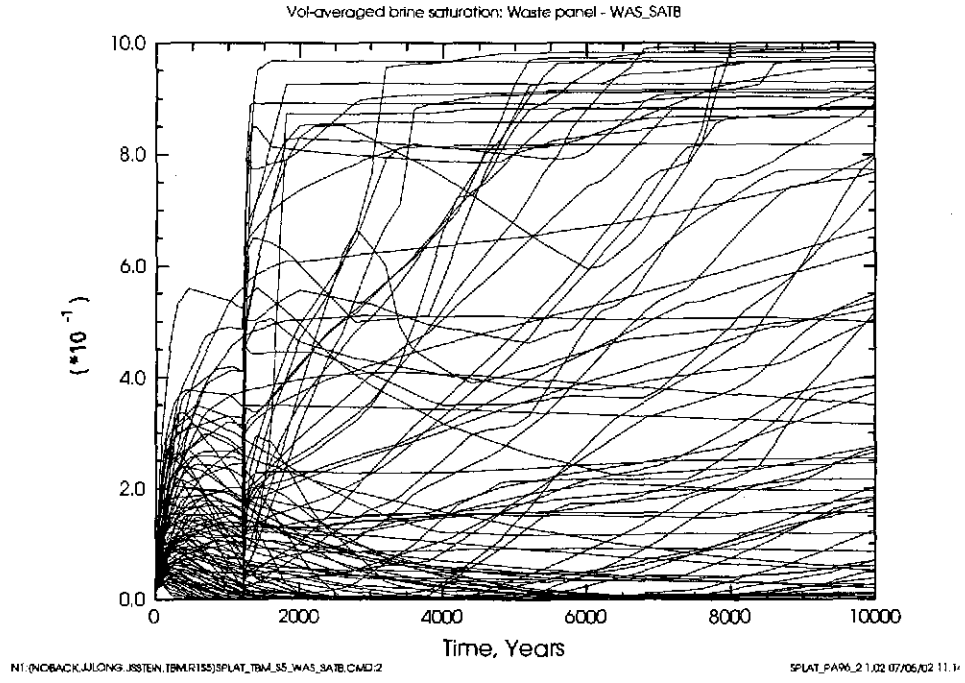

Figure 60. Disturbed Scenario (S5); Brine Saturation in the Waste Panel [WAS_SATB]; TBM

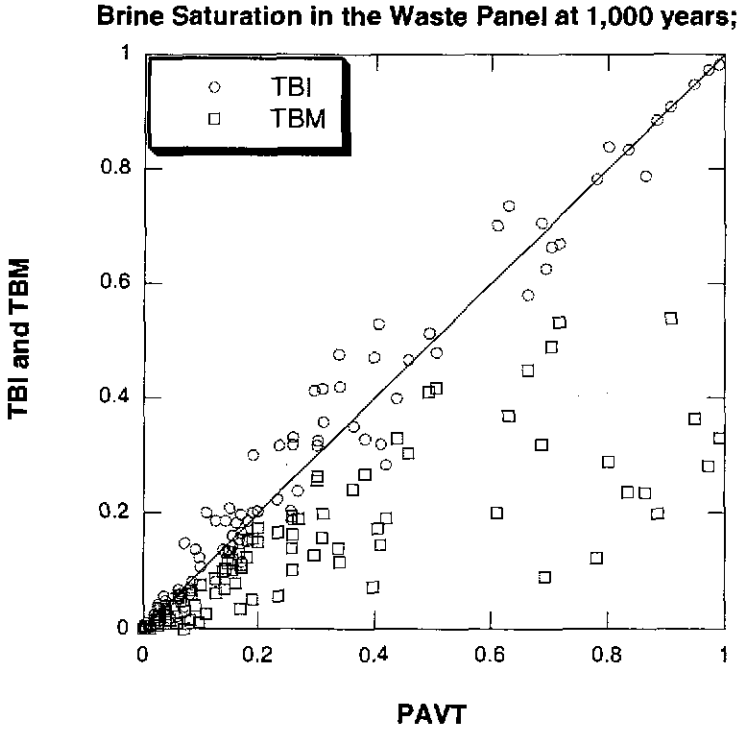

Figure 61. Disturbed Scenario (S5); Brine Saturation in the Waste Panel 1,000 Years [WAS_SATB]; Scatter Plot; TBM and TBI versus PAVT

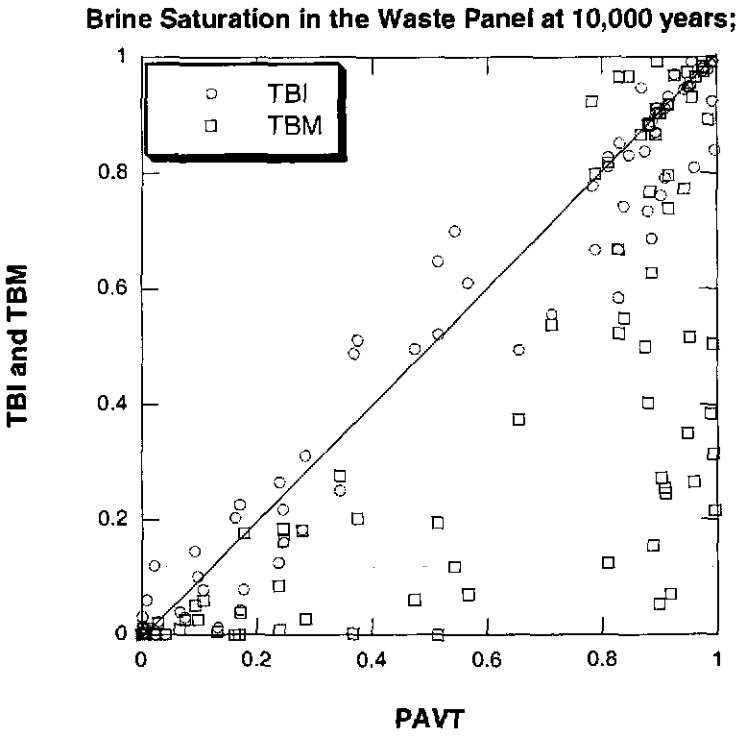

Figure 62. Disturbed Scenario (S5); Brine Saturation in the Waste Panel 10,000 Years [WAS_SATB]; Scatter Plot; TBM and TBI versus PAVT

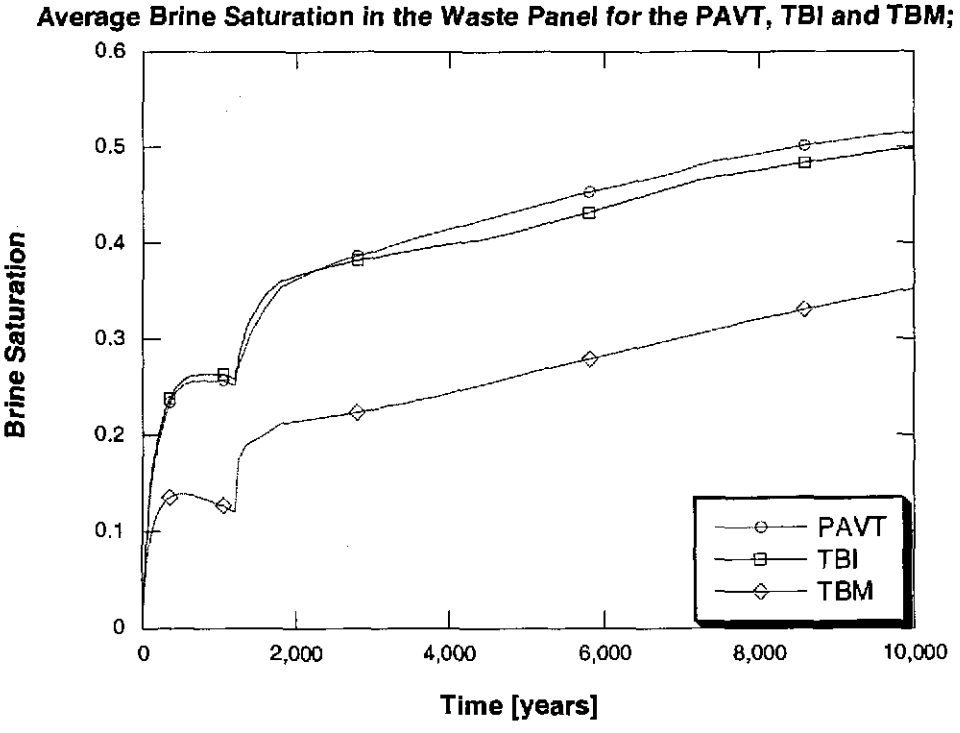

Figure 63. Disturbed Scenario (S5); Average Saturation in the Waste Panel [WAS_SATB]

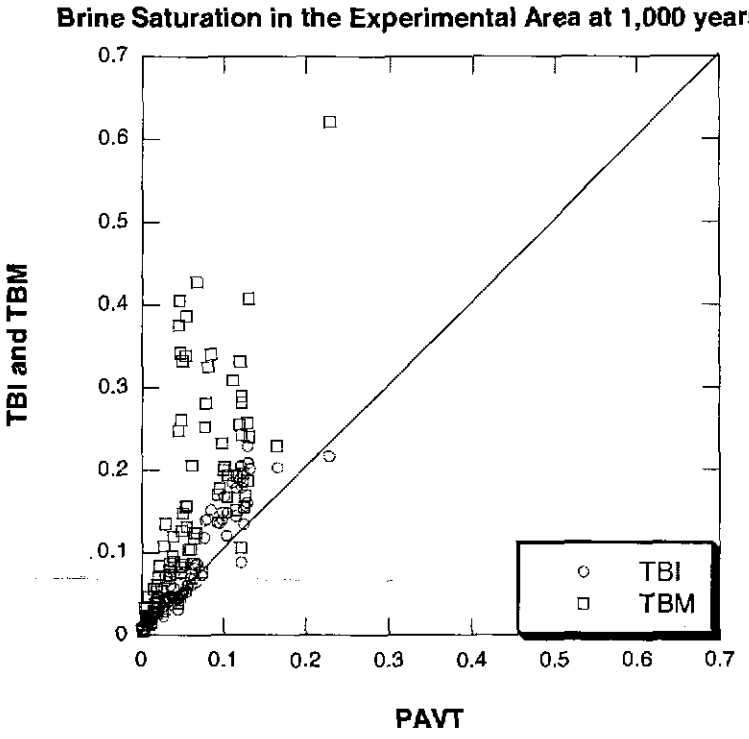

Figure 64. Disturbed Scenario (S5); Brine Saturation in the Experimental Area 1,000 Years [EXP_SATB]; Scatter Plot TBM and TBI versus PAVT

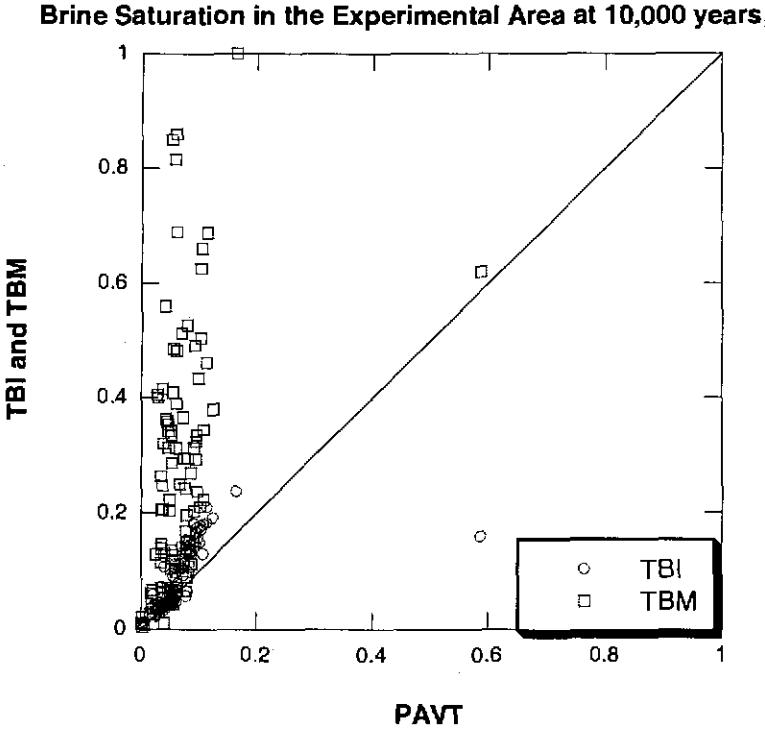

Figure 65. Disturbed Scenario (S5); Brine Saturation in the Experimental Area 10,000 Years [EXP_SATB]; Scatter Plot; TBM and TBI versus PAVT

4.5 PRESSURE

Pressure

The Option D panel closures are fundamentally different than what was included in the baseline PA in that they are designed to provide effective, long-term barriers to flow between panels. Their behavior in the model is consistent with their design. Pressure differences across the repository can remain significant for thousands of years. Brine that previously was able to flow between repository regions either through or below the panel closures is no longer able to follow that path.

Repository pressures for the TBI compare quite closely with the PAVT, indicating that changes to the grid including removal of the shaft, refining the grid spacing, and modifying the grid flaring did not substantially affect the model outcome. In contrast, the Option D panel closures increase waste panel pressures at early times, primarily because the full option D closures are less permeable than the PAVT and TBI closures, preventing movement of gas out of the waste panel. The increase in pressure is a transient effect, with 10,000-year pressures in all cases reaching comparable steady-state values. Additionally, after a drilling intrusion the Option D panel closures prevent pressure from equalizing throughout the repository. The higher pressures in the TBM may increase direct radionuclide releases from a drilling intrusion.

This section compares volume-averaged pressure in the waste panel, rest of repository and experimental areas for the TBM, TBI, and PAVT. This comparison identifies the effects on pressure of the implementation of the Option D panel closures and the correction to the molecular weight of cellulose, gridding, flaring, and shaft removal. Data are presented in two formats: (1) horsetail plots representing the behavior of all 100 vectors with time from 0 to 10,000 years for a single calculation, and (2) scatter-plots comparing calculations on a vector-by-vector basis.

4.5.1 Pressure Results for the TBI Calculation

A replicate analysis examining pressure for Scenarios S1, S3, and S5 was performed for the TBI. The changes distinguishing the TBI from the PAVT include incorporation of the new computational grid and removal of the fracturing in the upper DRZ. The following discussion deals first with the undisturbed scenario (S1), then the two disturbed scenarios (S3 and S5).

4.5.1.1 Undisturbed Scenario (S1)

Figures 66 and 67 show pressure in the waste panel and rest of repository over time for all 100 vectors in the S1 scenario. For comparison with the PAVT, the rest of repository in the TBI is defined as the average of the South and North Rest of Repository areas. In most vectors, pressures rise rapidly during the first 1000 years and then stabilize after about 2000 years with magnitudes ranging from 6 to 16 MPa. Pressure in the rest of repository behaves like pressure in the waste panel. This general pattern was also observed for the time evolution of pressures in the waste panel in the S1 scenario in the PAVT (MacKinnon and Freeze, 1997).

The rapid pressure rise during the first 1000 years is due to several mechanisms, including:

(1) inflow of brine from the surrounding formations,

(2) the generation of gas in the repository resulting from corrosion of iron and degradation of cellulose, plastic and rubber,

(3) creep closure in the repository.

Brine inflow and gas generation are both processes that have their largest impact within the first 1,000 years after repository closure. Brine inflow from the DRZ occurs with the first 50 years after repository closure. Around 1,000 years, cellulosics are exhausted and the gas generation in the waste regions slows considerably. As a result, from about 2,000 years onward, pressures in the waste panel remain nearly constant.

Figures 68 and 69 are scatter plots that compare pressures in the waste panel at 1,000 and 10,000 years for the TBI and PAVT. At both times, the TBI and PAVT pressures are nearly equal. This suggests that the change from the PAVT grid to the new grid does not introduce any significant changes to the waste panel pressures in the undisturbed scenario.

Figures 70 and 71 compare pressure in the rest of repository for the TBI and the PAVT at 1,000 and 10,000 years. These figures show that at both times the pressure in the rest of repository is not significantly affected by the change to the new grid.

Figure 72 shows the pressure in the experimental area for all 100 vectors in the S1 scenario. It is important to note that no waste is stored in the experimental or operations areas, so no gas is generated there as well as, no dynamic closure simulated there. The pressure is thus controlled by the initial conditions and subsequent gas and brine fluxes from adjacent regions. Pressure in the experimental area closely resembles pressure in the waste panel and rest of repository. This is because the panel closure system represented in the TBI and PAVT calculations allows for significant movement of gas between repository regions, resulting in rapid pressure equilibration.

The scatter-plots in Figures 73 and 74 compare pressures in the experimental area at 1,000 and 10,000 years for the PAVT and the TBI. Since all the data fall close to the diagonal line at both times, the experimental area pressures match quite closely. The one vector (vector 100) that stands conspicuously apart from the diagonal with PAVT pressure of near atmospheric was investigated further. The sampled 2-phase flow properties of the shaft material that separated the experimental region from the operations region (CONC_MON) for this vector resulted in zero permeability to gas for the entire simulation. This occurred because the initial saturation of this material was out of the range defined by the residual brine and gas saturations, in which flow is allowed. In the TBI, the shaft material was removed, thus eliminating this problem.

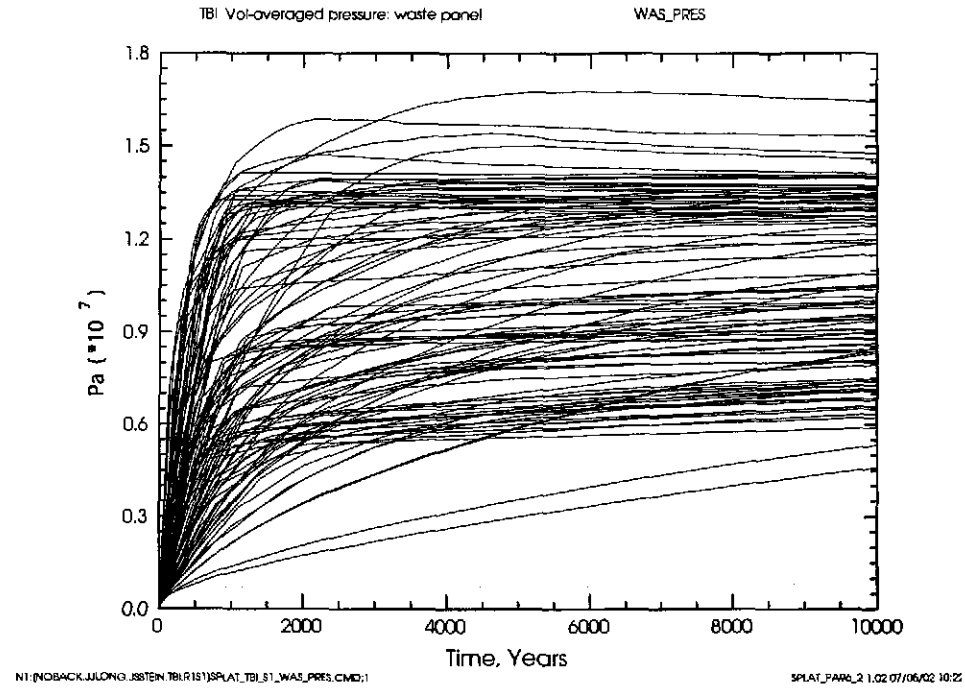

Figure 66. Undisturbed Scenario (S1); Pressure in the Waste Panel [WAS_PRES]; TBI

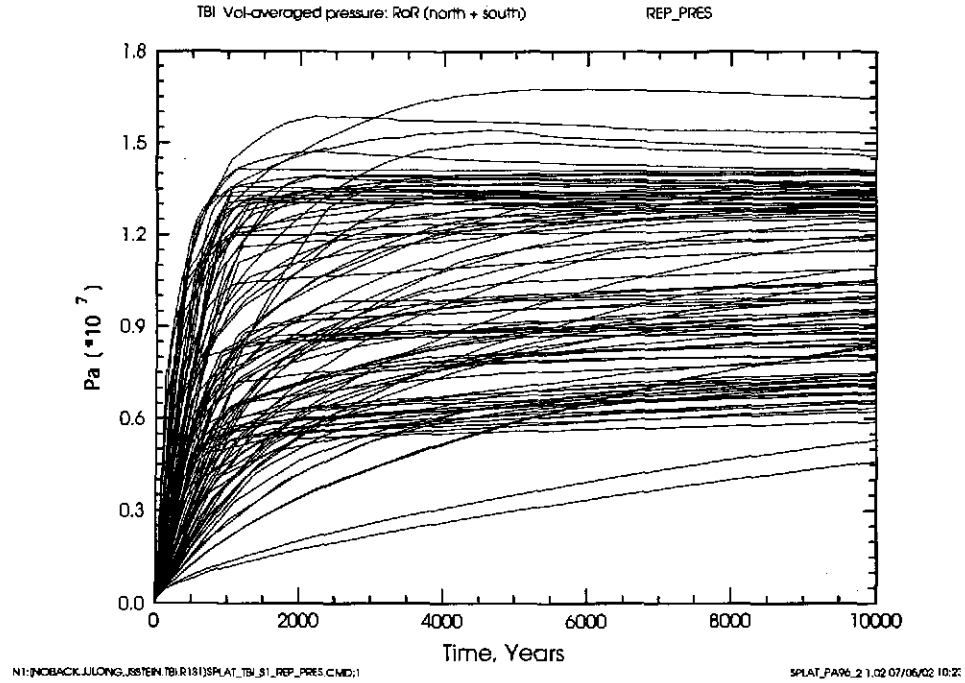

Figure 67. Undisturbed Scenario (S1); Pressure in the Rest of Repository [REP_PRES]; TBI

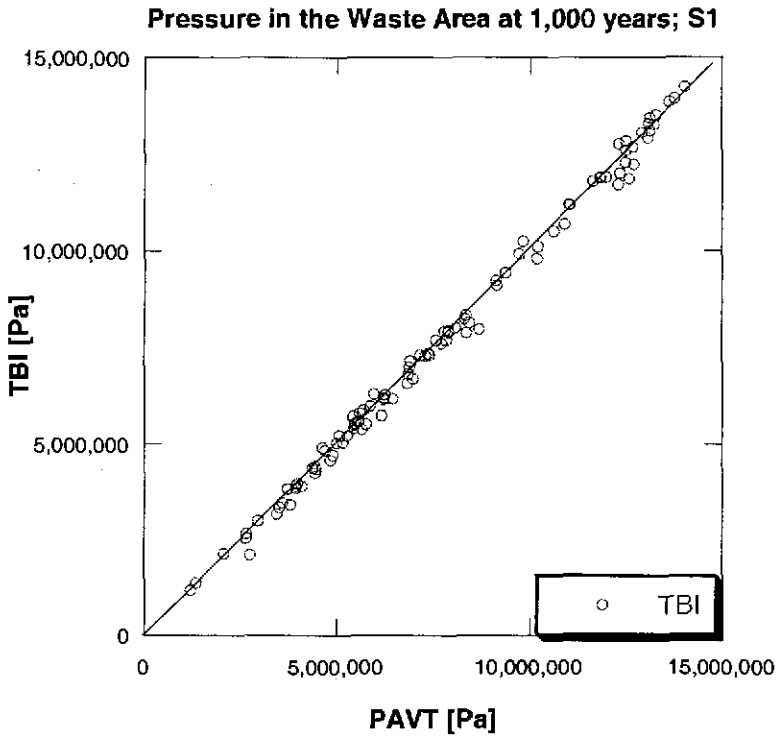

Figure 68. Undisturbed Scenario (S1); Pressure in the Waste Panel at 1,000 Years [WAS_PRES]; PAVT and TBI

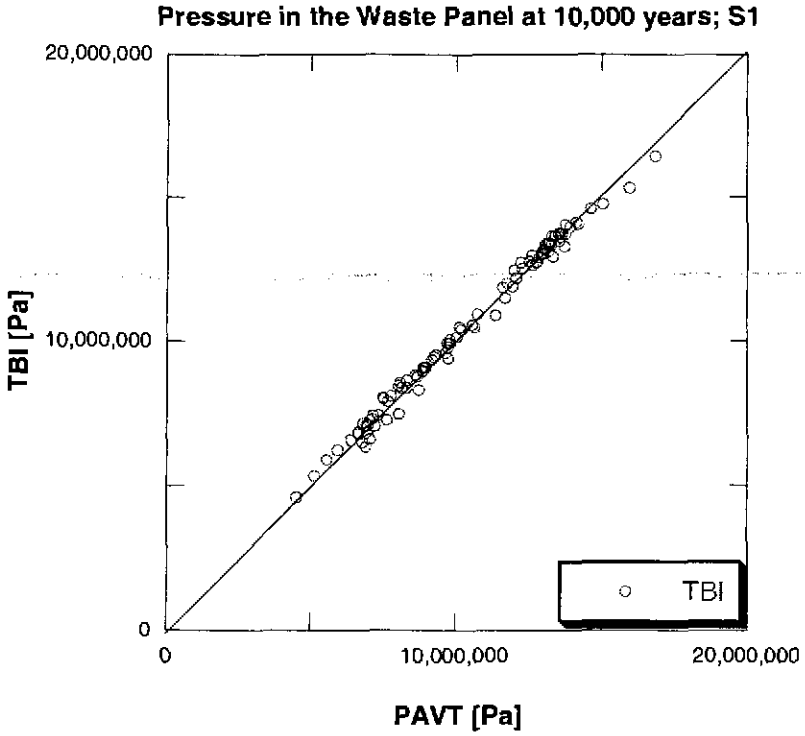

Figure 69. Undisturbed Scenario (S1); Pressure in the Waste Panel at 10,000 Years [WAS_PRES]; PAVT and TBI

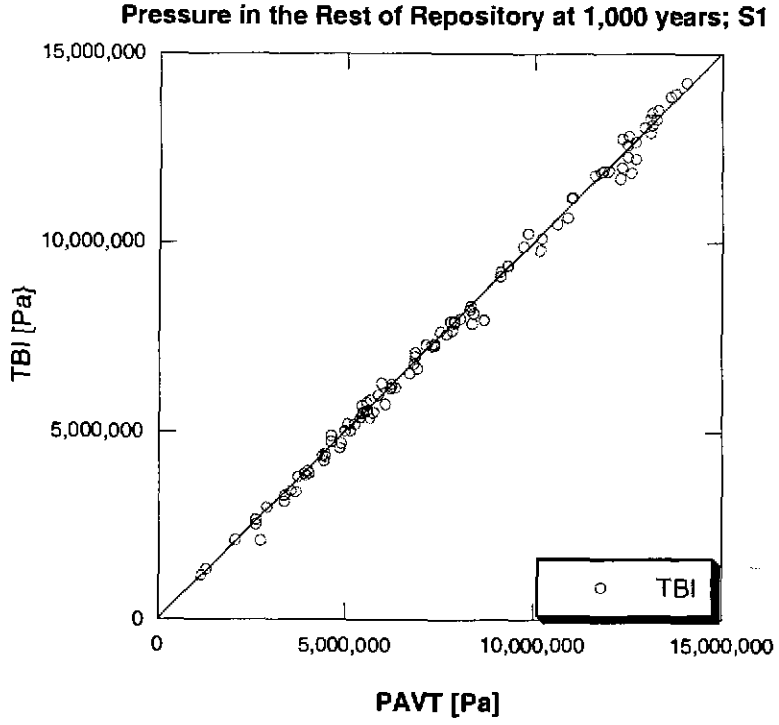

Figure 70. Undisturbed Scenario (S1); Pressure in the Rest of Repository at 1,000 Years [REP_PRES]; PAVT and TBI

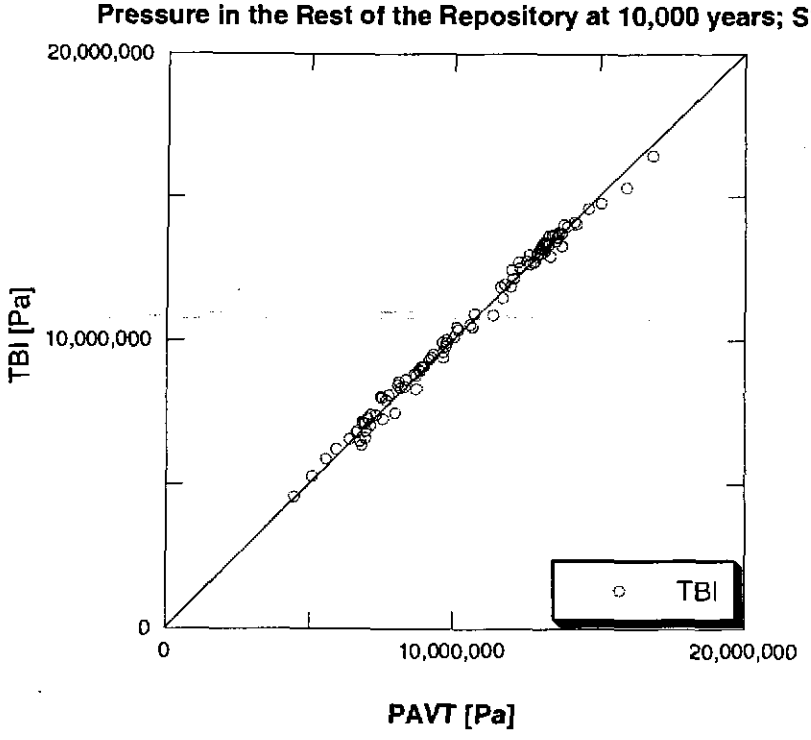

Figure 71. Undisturbed Scenario (S1); Pressure in the Rest of Repository at 10,000 Years [REP_PRES]; PAVT and TBI

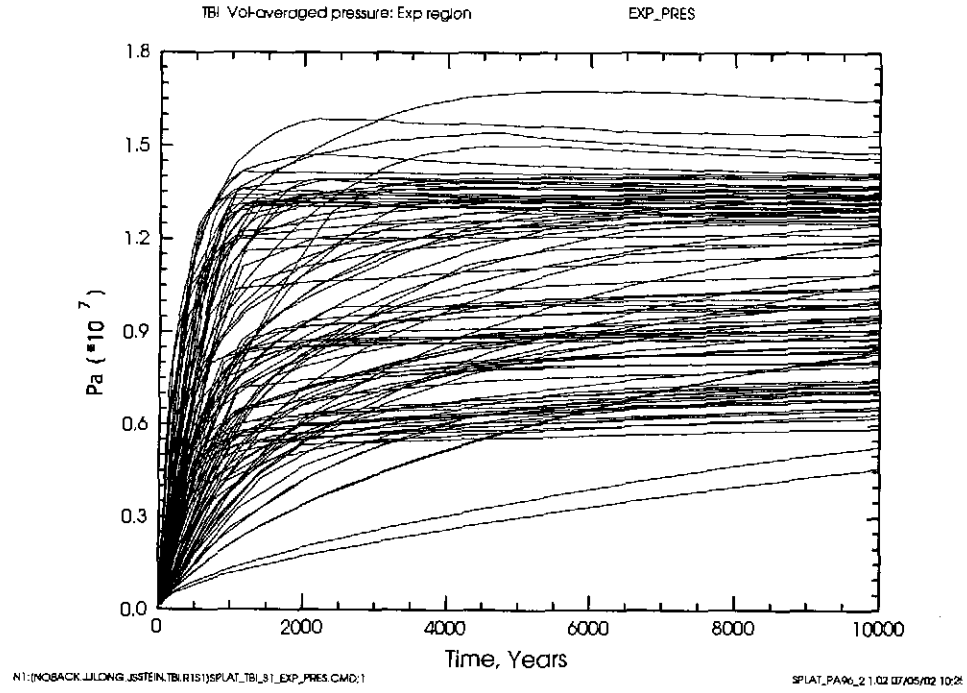

Figure 72. Undisturbed Scenario (S1); Pressure in the Experimental Area [EXP_PRES]; TBI

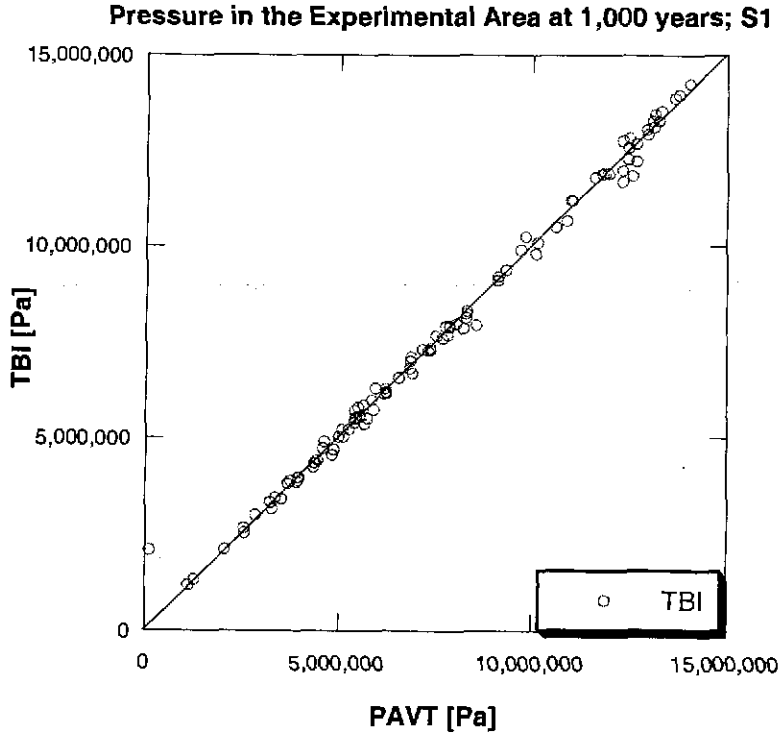

Figure 73. Undisturbed Scenario (S1); Pressure in the Experimental Area at 1,000 Years [EXP_PRES]; PAVT and TBI

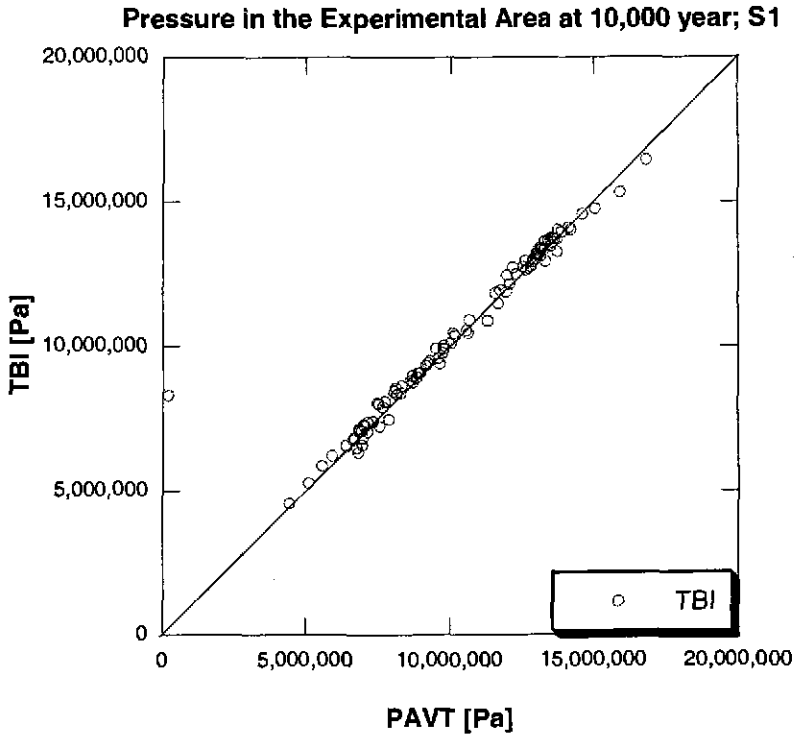

Figure 74. Undisturbed Scenario (S1); Pressure in the Experimental Area at 10,000 Years [EXP_PRES]; PAVT and TBI

4.5.2 Disturbed Scenarios (S3 and S5)

The S3 and S5 disturbed scenarios represent simulations in which drilling intrusions penetrate the repository at 1,000 years. Because both disturbed scenarios involve a drilling intrusion into the repository with subsequent depressurization, the profiles of pressure behavior versus time differ significantly from the undisturbed case. In S1, the pressure in the repository tended to increase rapidly until it reached a nearly steady-state pressure that endured from 2,000 years onward. In contrast, the S3 and S5 scenarios exhibit a rapid decrease in pressure following the drilling intrusion.

Figures 75 and 76 show the pressure in the waste panel over time for S3 and S5 scenarios. In each scenario, a borehole penetrates the repository at 1,000 years and is plugged above the repository for the next 200 years. After 200 years, the plug degrades, significantly increasing the borehole permeability and creating a path for pressurized brine and gas to escape and lower the repository pressure. Brine flow up the borehole from the Castile formation in the S3 scenario contributes to the generally higher pressures observed in the repository after 2000 years as compared to the S5 scenario.

Pressures in the disturbed scenarios are identical to the undisturbed scenario until the intrusion at 1000 years. Thereafter, pressure can change significantly as shown by Figures 75 and 76.

Figures 77 through 84 compare pressure in the waste panel and rest of repository at 3,000 years and at 10,000 years for the PAVT and the TBI, for both disturbed scenarios. Despite the transient effects on pressure of the intrusion, in either calculation pressures are similar, with no systematic increase or decrease of pressures. A few waste panel pressures for S5 appear lower in the TBI than PAVT (Figures 81 and 83), though the potential impact on radionuclide releases is likely irrelevant because the pressures fall well below the minimum 8 MPa necessary to initiate direct releases. There appears to be no significant effect on pressure in the waste-filled regions due to the change to the new grid or removal of the fracture model from the upper DRZ.

Figures 85 and 86 compare pressure in the experimental area for the PAVT and TBI at 10,000 years for both intrusion scenarios. These figures show that the change to the BRAGFLO grid does not significantly alter pressures outside the waste-filled regions.

This comparison of pressure between the PAVT and TBI concludes that the changes to the BRAGFLO grid do not significantly change the pressures in the repository.

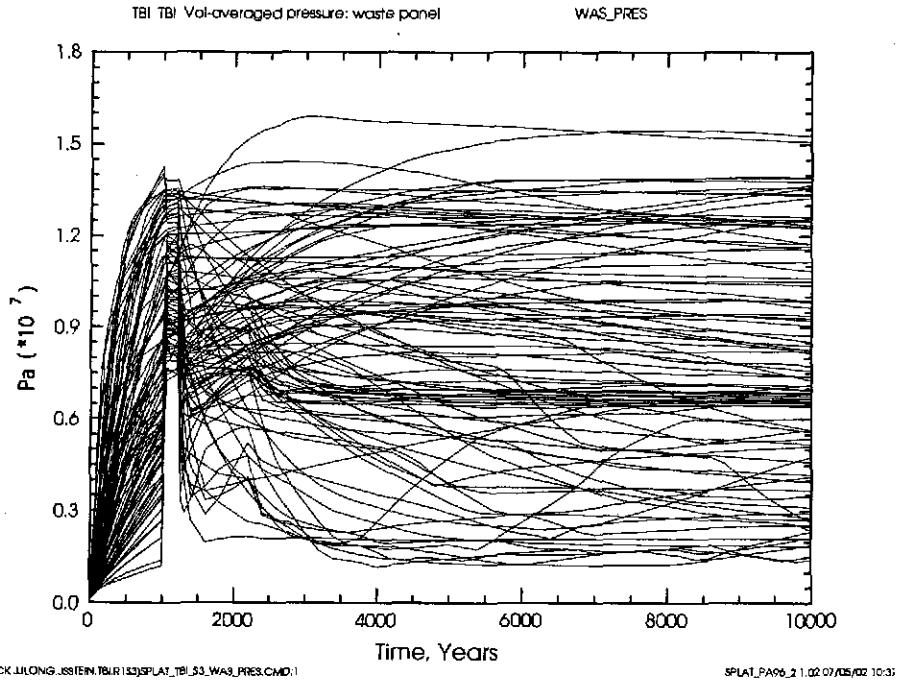

Figure 75. Disturbed Scenario (S3); Pressure in the Waste Panel [WAS_PRES]; TBI

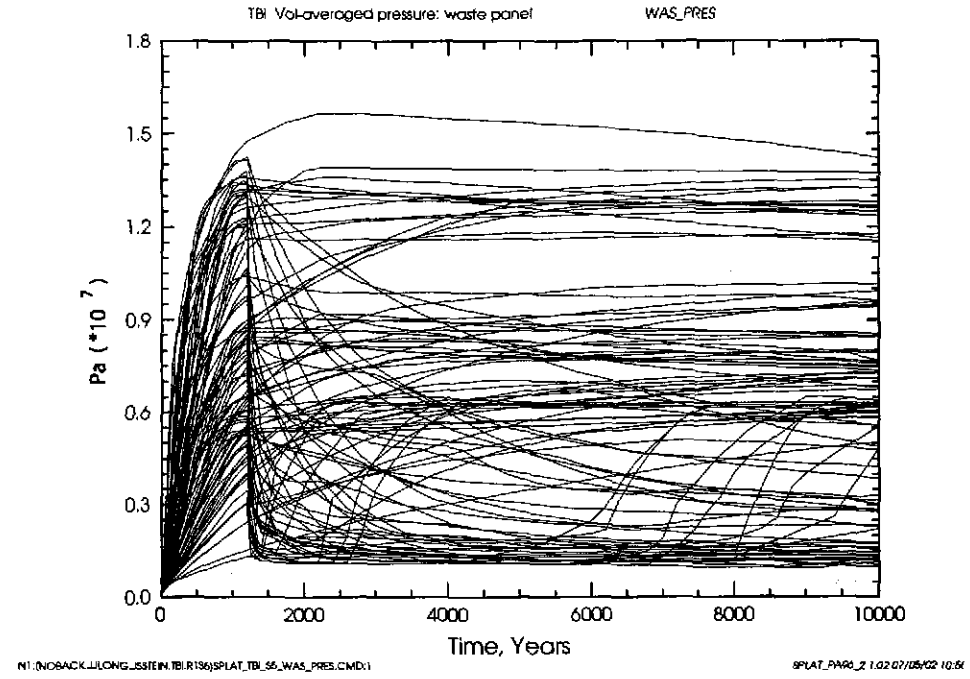

Figure 76. Disturbed Scenario (S5); Pressure in the Waste Panel [WAS_PRES]; TBI

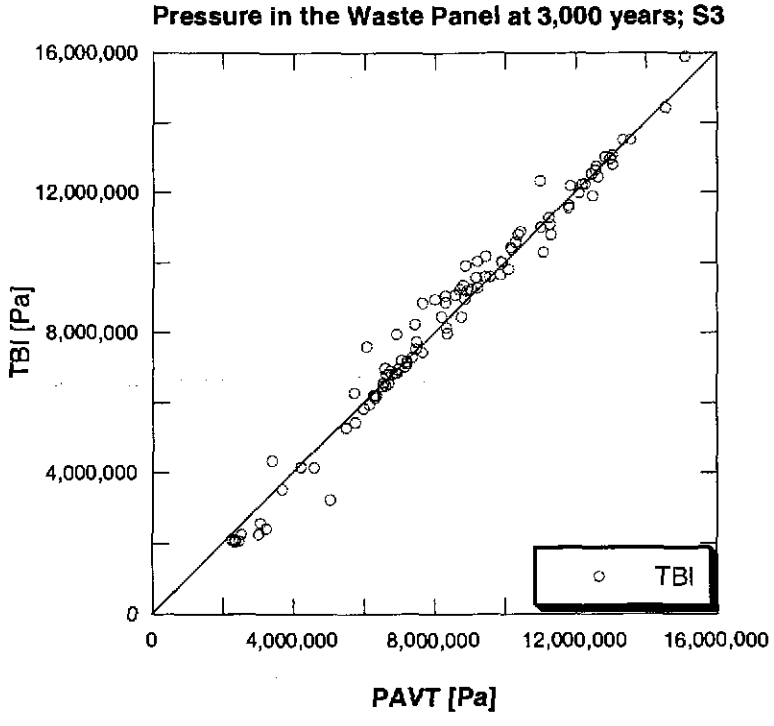

Figure 77. Disturbed Scenario (S3); Pressure in the Waste Panel 3,000 Years [WAS_PRES]; TBI versus PAVT

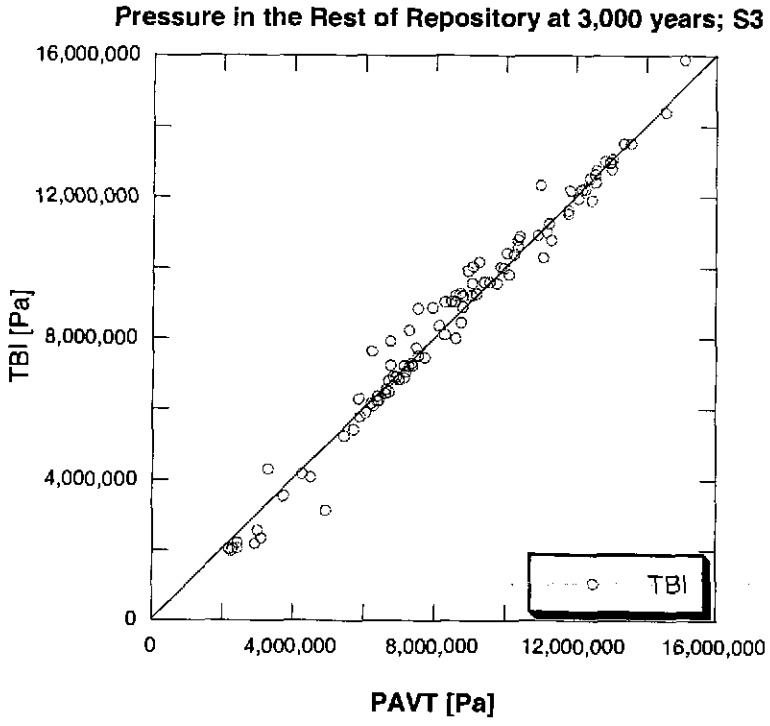

Figure 78. Disturbed Scenario (S3); Pressure in the Rest of Repository 3,000 Years [REP_PRES]; TBI versus PAVT

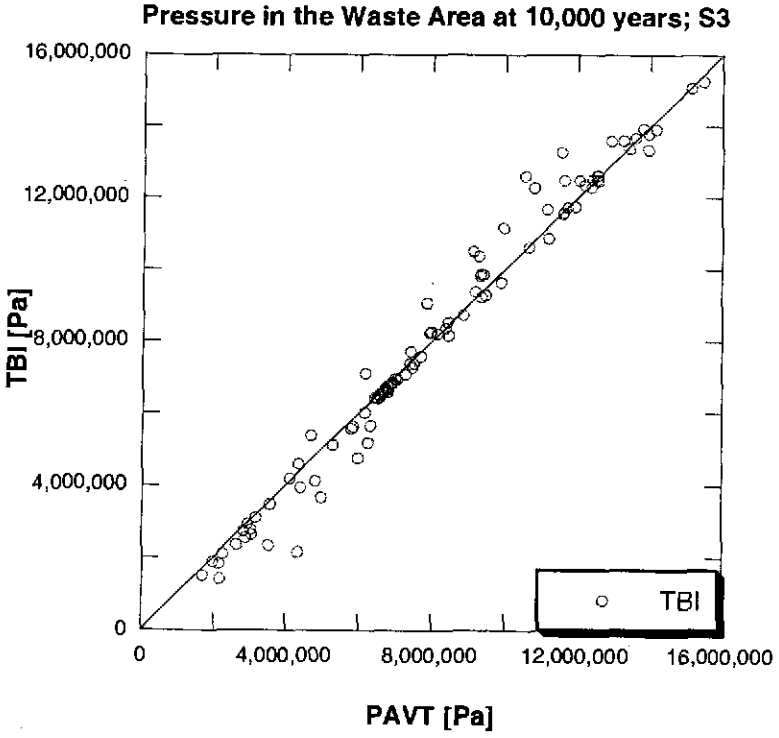

Figure 79. Disturbed Scenario (S3); Pressure in the Waste Panel 10,000 Years [WAS_PRES]; TBI versus PAVT

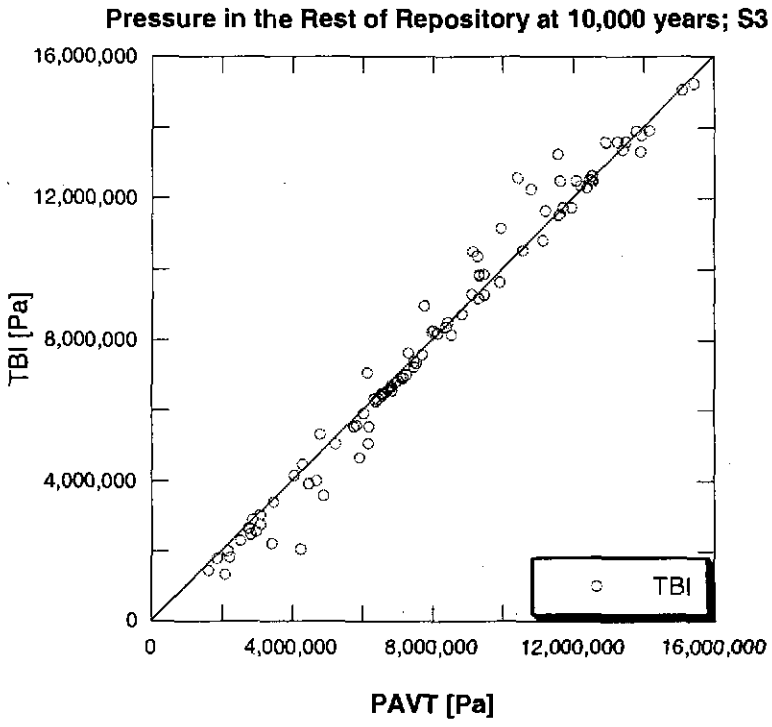

Figure 80. Disturbed Scenario (S3); Pressure in the Rest of Repository Area 10,000 Years [REP_PRES]; TBI versus PAVT

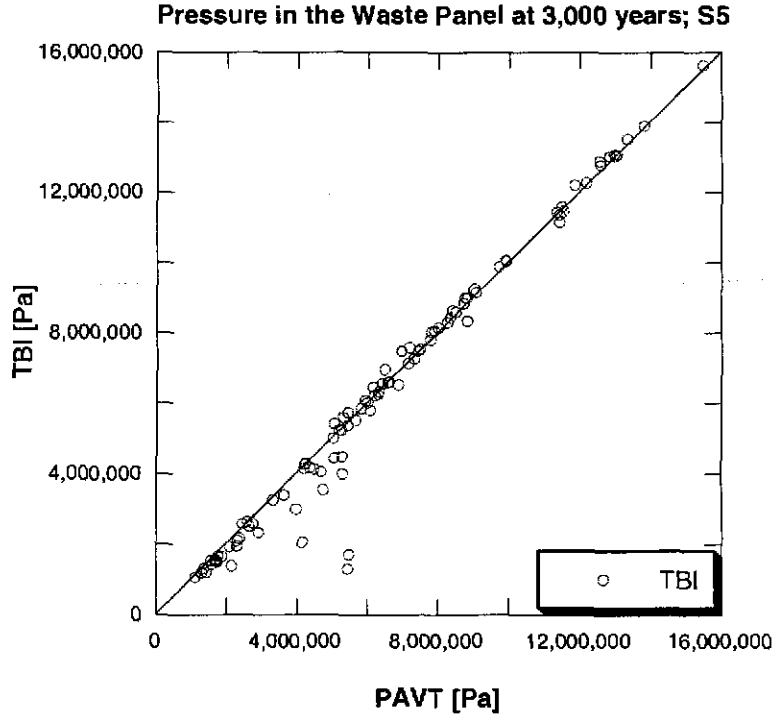

Figure 81. Disturbed Scenario (S5); Pressure in the Waste Panel 3,000 Years [WAS_PRES]; TBI versus PAVT

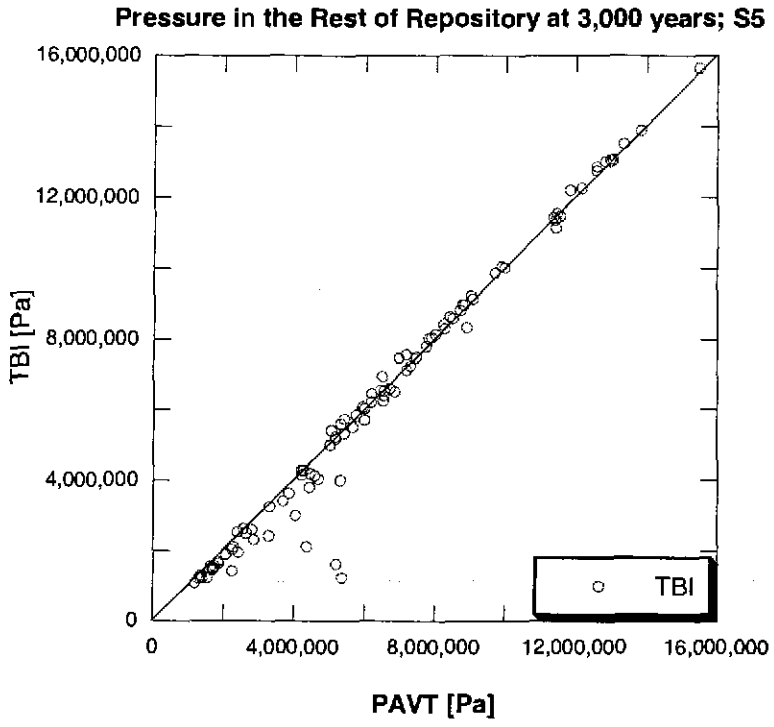

Figure 82. Disturbed Scenario (S5); Pressure in the Rest of Repository 3,000 Years [REP_PRES]; TBI versus PAVT

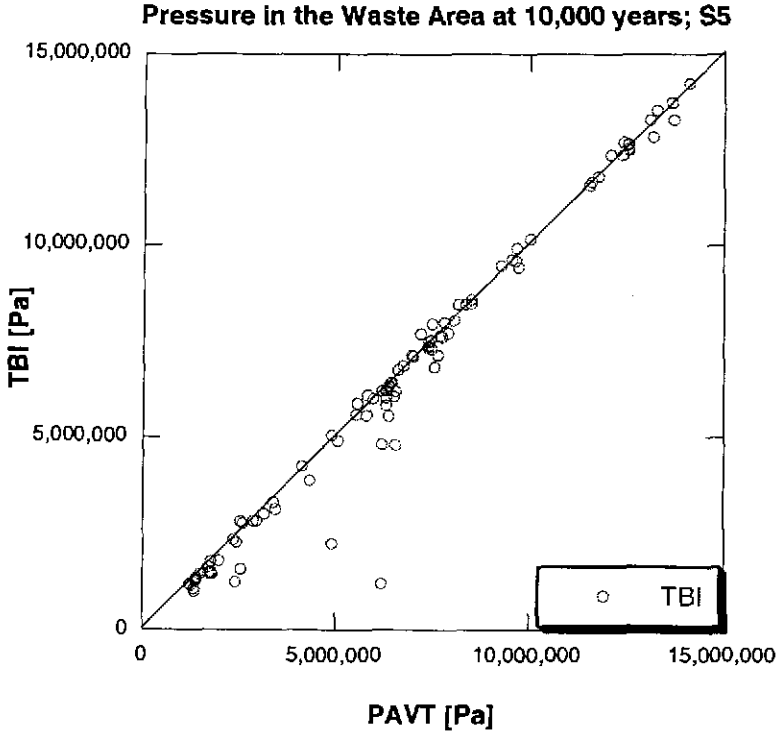

Figure 83. Disturbed Scenario (S5); Pressure in the Waste Panel 10,000 Years [WAS_PRES]; TBI versus PAVT

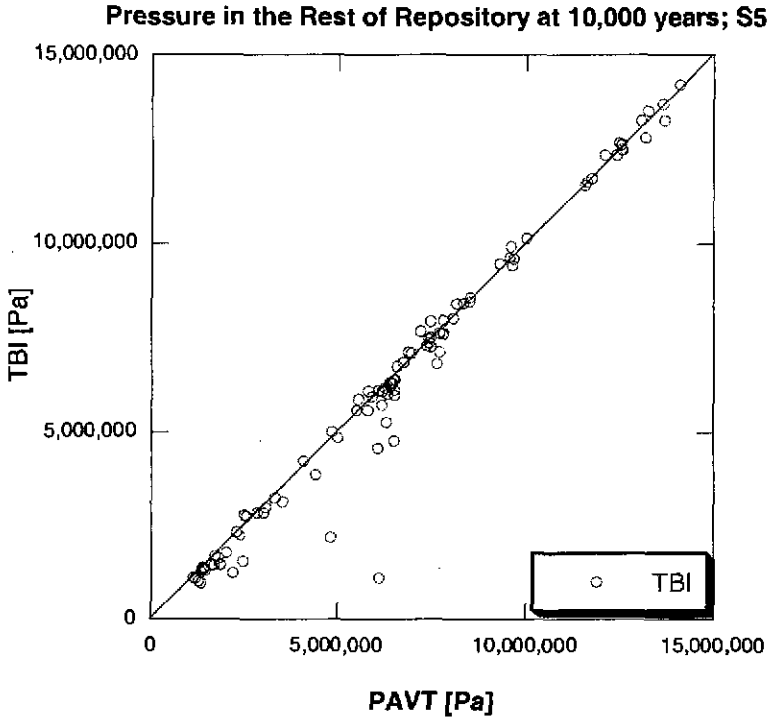

Figure 84. Disturbed Scenario (S5); Pressure in the Rest of Repository 10,000 Years [REP_PRES]; TBI versus PAVT

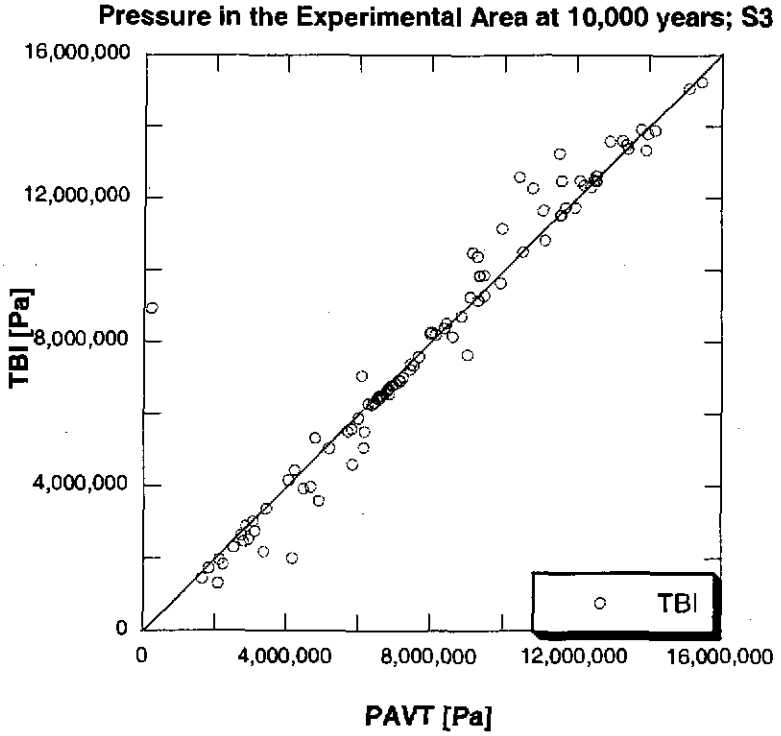

Figure 85. Disturbed Scenario (S3); Pressure in the Experimental Area 10,000 Years [EXP_PRES]; TBI versus PAVT

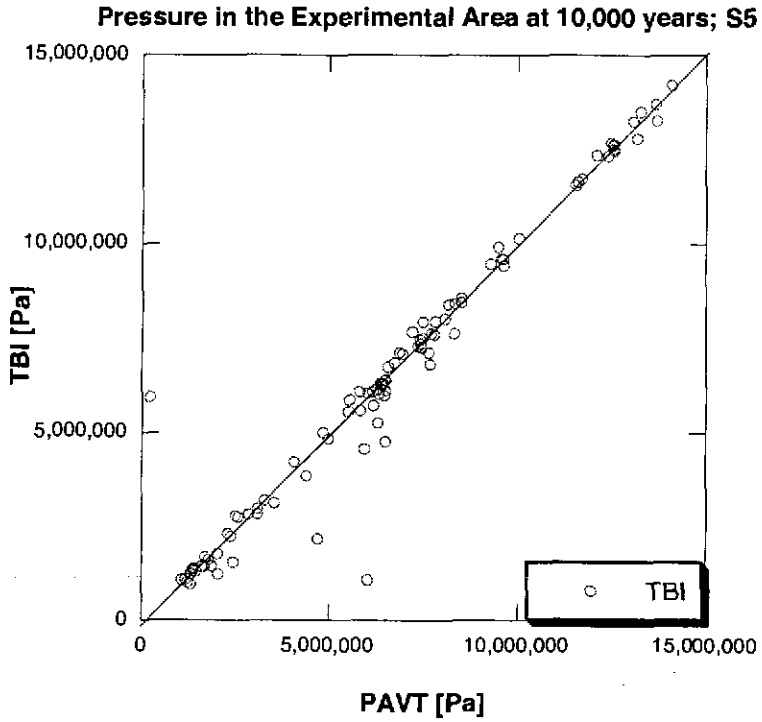

Figure 86. Disturbed Scenario (S5); Pressure in the Experimental Area 10,000 Years [EXP_PRES]; TBI versus PAVT

4.5.3 Pressure Results for the TBM Calculation

The comparison between the TBI and the PAVT showed no significant effects on repository pressure of implementing the new grid and removing of the fracture model from the upper DRZ. In this section, a replicate analysis of the TBM will be presented and compared to the PAVT and TBI. This will illustrate the effects on repository pressure of implementing the Option D panel closures and the correction to the molecular weight of cellulose. The Option D panel closure system inserts low-permeability barriers between repository areas that were not present in the TBI and PAVT. The Option D panel closures impede flow of gas and brine, as was shown in section 4.5, and thus will likely affect pressures in the repository. In addition, the molecular weight correction will slightly increase gas generation for some vectors which may impact repository pressure. The following discussion examines first the undisturbed scenario (S1), and then the two disturbed scenarios (S3 and S5).

4.5.3.1 Undisturbed Scenario (S1)

Figures 87, 88 and 89 show pressure in the waste panel, rest of repository and the experimental area over time for all 100 vectors in the undisturbed scenario. While the 10,000-year pressures are similar to the TBI, pressures at 1,000 years are slightly higher in the TBM. Several vectors exhibiting a characteristic pattern of rapid pressure increase forming a distinct peak, followed by a modest pressure decrease and subsequent leveling off with time, which is not seen in either the TBI or PAVT simulations. Also evident is a distinct time lag in the pressure rise in the experimental area for many vectors in the TBM calculation. This is likely the result of the Option D panel closures slowing the migration of gas from the waste regions to the operations and experimental

areas. Figure 89 shows that the Option D panel closures in the TBM calculations affect the transient behavior of pressure differently in different regions of the repository.

The existence of higher pressures in the TBM at early times is especially evident in the scatter-plots comparing pressure in the waste panel for the TBM, TBI and PAVT at 1,000 and 10,000 years (Figures 90 and 91). While the TBI and PAVT match quite closely, the TBM values at 1,000 years are y higher (Figure 90). This is a transient condition, however, as waste panel pressures for all three cases are nearly equal at 10,000 years (Figure 91). Similar effects are observed for the pressure in the rest of repository.

To confirm that the difference in pressure shown in Figure 90 is due to the Option D panel closures and not to the correction to the molecular weight of cellulose, BRAGFLO was run with the Option D panel closures in the new grid but with the uncorrected molecular weight of cellulose. This calculation produced pressures that differed significantly from the TBI but closely matched those of the TBM. Thus, the Option D panel closures are responsible for the transient increase in waste region pressures observed in the TBM.

The scatter-plots for the experimental area in the TBM undisturbed (S1) scenario (Figures 92 and 93) show very clearly that pressure in this region is significantly lower in the TBM at 1,000 years than in the TBI and PAVT. This difference does not endure, however, by 10,000 years pressure is equivalent in all calculations. The combination of higher pressure in the waste regions and lower pressure in the experimental area at 1,000 years is evidence that the Option D panel closures are significantly slowing the movement of gas between these regions and causing pressure differences. The scatter-plots are quite different from the TBI calculation (Figures 73 and 74) where all excavated area pressures equalize rapidly and behave just like the PAVT. As described in Section 4.6.1.1 and shown onFigures 73 and 74, vector 100 is anomalous due to the sampled 2-phase flow properties of the shaft material, CONC_MON in the PAVT for this vector. This anomalous behavior is evident in Figures 92 and 93 as well.

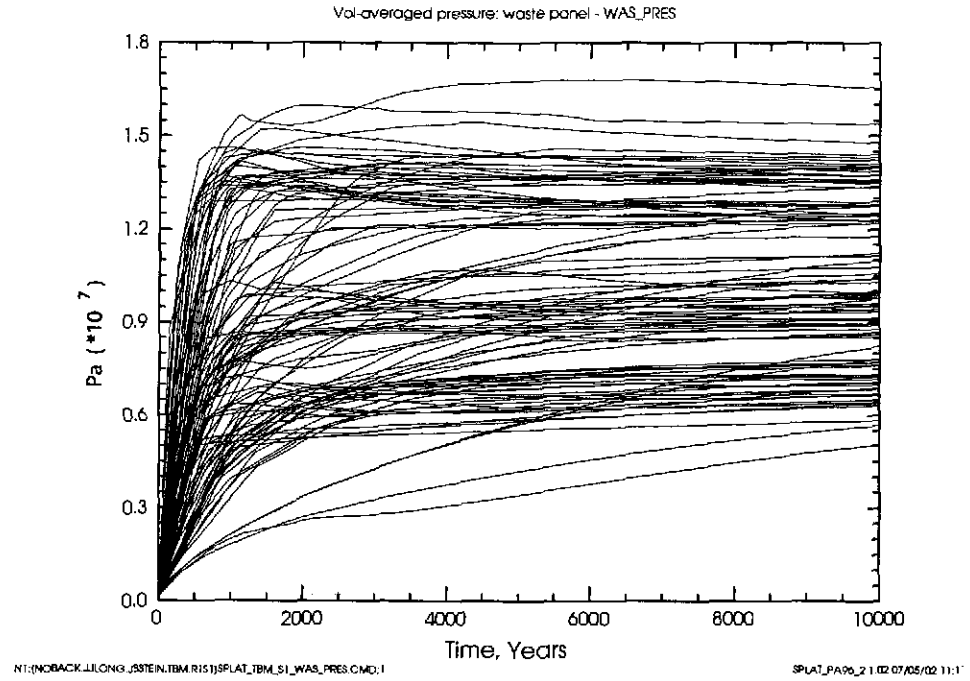

Figure 87. Undisturbed Scenario (S1); Pressure in the Waste Panel [WAS_PRES]; TBM

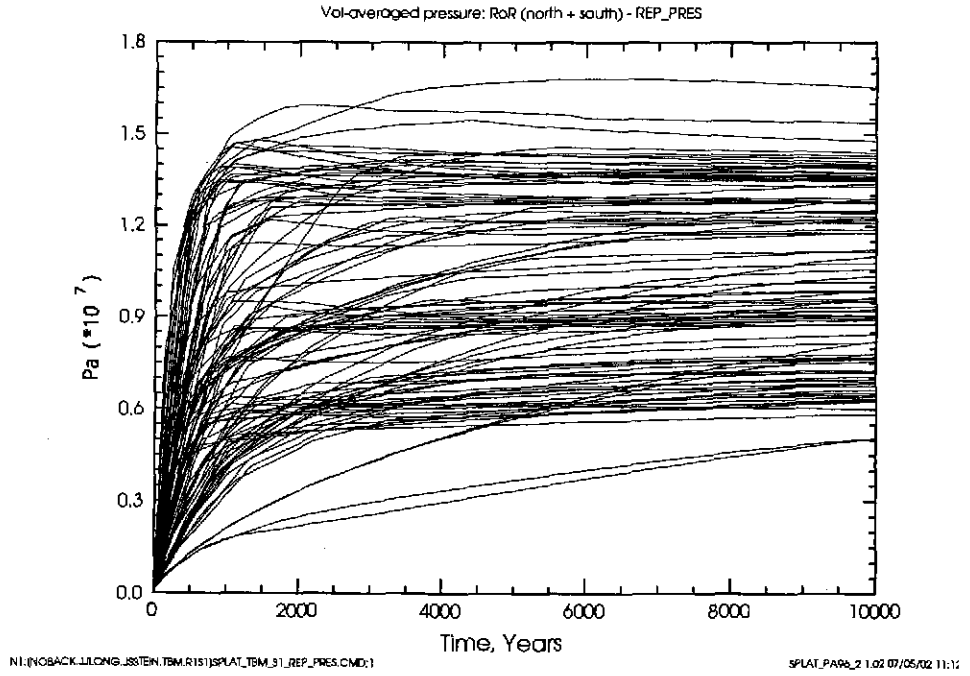

Figure 88. Undisturbed Scenario (S1); Pressure in the Rest of Repository [REP_PRES]; TBM

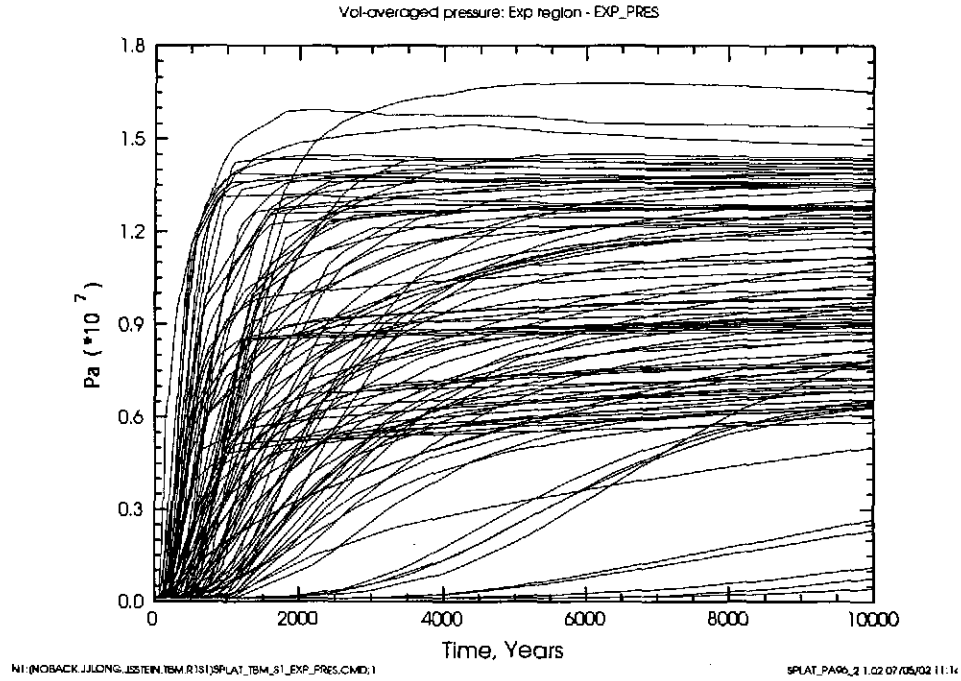

Figure 89. Undisturbed Scenario (S1); Pressure in the Experimental Area [EXP_PRES]; TBM

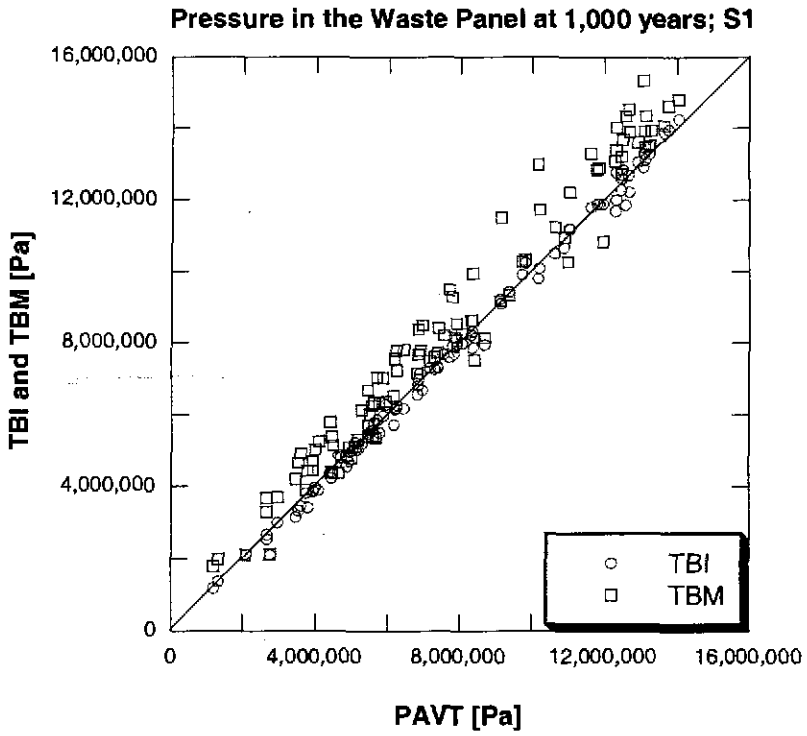

Figure 90. Undisturbed Scenario (S1); Pressure in the Waste Panel at 1,000 Years [WAS_PRES]; TBM and TBI versus PAVT

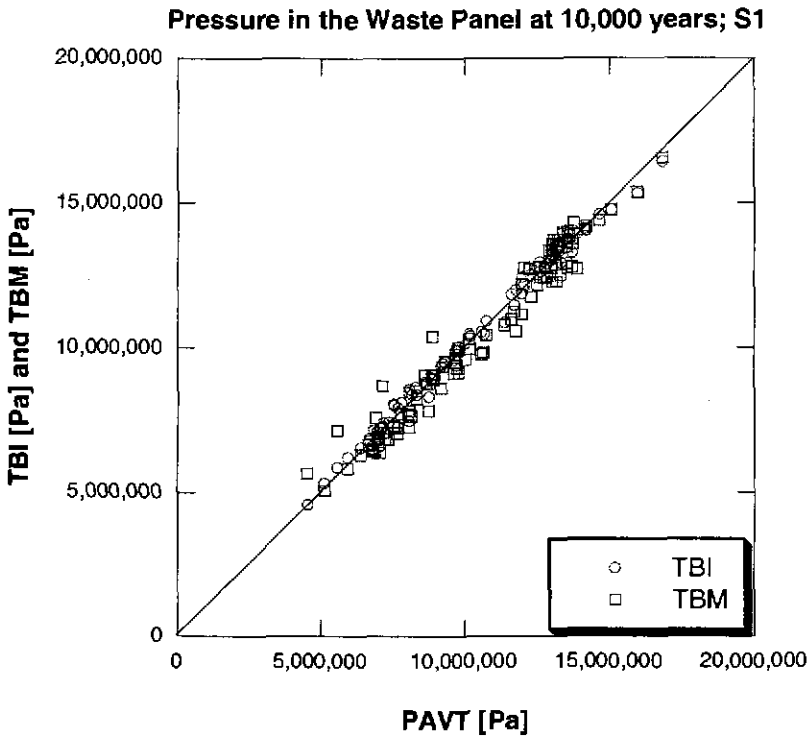

Figure 91. Undisturbed Scenario (S1); Pressure in the Waste Panel at 10,000 Years [WAS_PRES]; TBM and TBI versus PAVT

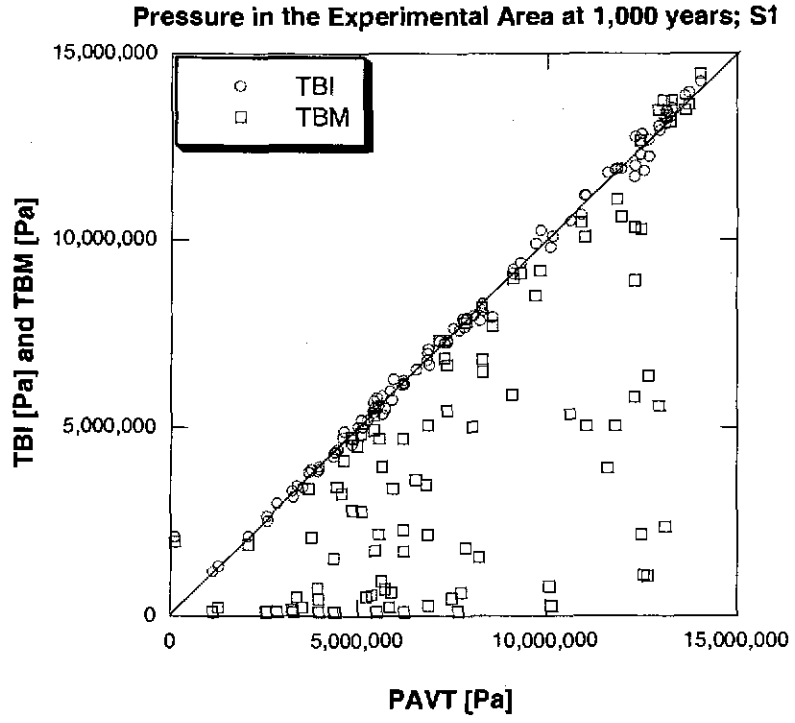

Figure 92. Undisturbed Scenario (S1); Pressure in the Experimental Area at 1,000 Years [EXP_PRES]; TBM and TBI versus PAVT

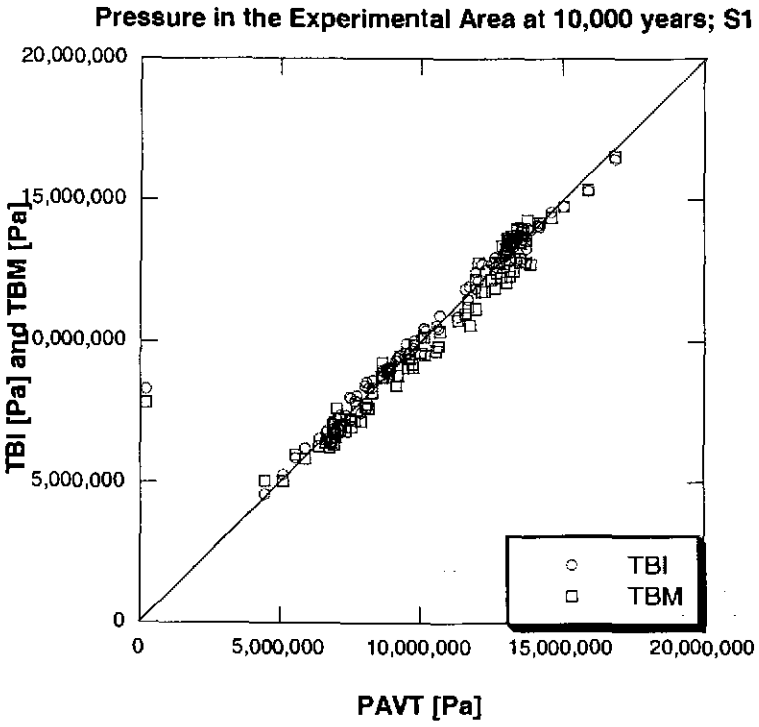

Figure 93. Undisturbed Scenario (S1); Pressure in the Experimental Area at 10,000 Years [EXP_PRES]; TBM and TBI versus PAVT

4.5.3.2 Disturbed Scenario (S3)

Figure 94 shows pressure in the waste panel over time for all 100 vectors in the S3 scenario, in which a drilling intrusion takes place at 1,000 years, penetrating both the repository and a pressurized brine pocket. At the time of intrusion, borehole plugs effectively prevent brine from flowing up the borehole above the repository. Once borehole plugs degrade 200 years after the intrusion, brine can flow from the Castile into the waste panel. The low-pressure vectors exhibit a rapid increase in pressure following the intrusion. This occurs when the pressure in the Castile is significantly higher than in the repository and these units are suddenly connected by the borehole. Similarly, high pressure vectors can experience a pressure reduction following intrusion if pressure in the Castile is lower than in the repository.

Just prior to intrusion, pressures in the S3 scenario are identical to those in the undisturbed scenario, so Figures 90 and 92 apply to S3 at 1,000 years. Recall that TBM waste panel pressures are systematically higher than the TBI or PAVT, and experimental area pressures are significantly lower. After the intrusion, pressures are subject to significant transient effects. Figures 95 and 96 compare pressure in the waste panel and the rest of repository at 3,000 years in the TBM, TBI and PAVT. Figures 97 and 98 compare pressures in the waste panel and experimental areas at 10,000 years for the PAVT, TBI, and TBM S3 scenario, respectively. These figures show that the TBM pressures are significantly different than in the TBI or PAVT. The difference in pressurebetween the TBI and PAVT are more modest. The difference in pressures is due to effects of the panel closures.

Although the pressures in the TBM vary significantly from those in the TBI and PAVT, the overall distribution of pressures is similar. Figures 99 and 100 compare the mean, median, 10^{th} and 90^{th} quantiles for pressure in the waste panel and rest of repository for the TBM and PAVT. Since the distribution of pressures is similar, pressure-dependent releases such as spallings and DBR are likely to be similar. Thus, the differences in pressure may not translate to significantly different releases in this scenario.

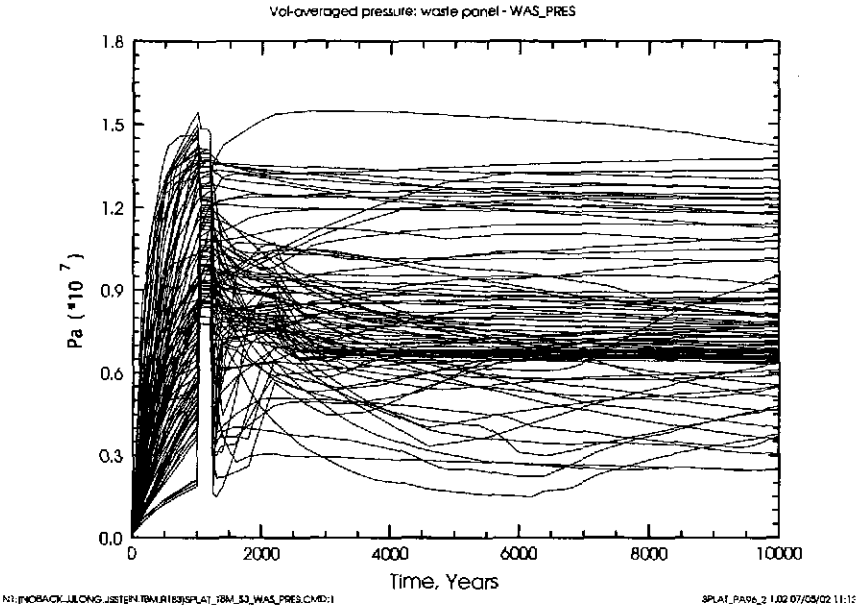

Figure 94. Disturbed Scenario (S3); Pressure in the Waste Panel [WAS_PRES]; TBM

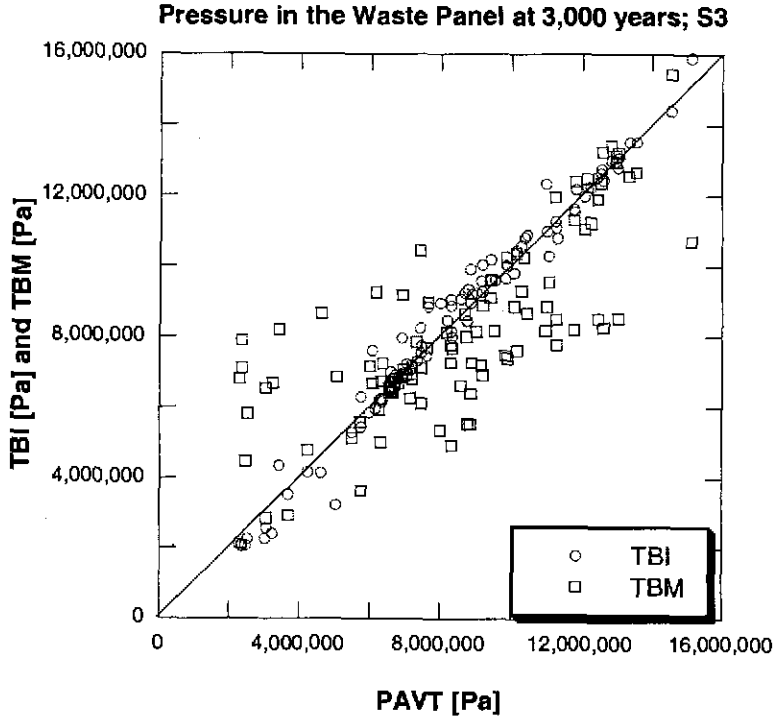

Figure 95. Disturbed Scenario (S3); Pressure in the Waste Panel at 3,000 Years [WAS_PRES]; TBM and TBI versus PAVT

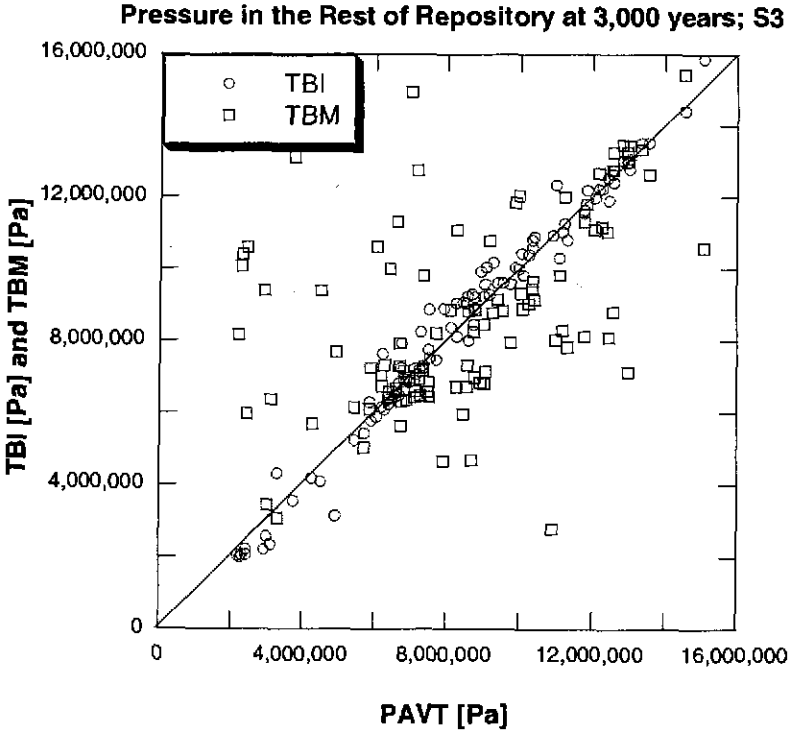

Figure 96. Disturbed Scenario (S3); Pressure in the Rest of Repository at 3,000 Years [REP_PRES]; TBM and TBI versus PAVT

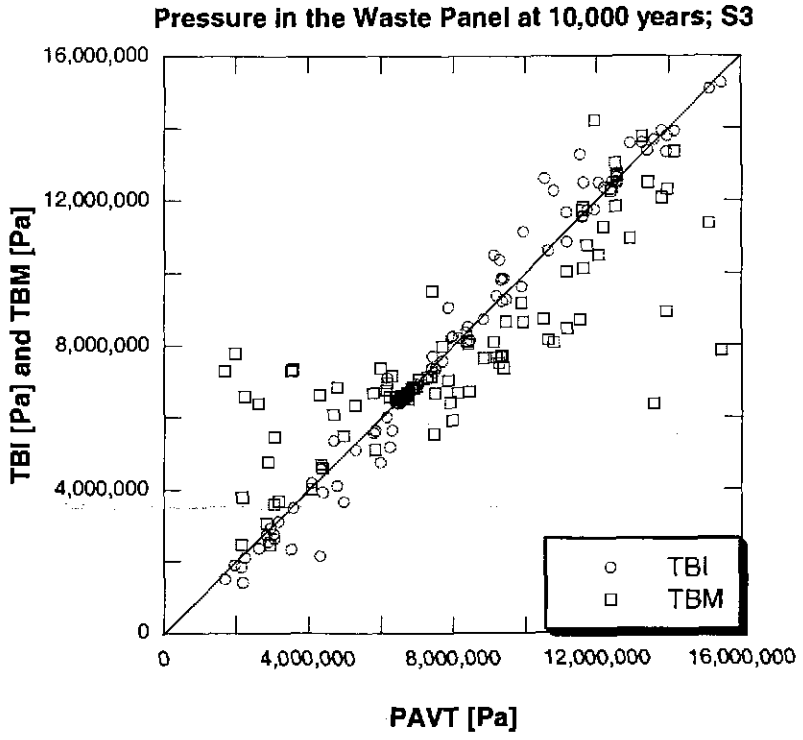

Figure 97. Disturbed Scenario (S3); Pressure in the Waste Panel at 10,000 Years [WAS_PRES]; TBM and TBI versus PAVT

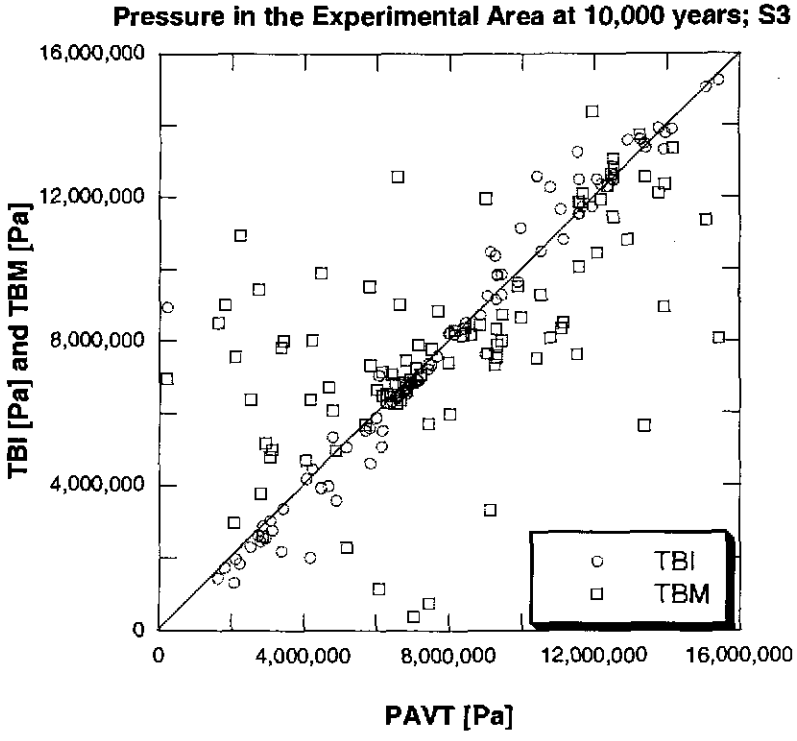

Figure 98. Disturbed Scenario (S3); Pressure in the Experimental Area at 10,000 Years [EXP_PRES]; TBM and TBI versus PAVT

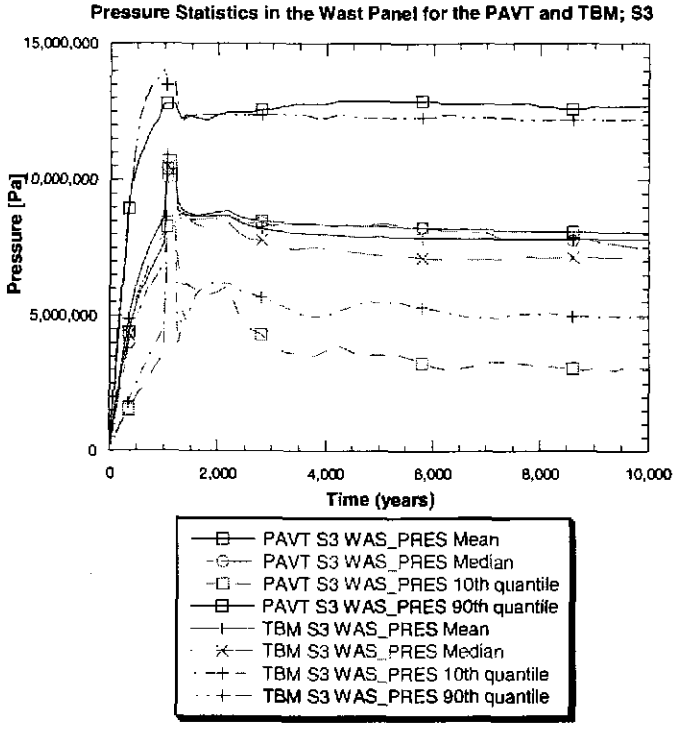

Figure 99. Disturbed Scenario (S3); Mean, Median, 10th And 90th Quantiles For Pressure In The Waste Panel; TBM and PAVT

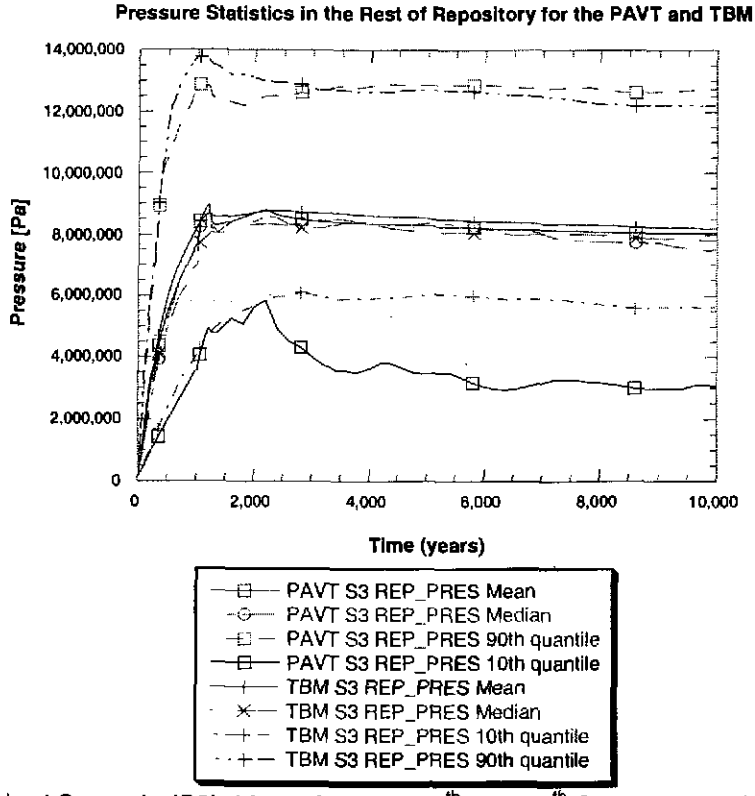

Figure 100. Disturbed Scenario (S3); Mean, Median, 10th And 90th Quantiles For Pressure In Rest Of Repository; TBM and PAVT

4.5.3.3 Disturbed Scenario (S5)

Figures 101 and 102 show pressure in the waste panel and rest of repository for all 100 vectors of the S5 scenario in the TBM. Before the intrusion at 1,000 years, pressure behaves as in the undisturbed scenario. The borehole plug degrades 200 years after the intrusion, allowing gas and brine to flow in the borehole, and generally depressurizing the waste panel. After depressurization, most vectors stabilize between 2 and 9 MPa. Pressure in the rest of repository is reduced by the intrusion albeit at a much slower rate than in the waste panel.

Figures 103 and 104 compare pressure in the waste panel and rest of repository at 3,000 years for the TBM, TBI, and PAVT. Pressure in the waste panel is generally similar in the TBM and the TBI. However, pressure in the rest of repository is higher in the TBM than in the TBI or PAVT. Figures 105 and 106 compare average pressure in the waste panel and rest of repository for the TBM and the PAVT. Figure 106 shows that after the intrusion, pressures in the PAVT rapidly equalize between these two repository areas. However, in the TBM, pressures equilibrate very slowly across the Option D panel closures in the S5 scenario.

Figures 107 and 108 compare pressure in the waste panel and rest of repository at 10,000 years for the TBM, TBI, and PAVT for the S5 scenario. As opposed to the elevated pressures in the waste regions at 1,000 years, the 10,000-year comparison shows equal pressures in the waste panel. However, pressures in the rest of repository remain higher for some vectors in the TBM than in the TBI or PAVT even after 10,000 years.

Figure 109 shows pressure in the experimental area for all 100 vectors in the S5 scenario for the TBM. Figure 109 shows that pressure in the experimental area does not respond to drilling intrusions as rapidly as the rest of repository (Figure 102) due to the presence of the panel closures. Pressures at 10,000 years in the experimental area are generally lower than in the undisturbed scenario (Figure 89) due to long-term depressurization of the entire repository arising from the drilling intrusion. Figure 110 compares pressure in the experimental area at 10,000 years for the TBM, TBI and PAVT. This figure shows that the TBM maintains higher pressures due to the Option D panel closures.

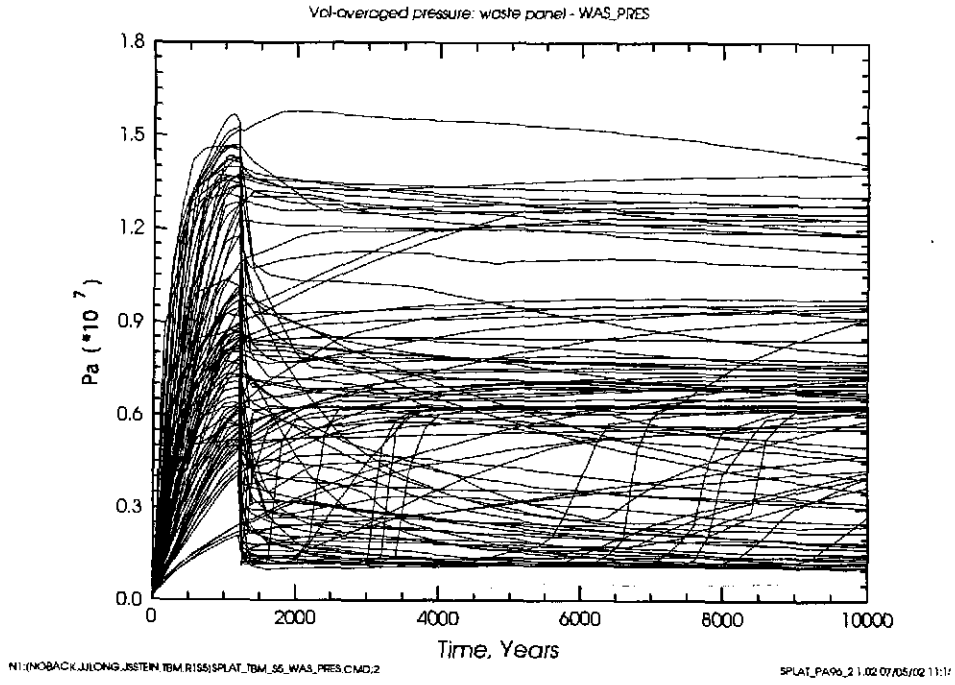

Figure 101. Disturbed Scenario (S5); Pressure in the Waste Panel [WAS_PRES]; TBM

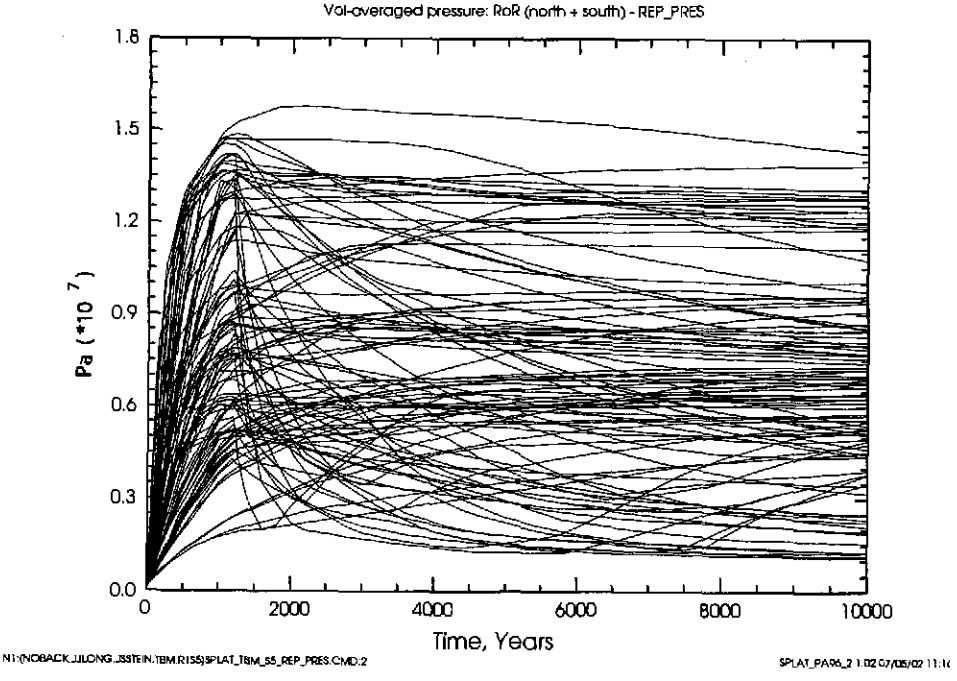

Figure 102. Disturbed Scenario (S5); Pressure in the Rest of Repository [REP_PRES]; TBM

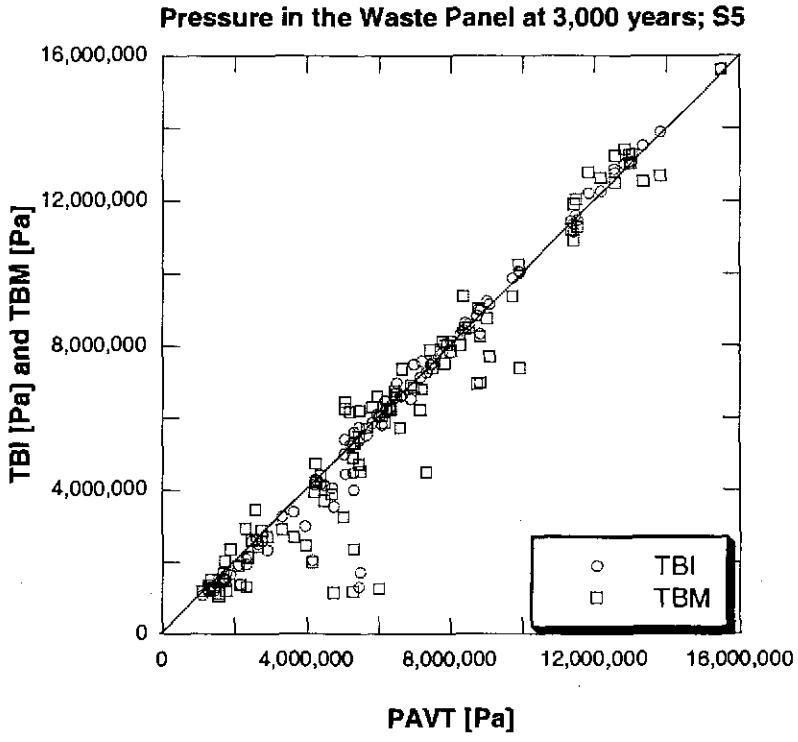

Figure 103. Disturbed Scenario (S5); Pressure in the Waste Panel at 3,000 Years [WAS_PRES]; TBM and TBI versus PAVT

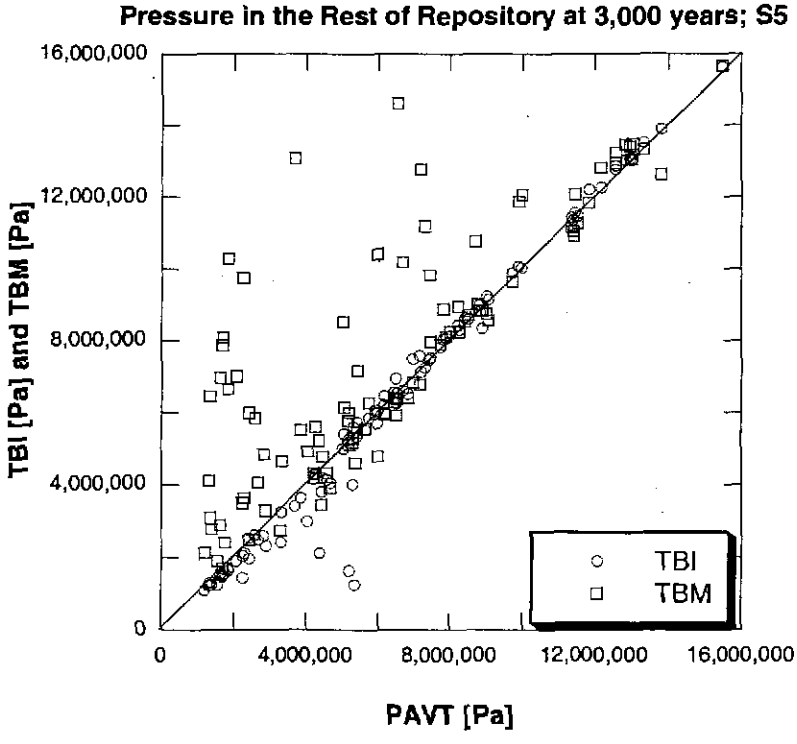

Figure 104. Disturbed Scenario (S5); Pressure in the Rest of Repository at 3,000 Years [REP_PRES]; TBM and TBI versus PAVT

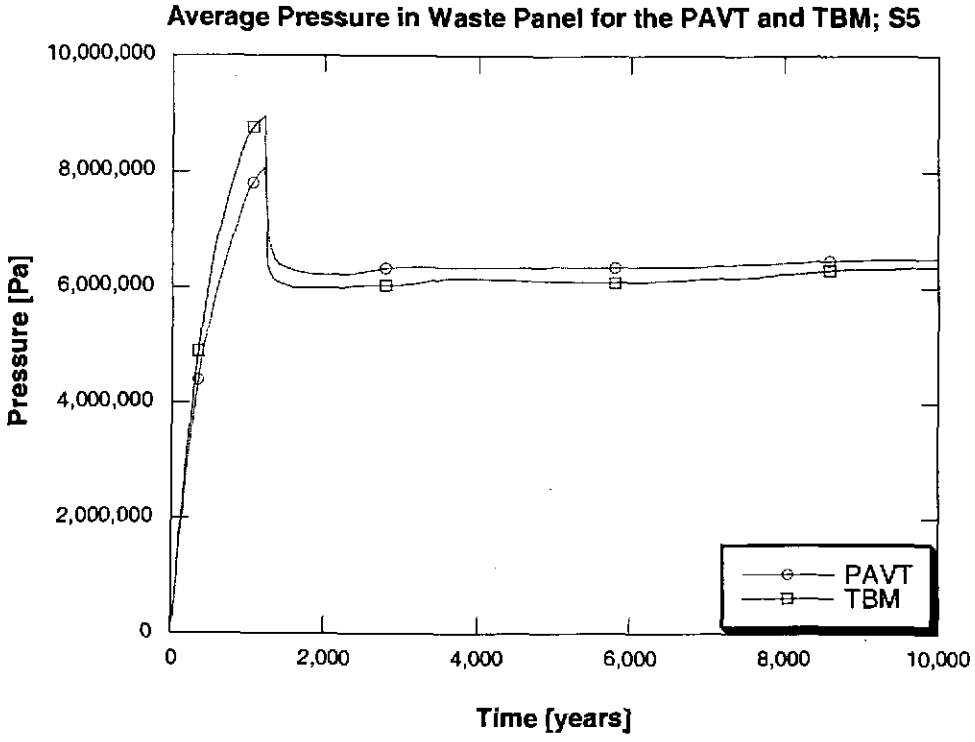

Figure 105. Disturbed Scenario (S5); Average Pressure In The Waste Panel [WAS_PRES]; TBM and PAVT

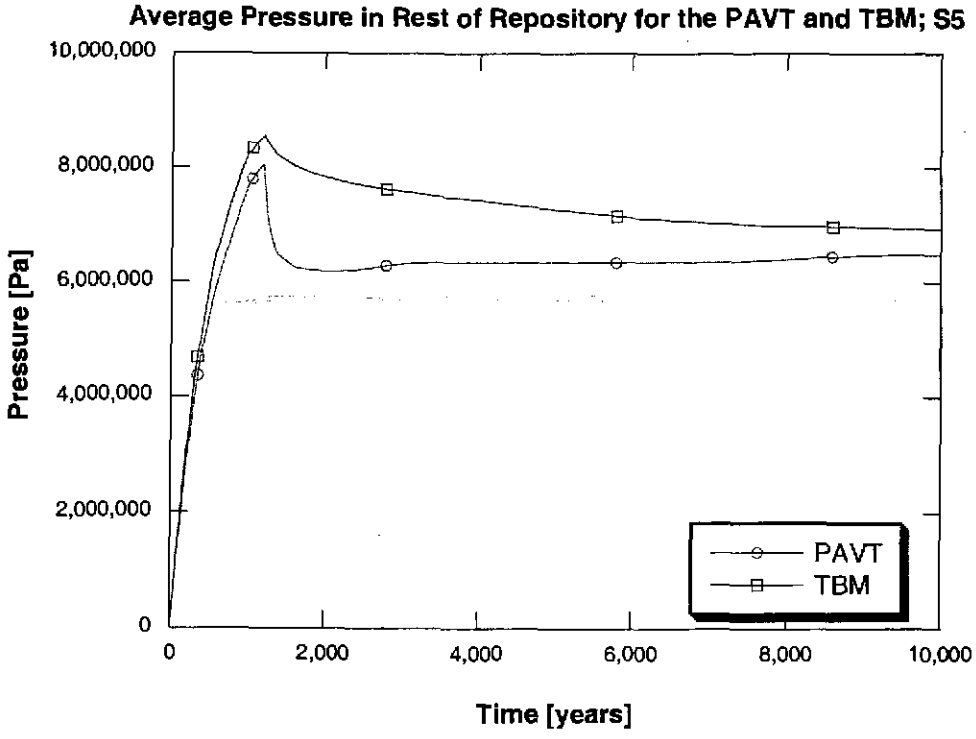

Figure 106. Disturbed Scenario (S5); Average Pressure In The Rest Of Repository [REP_PRES]; TBM and PAVT

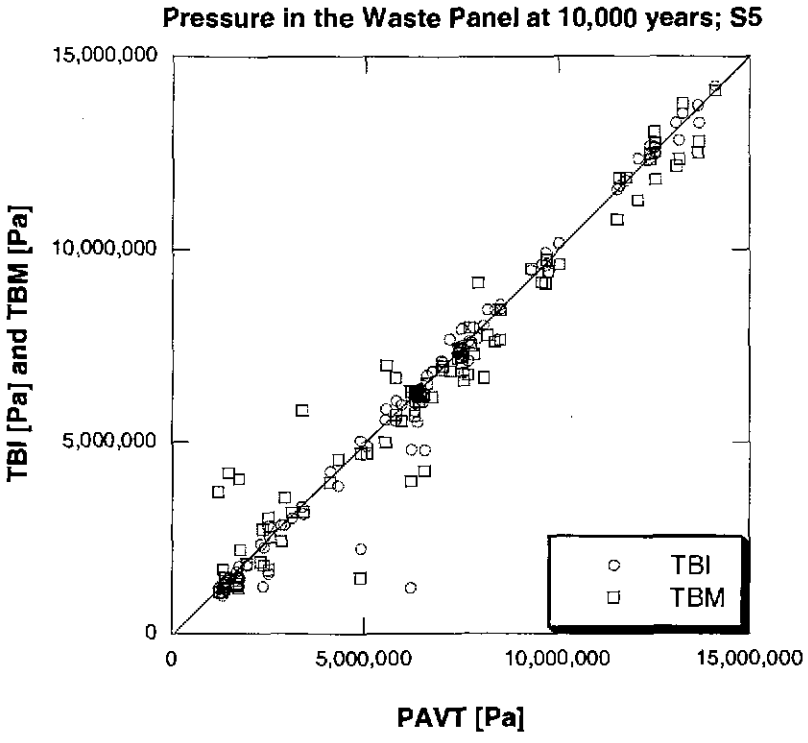

Figure 107. Disturbed Scenario (S5); Pressure in the Waste Panel at 10,000 Years [WAS_PRES]; TBM and TBI versus PAVT

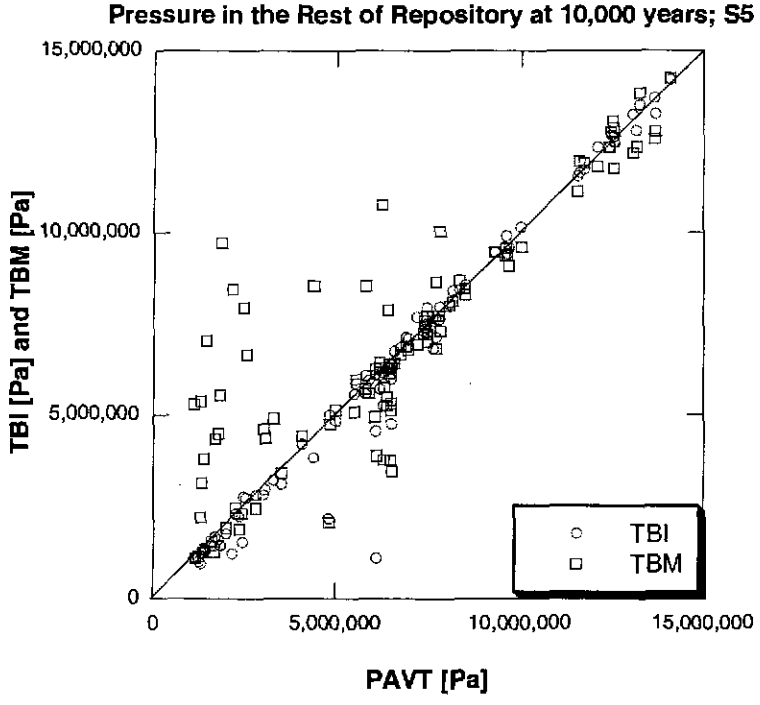

Figure 108. Disturbed Scenario (S5); Pressure in the Rest of Repository at 10,000 Years [REP_PRES]; TBM and TBI versus PAVT

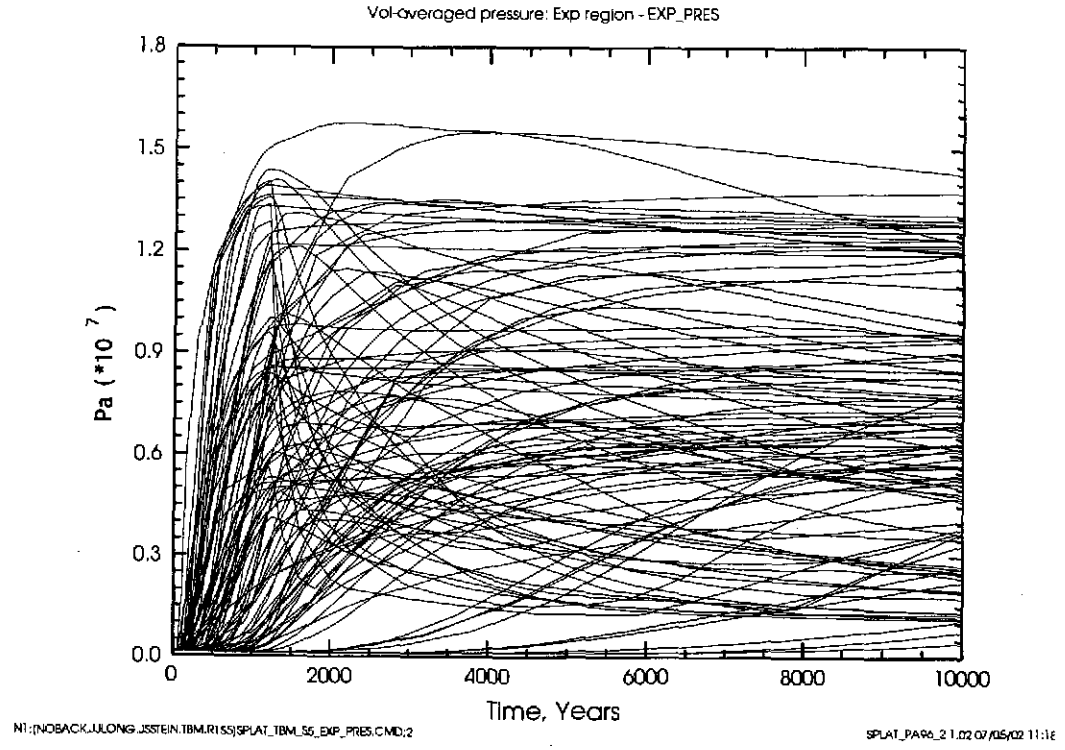

Figure 109. Disturbed Scenario (S5); Pressure in the Experimental Area [EXP_PRES]; TBM

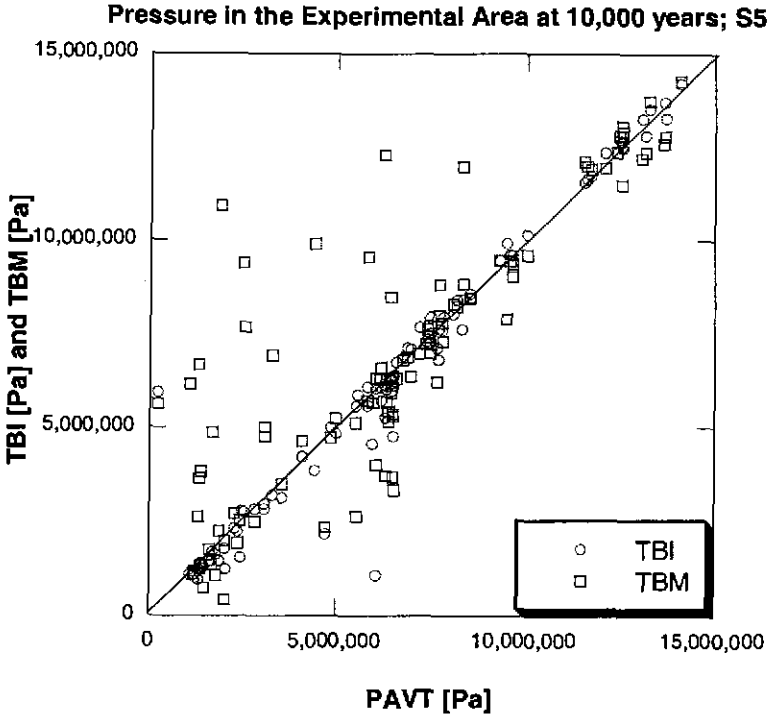

Figure 110. Disturbed Scenario (S5); Pressure in the Experimental Area at 10,000 Years [EXP_PRES]; TBM and TBI versus PAVT

4.6 BRINE FLOW FROM THE REPOSITORY

This section compares brine flow away from the repository between the TBM, TBI and PAVT. BRAGFLO calculates brine flow away from the repository over the 10,000 year period; other PA codes use these brine flow results to estimate releases of radionuclides by transport. Direct releases of brine to the surface at the time of a drilling intrusion are calculated by the direct brine release codes and are not considered here.

The primary paths for brine flow from the repository are:

1. out the marker beds
2. up the borehole to the Culebra in disturbed scenarios

Other brine flow paths, such as through the Salado or up the shaft, have been shown to be negligible, and are not considered here.

4.6.1 Brine Flow Out Marker Beds

In the PAVT, a few vectors showed significant flow out the marker beds to the land withdrawal boundary (LWB). However, analysis of these vectors concluded that the brine reaching the LWB had never contacted waste, and thus did not transport any radionuclides. Figure 111 compares the brine flow reaching the LWB for the TBM, TBI, and PAVT for those vectors which had total flow greater than 0.1 m^3 to the LWB. In this case the scatter plot is shown on a log-log scale to more clearly show the range in the data. The changes made to BRAGFLO do not appear to significantly affect these flows; all three calculations produce flow to the LWB in the same vectors and with about the same magnitude.

4.6.2 Brine Flow Up the Borehole

Brine flow up the borehole is a complex, dynamic process. In the disturbed scenarios, brine can flow in either direction in the borehole, depending on the pressure gradient and saturation at the moment. Brine flow is also complicated by the two-phase flow properties of the materials in the borehole, which change over time to simulate the degradation of the borehole plugs. This analysis examines only cumulative brine flow up the borehole above the upper DRZ, comparing the TBI and TBM to the PAVT.

Figure 112 compares cumulative brine flow up the borehole after 10,000 years in the S3 scenario for the TBM, TBI, and PAVT. Most vectors have little to no brine flow up the borehole; in these vectors it is likely that gas flow dominates. For those vectors that do have brine flow up the borehole, cumulative flow in the TBI is quite similar to that in the PAVT and cumulative flow in the TBM is generally greater. The modest increase in brine flow in the TBM is due to the Option D panel closures. In the S3 scenario, brine generally flows up the borehole from the Castile. Once the waste panel is saturated, additional brine can only flow up the borehole above the repository because the Option D panel closures prevent it from flowing laterally to other parts of the repository. Figure 24 shows that, in the TBM, less brine enters the repository from the Castile than in the TBI or the PAVT. Figure 29 shows that, in the TBM, there is significantly less brine present in the excavated

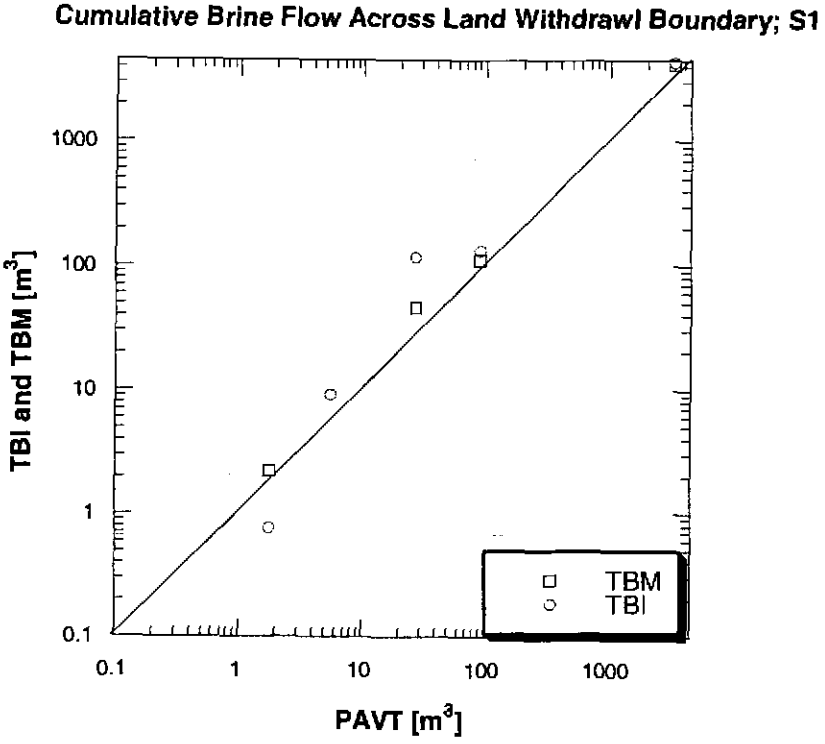

Figure 111. Undisturbed Scenario (S1); Cumulative Brine Flow Across Land Withdrawal Boundary at 10,000 Years; Scatter Plot; TBM and TBI versus PAVT

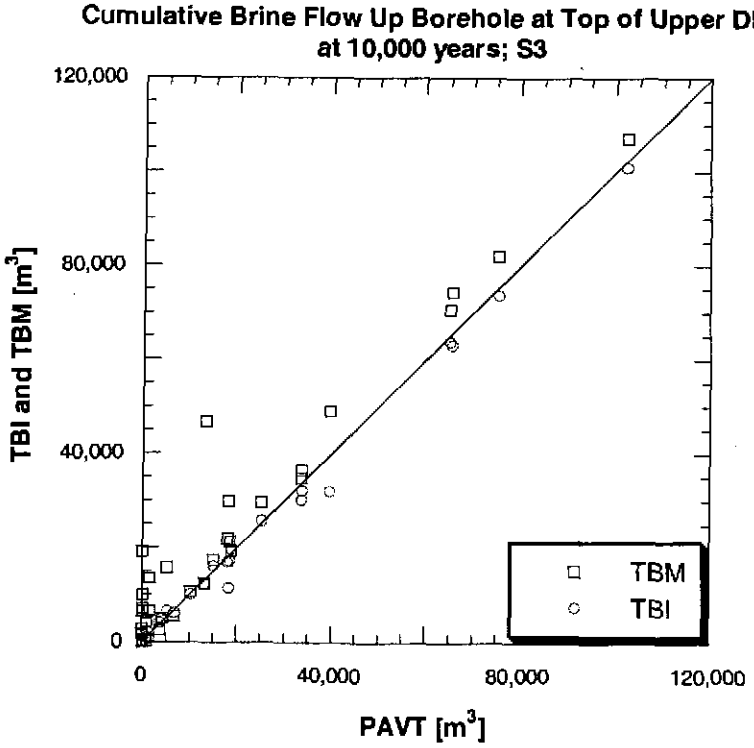

Figure 112. Disturbed Scenario (S3); Cumulative Brine Flow Up Borehole at Top of Upper DRZ at 10,000 Years; Scatter Plot; TBM and TBI versus PAVT

area as a whole than in either the TBI or the PAVT. Thus, in the S3 scenario for the TBM, brine flowing from the Castile fills the waste panel and then either stops or flows up the borehole above the repository. The Option D panel closures prevent lateral flow in to the rest of the repository. In contrast, without the Option D panel closures, brine flows from the Castile to the waste panel then flows laterally into the rest of repository as well as up the borehole. The S5 scenario is quite different than the S3 scenario. In the S5 scenario, brine in the borehole can only move in one direction at any specific time (a limitation caused by the coarse grid refinement). Generally, after the borehole plugs degrade, brine flows down the borehole from the Culebra at a rate determined by the borehole permeability. The additional brine flowing into the waste panel may increase gas generation and thus increase pressure in the waste panel. If pressures increase enough, brine flow can reverse and brine can move up the borehole towards the Culebra.

Figure 113 compares cumulative brine flow up the borehole after 10,000 years in the S5 scenario for the TBM, TBI, and PAVT. In all three calculations, the distribution of brine flow up the borehole is similar. Most vectors have little to no flow. For vectors that have significant flow up the borehole, the TBI and PAVT are similar, indicating that the new grid does not alter brine flow up the borehole in the S5 scenario. However, when the Option D panel closures are added, some vectors that had large flows in the PAVT have no flow in the TBM, while other vectors that had no flow in the PAVT have large flow in the TBM. An analysis that explains why the flows change for specific vectors would be too detailed for this report. Brine flow up the borehole is significant only in the calculation of releases through the Culebra. Thus, the differences in flow for each vector will be analyzed in a subsequent report to the extent necessary to understand their effect on releases through the Culebra.

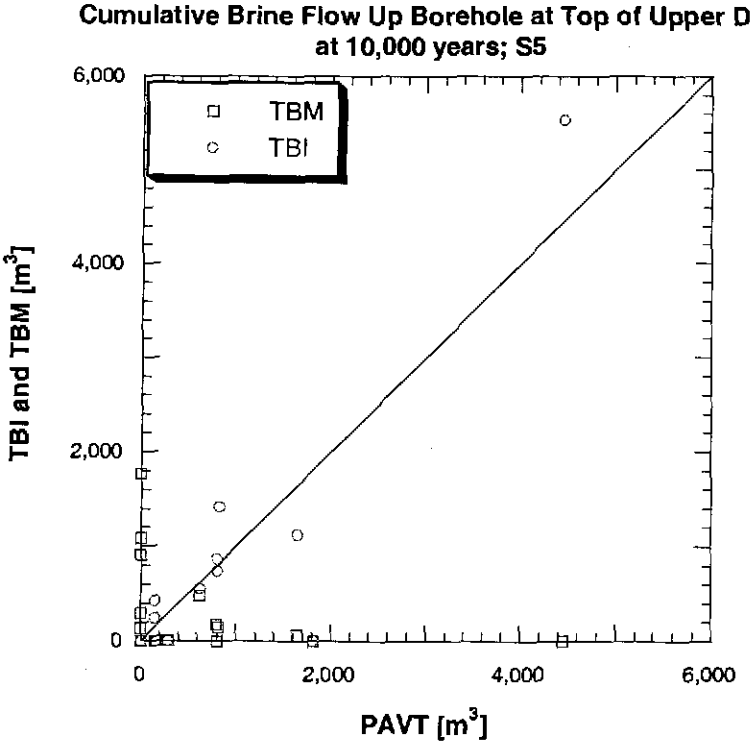

Figure 113. Disturbed Scenario (S5); Cumulative Brine Flow Up Borehole at Top of Upper DRZ at 10,000 Years; Scatter Plot; TBM and TBI versus PAVT

4.7 SENSITIVITY ANALYSES

A sensitivity analysis determines the effects of uncertain model inputs on model outcome and is widely recognized as an essential component of studies like performance assessment. The importance of identifying and characterizing the sensitivity of performance assessment results to uncertain model inputs was recognized at each step in the WIPP certification process, and as a result, a sensitivity analysis was performed as part of the PAVT (SNL, 1997). That analysis was compared with the sensitivity analysis conducted in much greater detail for the Compliance Certification Application (CCA), which is summarized in (Helton et al, 2000a; Helton et al, 2000b) and documented in (Helton et al., 1998).

To verify the conclusions made thus far about the reasons for the differences between the results generated with the TBM model and the PAVT results, a sensitivity analysis on the TBM BRAGFLO results was performed and compared with the sensitivity analysis conducted for the BRAGFLO portion of the PAVT. In each analysis, partial correlation coefficients for the BRAGFLO output variables were calculated at specific times, using the sampled input variables as the independent variables. The sensitivity analyses identify which sampled variables have the strongest correlation to the uncertainty in the BRAGFLO output variables at each point in time. As explained earlier, the TBM calculations used the same variable sampling as was used in the PAVT for those parameters in common with the different analyses. If the conceptual model changes to BRAGFLO have altered the stochastic relationship between sampled inputs and BRAGFLO outputs, the alterations should be observed as differences between the two sensitivity analyses.

4.7.1 Comparison between PAVT and TBM Sensitivity Analyses

The comparison between sensitivity analyses did not consider all BRAGFLO output variables, restricting the comparison to those variables documented for the PAVT sensitivity analysis (SNL, 1997). Table 2 lists the BRAGFLO output variables that were compared between the two analyses. The complete sensitivity analysis for the TBM resulted in three volumes of printed rankings for the BRAGFLO variables over time for the three scenarios, S1, S3, and S5 (Garner, 2002a; Garner 2002b; Garner, 2002c)

The PAVT sensitivity analysis identified the sampled variables that had a correlation greater than 0.5 or less than –0.5 at any time interval during the calculation. For the TBM sensitivity analysis the correlation threshold was relaxed to show sampled variables with correlations of at least 0.25 in magnitude.

To illustrate the comparison between the sensitivity analyses, Figures 114 and 115 show the PAVT and TBM partial correlation results for the BRAGFLO output variable WAS_PRES, pressure in the waste panel, for the undisturbed scenario (S1). These figures plot the correlation between the most correlated input variables and the output variable over time. Figure 114 shows that the variation in the values of WAS_PRES in the PAVT is almost completely explained by the variation in the input variable WMICDFLG, a flag which indicates whether microbial degradation of cellulose is taking place. Figure 114 shows that the remaining variation in WAS_PRES after 3,000 years (after accounting for WMICDFLG) is best explained by the variation in HALPOR, the porosity of the surrounding halite, and by DRZPRM, the permeability of the DRZ.

Table 2. BRAGFLO Variables Considered in Comparison of Sensitivity Analyses

Output variable	Scenario	Definition
BRAALIC	S1, S5, S3	Cumulative brine flow out of all marker beds towards the repository (m^3)
BRNREPTC	S1, S3, S5	Cumulative brine flow into waste-filled regions (m^3)
FE_MOLE	S1, S3, S5	Fraction of iron remaining (moles)
GAS_MOLE	S1, S3, S5	Cumulative amount of gas generated (moles)
WAS_PRES	S1, S3, S5	Pressure in waste panel (Pa)
WAS_SATB	S1, S3, S5	Brine saturation in waste panel
BNBHDNUZ	S3, S5	Cumulative brine flow down borehole at the top of the upper DRZ
BNBHLDRZ	S3	Cumulative brine flow up borehole at the bottom of the lower DRZ

In the TBM, Figure 115 shows that the variation in WAS_PRES is also almost completely explained by WMICDFLG, and that the remaining variation is also explained HALPOR after 3,000 years. However, the legend on Figure 115 indicates that the magnitude of the correlation of DRZPRM with WAS_PRES has decreased somewhat. In the PAVT, this correlation was slightly above 0.5 from 3,000 to 10,000 years; in the TBM, the correlation did not exceed 0.425.

Despite this difference, the two figures demonstrate that, in both calculations, the output variable WAS_PRES correlates to the same set of input variables with roughly the same correlation values. Thus, the relationship between WAS_PRES and the sampled input variables has not significantly changed.

Overall, the sensitivity analysis comparison did not turn up any significant differences between the PAVT and the TBM in partial correlations. For many output variables, the correlations of sampled variables changed slightly, becoming stronger or weaker; for a few output variables, the relative ranking of correlations of sampled variables changed, with some sampled variables becoming of higher rank than others. However, the set of the most correlated sampled variables remained the same between the PAVT and the TBM for each output variable

Although the correlations for only a few BRAGFLO output variables were compared, the comparison was sufficient to detect any significant change in the stochastic relationships between sampled variables and BRAGFLO output. Consequently, the conceptual model changes made to

BRAGFLO for the TBM did not alter the dependence of BRAGFLO's uncertain output variables on the sampled input variables.

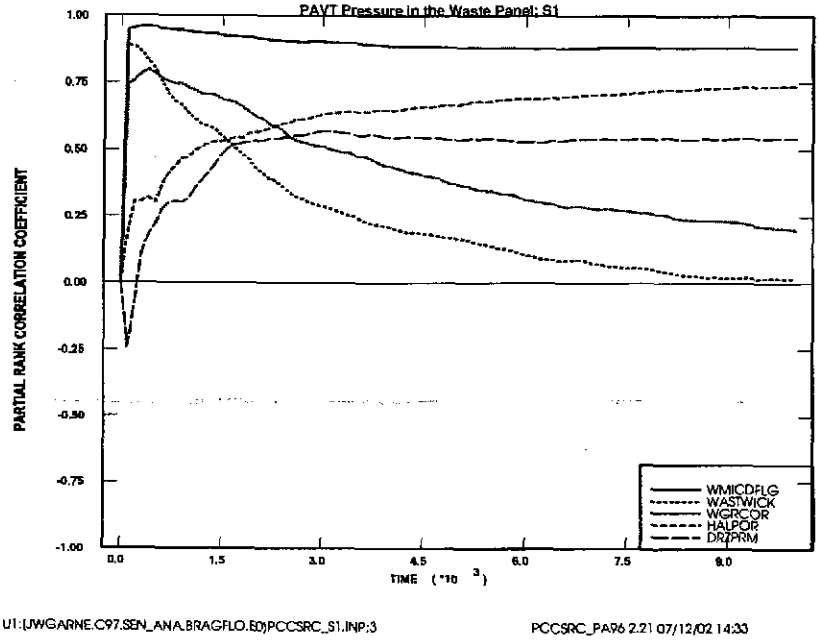

Figure 114. Partial Rank Correlation Coefficients for the Pressure in the Waste Panel [WAS_PRES]; PAVT

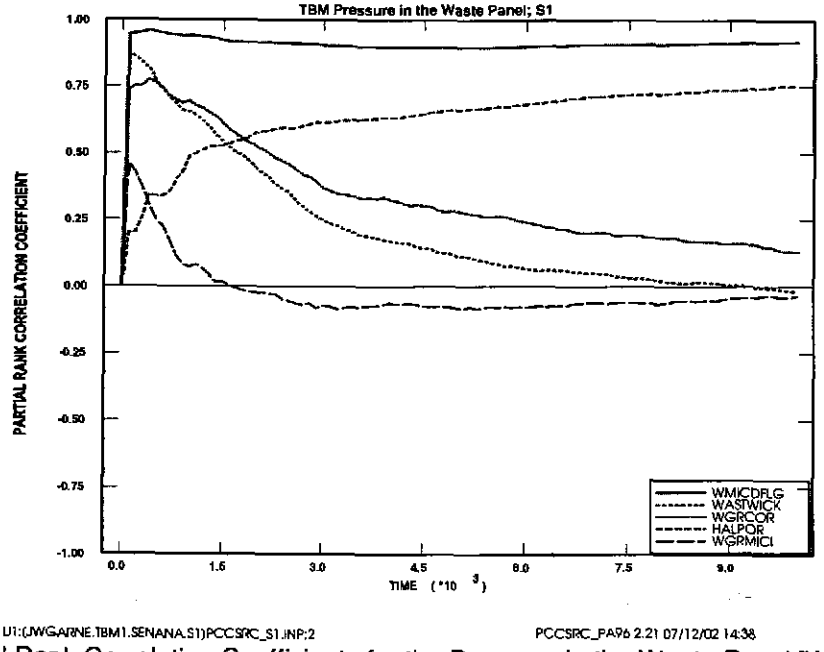

Figure 115. Partial Rank Correlation Coefficients for the Pressure in the Waste Panel [WAS_PRES]; TBM

5. CONCLUSIONS

The Technical Baseline Migration (TBM) is a PA calculation conducted to support changes to conceptual models, parameter corrections, and grid refinement corrections. The aim of these calculations is to adequately model the effect of the Option D panel closures; demonstrate that the shaft seal model as implemented in the baseline BRAGFLO grid is as effective as the surrounding rocks in preventing releases and thus can be simplified or removed from the model domain; and incorporate a number of parameter and grid refinement corrections that better reflect our increased scientific understanding of physical processes since the time of the CCA.

The TBM calculations implemented a series of grid and parameter changes to account for advances in SNL's understanding of WIPP processes since the time of the CCA and PAVT. A single vector analysis was conducted to estimate the relative contribution of each incremental change and then two replicate analyses were conducted to demonstrate that while certain changes have little effect on results, some changes significantly affect the relative magnitude of the various release mechanisms and pathways.

The single vector analysis suggested that the changes included in TBI, including adding grid cells near the repository, dividing the rest of repository into two regions, removing the explicit representation of the shaft from the grid, and removing fracturing in the upper DRZ together had little effect on results. This evidence led to a full replicate analysis of this intermediate case, in which the TBI was compared to the PAVT for 100 vectors. This analysis confirmed that these changes to the grid and conceptual models only cause slight differences in pressure and saturation results across the full replicate. This suggests that the original BRAGFLO grid was adequate. The TBM calculation incorporated all the changes included in the TBI and also added a correction the molecular weight of cellulosics and the explicit representation of the Option D panel closures. A full replicate analysis was conducted for the TBM and results were compared to the TBI and PAVT on a vector-by-vector basis. The TBM confirmed that the Option D panel closures and molecular weight correction affected brine flow patterns, pressure, and saturation conditions in the repository.

The molecular weight correction only affects the 50% of vectors that include biodegradation and results in a 10% increase gas production from biodegradation. Since gas is also produced by corrosion, the total increase in gas produced is less than 10% for these vectors.

The Option D panel closures have a more dramatic effect on results. The panel closures effectively slow the movement of brine and gas between different regions in the repository that are separated by panel closures. One result, is less brine flows into the southern waste filled regions since it no longer can flow laterally across the repository from the northern experimental area. Less brine flowing into the waste regions results in lower brine saturations in the waste regions. One possible effect of this is to reduce the direct brine releases since these require ample brine to be present. However, despite the drier conditions, gas is still produced in the waste regions and pressures are typically higher in these regions than in the PAVT because the gas is unable to flow to the northern areas and equalize pressures nearly as quickly as occurred in the PAVT. Since DBR releases are dependant on saturation and pressures the DBR calculations must be run to fully evaluate the effect of the Option D panel closures on DRR.

The higher waste region pressures are also important following a drilling intrusion when the intruded panel is typically depressurizied. In the PAVT a single drilling intrusion effectively depressurized the entire repository, with the pressure in all regions changing at the same time. In the TBM, the Option D panel closures isolate the intruded panel and pressures do not change as rapidly in other parts of the repository. This result is quite important for estimating direct releases to the surface from spallings and DBR, since in the PAVT, only minor releases were seen for subsequent intrusions after the repository was depressurized. In the TBM, the subsequent intrusions are likely to penetrate waste panels that have not been previously depressurized. For this reason it is likely that frequency of spallings and DBR releases will be greater in the TBM than in the PAVT. A full set of spallings calculations is planned to address this question.

In summary, based on the BRAGFLO results from the TBI, there was no significant effect on results from refining the grid, removing the explicit representation of the shaft and removing the fracturing in the upper DRZ. However, these changes are expected to improve the accuracy of the transport calculation that are planned next. The TBM calculation demonstrates that the Option D panel closures change the dynamics within the repository by altering brine and gas flow patterns that result in reduced saturation and increased pressure in the waste regions. These effects will change the direct releases. It is still uncertain how much the total releases will change, but it is clear that the even if the total releases do not change significantly, the relative contribution of each release mechanism will change. It is imperative that the PA accurately represents the actual processes that are expected to occur at WIPP in the future. If panels are to be sealed with closures that behave like Option D, it is incumbent on SNL to represent them adequately in the PA. The TBM calculation suggests that the current PAVT baseline may need to be revised to incorporate new knowledge about the importance of panel closures to long term PA.

6. REFERENCES

Anderson, M.P., and Woessner, W.W. 1992. *Applied Groundwater Modeling: Simulation of Flow and Advective Transport*. San Diego: Academic Press.

Caporuscio, F., Gibbons, J., and Oswald, E. 2002. *Waste Isolation Pilot Plant: Salado Flow Conceptual Models Peer Review Report*. Report prepared for the U.S. Department of Energy, Carlsbad Area Office, Office of Regulatory Compliance.

Economy, K.M., Helton, J.C., and Vaughn, P. 1999. *Brine and Gas Flow Patterns Between Excavated Areas and Disturbed Rock Zone in the 1996 Performance Assessment for the Waste Isolation Pilot Plant for a Single Drilling Intrusion that Penetrates Repository and Castile Brine Reservoir*. SAND99-1043. Albuquerque, NM: Sandia National Laboratories.

Garner, J.W. 2002a. *TBM STEPWISE Analysis S1 Scenario*. ERMS# 522808. Carlsbad, NM: Sandia National Laboratories.

Garner, J.W. 2002b. *TBM STEPWISE Analysis S3 Scenario*. ERMS# 522809. Carlsbad, NM: Sandia National Laboratories.

Garner, J.W. 2002c. *TBM STEPWISE Analysis S5 Scenario*. ERMS# 522810. Carlsbad, NM: Sandia National Laboratories.

Helton, J.C., Bean, J.E., Berglund, J.W., Davis, F.J., Garner, J.W., Johnson, J.D., MacKinnon, R.J., Miller, J., O'Brien, D.G., Ramsey, J.L., Schreiber, J.D., Shinta, A., Smith, L.N., Stoelzel, D.M., Stockman, C., and Vaughn, P. 1998. *Uncertainty and Sensitivity Analysis Results Obtained in the 1996 Performance Assessment for the Waste Isolation Pilot Plant*. SAND98-0365. Albuquerque, NM: Sandia National Laboratories.

Helton, J.C., Bean, J.E., Economy, K., Garner, J.W., MacKinnon, R.J., Miller, J., Schreiber, J.D., and Vaughn, P. 2000a. "Uncertainty and sensitivity analysis for two-phase flow in the vicinity of the repository in the 1996 performance assessment for the Waste Isolation Pilot Plant: undisturbed conditions," *Reliability Engineering & System Safety*. Vol. 69, no. 1-3, 227-261.

Helton, J.C., Bean, J.E., Economy, K., Garner, J.W., MacKinnon, R.J., Miller, J., Schreiber, J.D., and Vaughn, P. 2000b. "Uncertainty and sensitivity analysis for two-phase flow in the vicinity of the repository in the 1996 performance assessment for the Waste Isolation Pilot Plant: disturbed conditions," *Reliability Engineering & System Safety*. Vol. 69, no. 1-3, 263-304.

Hurtado, L.D., Knowles, M.K., Kelley, V.A., Jones, T.L., Ogintz, J.B., and Pfeifle, T.W. 1997. *WIPP Shaft Seal System Parameters Recommended to Support Compliance Calculations*. SAND97-1287. Albuquerque, NM: Sandia National Laboratories.

MacKinnon, R.J., and Freeze, G. 1997. *Supplemental Summary of EPA-Mandated Performance Assessment Verification Test (All Replicates) and Comparison with the Compliance Certification Application Calculations*. WPO# 46702. Albuquerque, NM: Sandia National Laboratories.

SNL. 1997. *Summary of Uncertainty and Sensitivity Analysis Results for the EPA-Mandated Performance Assessment Verification Test*. WPO# 420667. Albuquerque, NM: Sandia National Laboratories.

Stein, J.S. 2002a. "Analysis Plan for Calculations of Salado Flow: Technical Baseline Migration (TBM)." AP-086. Carlsbad, NM: Sandia National Laboratories. ERMS# 520612.

Stein, J. 2002b. "Parameter values for new materials CONC_PCS and DRZ_PCS." Memorandum to M.K. Knowles, Feb 13, 2002. Carlsbad, NM: Sandia National Laboratories. ERMS# 520524.

Stein, J. 2002c. "Minor difference found in TBM grid volumes." Memorandum to M.K. Knowles, May 20, 2002. Carlsbad, NM: Sandia National Laboratories. ERMS# 522357.

Thompson, T.W., and Hansen, F.D. 1996. "Long-term Performance of Panel Closures." Memorandum to M. G. Marietta, August 2, 1996. Albuquerque, NM: Sandia National Laboratories. ERMS# 240418.

Tisinger, S. 2001. *Analysis Report for the Migration of WIPP PA Parameter Data to the PAPDB Data Model*. Carlsbad, NM: Sandia National Laboratories. ERMS# 520780.

U.S. DOE (U.S. Department of Energy). 1996. *Title 40 CFR Part 191 Compliance Certification Application for the Waste Isolation Pilot Plant*. DOE/CAO-1996-2184. Carlsbad, NM: U.S. Department of Energy, Waste Isolation Pilot Plant, Carlsbad Area Office.

U.S. EPA (U.S. Environmental Protection Agency). 1996. "40 CFR Part 194: Criteria for the Certification and Recertification of the Waste Isolation Pilot Plant's Compliance With the 40 CFR Part 191 Disposal Regulations; Final Rule," *Federal Register*. Vol. 61, no. 28, 5224-5245.

U.S. EPA (U.S. Environmental Protection Agency). 1998. *Technical Support Document for Section 194.23: Parameter Justification Report*. Docket No: A-93-02 V-B-14. Washington DC: U.S. Environmental Protection Agency, Center for the Waste Isolation Pilot Plant, Office of Radiation and Indoor Air.

Vaughn, P. 1996. "FEP Screening Analysis, S1: Verification of 2D-Radial Flaring Using 3D Geometry, CCA Appendix MASS Attachment 4-1." Memorandum to D.R. Anderson. Albuquerque, NM: Sandia National Laboratories. ERMS# 415853.

WIPP PA (Performance Assessment). 1992-1993. *Preliminary Performance Assessment for the Waste Isolation Pilot Plant, December 1992*. SAND92-0700/1-5. Albuquerque, NM: Sandia National Laboratories Vols. 1-5.

APPENDIX A
COMPUTATIONAL GRIDS FOR PAVT AND TBM

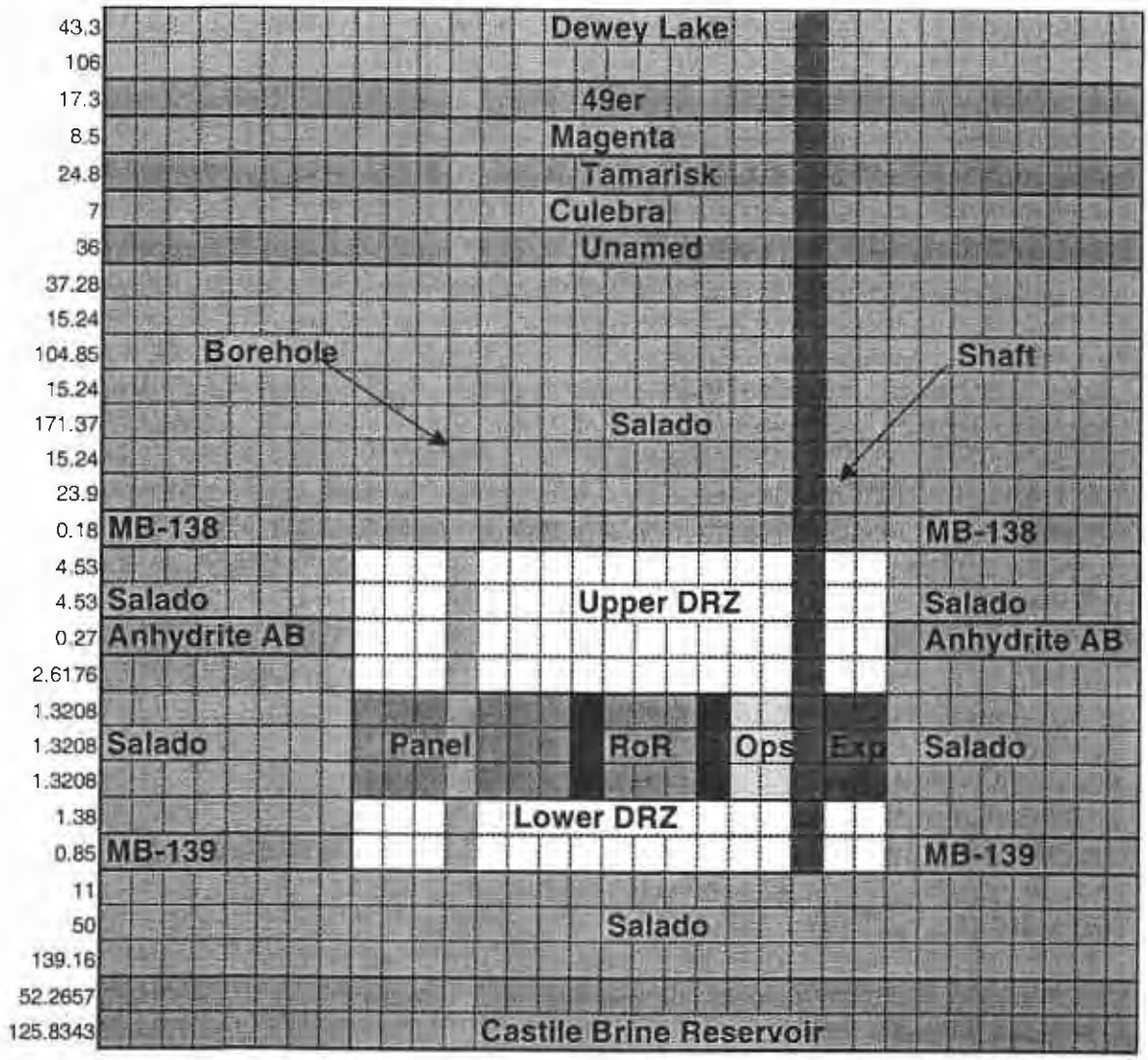

ΔX [m]	ΔZ [m]
15000	61314.3
5000	21314.3
1000	8748.8
750	6561.6
500	3314.3
100	2114.3
40	1834.3
10	1734.3
43.8	126.2
10	28.8
2	4.8
0.27575	0.27575
2	4.8
10	28.8
43.8	126.2
40	10
231.67	141.61
231.67	141.61
231.67	141.61
80	18.9
283	18.9
50	18.9
10	9.5
60	20.5
500	53.1
10	1258.9
40	1458.9
100	2018.9
500	3928
750	6910.6
1000	9214.1
5000	21726.9
15000	61726.9

Figure A-1. Baseline Computational Grid

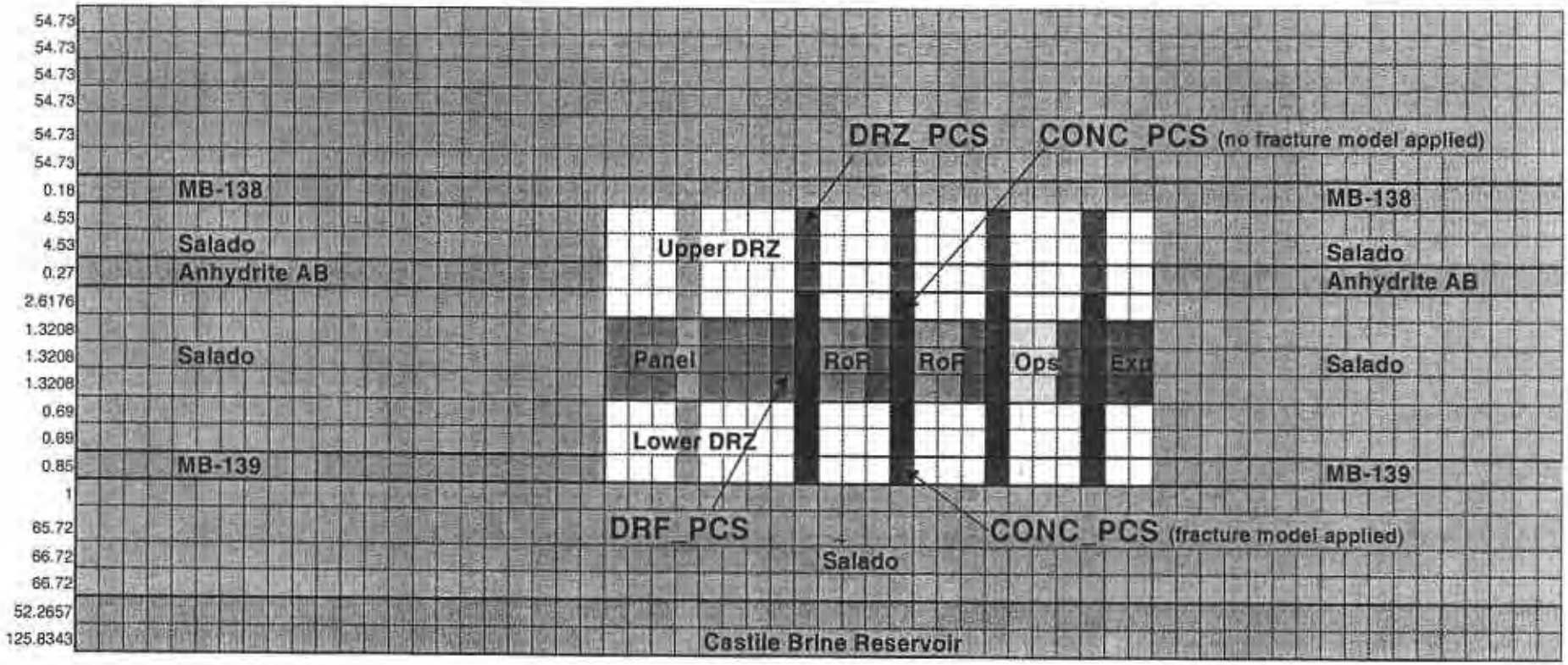

ΔZ [m]	ΔX [m]
54.73	12203.828
54.73	3126.85363
54.73	2156.45078
54.73	1487.20744
54.73	1025.6603
54.73	707.351931
0.18	526.683884
4.53	363.230264
4.53	250.503631
0.27	172.761125
2.6176	119.145603
1.3208	82.1693815
1.3208	56.668539
1.3208	39.081751
0.69	26.9529317
0.69	18.5882288
0.85	12.8194681
1	8.8410125
65.72	6.09725
66.72	4.205
66.72	2.9
52.2657	2
125.8343	43.8
66176.7756	10
35515.4124	2
24948.8035	0.28
17661.4871	2
12635.7516	10
9169.72718	43.8
6701.65555	32.1
4921.82725	7.9
3694.35946	140.2
2847.82995	140.2
2264.0165	32.1
1861.38653	7.9
1583.71069	140.2
1392.21011	140.2
1260.14074	32.1
1169.05842	7.9
1106.24303	137
1062.92206	137
1033.04554	32.1
1012.44104	7.9
998.23104	361.65
988.43104	361.65
126.2	2
28.8	2.9
4.8	4.205
0.28	6.09725
4.8	8.8410125
28.8	12.8194681
126.2	18.5882288
20	26.9529317
20	39.081751
175.436259	56.668539
175.436259	82.1693815
40	119.145603
40	172.761125
175.436259	250.503631
175.436259	363.230264
40	526.683884
40	707.351931
30.61	
30.61	
40	
40	
30.61	
30.61	
2839.27104	
2849.07104	
2863.28104	
2883.88554	
2913.76206	
2957.08303	
3019.89842	
3110.98074	
3243.05011	
3434.55069	
3712.22653	
4114.8565	
4698.66995	
5545.19946	
6772.66725	
8552.49555	
11020.5672	

Figure A-2. TBM Computational Grid

APPENDIX B
PROPERTIES FOR CONC_PCS

CONC_T1 Param. ID	Property	Description	Units	Distribution	Values
2463	CAP_MOD	Model number, capillary pressure model	NONE	Constant	2.0000000e+000
2464	COMP_RCK	Bulk Compressibility	Pa^-1	Constant	1.2000000e-009
2680	COMPRES	Brine Compressibility	Pa^-1	Constant	0.0000000e+000
2681	KPT	Flag for Permeability Determined Threshold	NONE	Constant	0.0000000e+000
2465	PC_MAX	Maximum allowable capillary pressure	Pa	Constant	1.0000000e+008
2682	PCT_A	Threshold Pressure Linear Parameter	Pa	Constant	5.6000000e-001
2683	PCT_EXP	Threshold pressure exponential parameter	NONE	Constant	-3.4600000e-001
2468	PO_MIN	Minimum brine pressure for capillary model KPC=3	Pa	Constant	1.0132500e+005
2466	PORE_DIS	Brooks-Corey pore distribution parameter	NONE	Cumulative	P(PORE_DIS = 1.100e-001) = 0.0 P(PORE_DIS = 9.400e-001) = 0.5 P(PORE_DIS = 8.100e+000) = 1.0
2467	POROSITY	Effective porosity	NONE	Constant	5.0000000e-002
2469	PRESSURE	Brine far-field pore pressure	Pa	Constant	1.0132500e+005
2470	PRMX_LOG	Log of intrinsic permeability, X-direction	log(m^2)	Triangular	Minimum -2.0699000e+001 Mode -1.8749600e+001 Maximum -1.7000000e+001
2471	PRMY_LOG	Log of intrinsic permeability, Y-direction	log(m^2)	Triangular	Minimum -2.0699000e+001 Mode -1.8749600e+001 Maximum -1.7000000e+001
2472	PRMZ_LOG	Log of intrinsic permeability, Z-direction	log(m^2)	Triangular	Minimum -2.0699000e+001 Mode -1.8749600e+001 Maximum -1.7000000e+001
2473	PTHRESH	Capillary threshold displacement pressure	Pa	Constant	1.5000000e+000
2474	PTINDEX	Index for computing uncertainty in threshold displacement pressure	NONE	Constant	7.0000000e-001
2475	REF_PRES	Reference pressure for porosity	Pa	Constant	1.0100000e+005
2476	RELP_MOD	Model number, relative permeability model	NONE	Constant	4.0000000e+000
2477	SAT_IBRN	Initial Brine Saturation	NONE	Constant	9.9999990e-001
2478	SAT_RBRN	Residual Brine Saturation	NONE	Cumulative	P(SAT_RBRN = 0.000e+000) = 0.0 P(SAT_RBRN = 2.000e-001) = 0.5 P(SAT_RBRN = 6.000e-001) = 1.0
2479	SAT_RGAS	Residual Gas Saturation	NONE	Uniform	Minimum 0.0000000e+000 Maximum 4.0000000e-001
2684	SBMIN	Minimum brine saturation when using capillary model number KPC(I) = 3	NONE	Constant	2.1000000e-001

APPENDIX C
PROPERTIES FOR DRZ_PCS

DRZ_1 Param. ID	Property	Description	Units	Distribution	Values
190	CAP_MOD	Model number, capillary pressure model	NONE	Constant	1.0000000e+000
191	COMP_RCK	Bulk Compressibility	Pa^-1	Constant	7.4100000e-010
3116	KPT	Flag for Permeability Determined Threshold	NONE	Constant	0.0000000e+000
193	PC_MAX	Maximum allowable capillary pressure	Pa	Constant	1.0000000e+008
3128	PCT_A	Threshold Pressure Linear Parameter	Pa	Constant	0.0000000e+000
3129	PCT_EXP	Threshold pressure exponential parameter	NONE	Constant	0.0000000e+000
196	PO_MIN	Minimum brine pressure for capillary model KPC=3	Pa	Constant	1.0132500e+005
194	PORE_DIS	Brooks-Corey pore distribution parameter	NONE	Constant	7.0000000e-001
195	POROSITY	Effective porosity	NONE	Cumulative	P(POROSITY = 3.90e-003) = 0.0 P(POROSITY = 1.29e-002) = 0.5 P(POROSITY = 3.29e-002) = 1.0
198	PRMX_LOG	Log of intrinsic permeability, X-direction	log(m^2)	Triangular	Minimum -2.06990e+001 Mode -1.87496e+001 Maximum -1.70000e+001
199	PRMY_LOG	Log of intrinsic permeability, Y-direction	log(m^2)	Triangular	Minimum -2.06990e+001 Mode -1.87496e+001 Maximum -1.70000e+001
200	PRMZ_LOG	Log of intrinsic permeability, Z-direction	log(m^2)	Triangular	Minimum -2.06990e+001 Mode -1.87496e+001 Maximum -1.70000e+001
203	RELP_MOD	Model number, relative permeability model	NONE	Delta	P(RELP_MOD = 1) = 0.33 P(RELP_MOD = 2) = 0.00 P(RELP_MOD = 3) = 0.67 P(RELP_MOD = 4) = 0.00
205	SAT_RBRN	Residual Brine Saturation	NONE	Constant	0.0000000e+000
206	SAT_RGAS	Residual Gas Saturation	NONE	Constant	0.0000000e+000

APPENDIX D
SINGLE VECTOR ANALYSIS

D.1 RATIONALE FOR SINGLE VECTOR ANALYSIS

The single vector analysis directly compares results of different model cases for a single vector of input parameter values. A single vector analysis has the advantage over the standard 100-vector replicate analysis in model development because changes in a single output curve are easier to monitor and understand than are a family of 100 curves generated from uncertainty analysis. The caveat of this approach, however, is that the input data only represent one unique condition in a large space of parameter uncertainty. It is thus important to remember that the single-vector results do not define the system response to incremental changes in model cases. For this reason, single-vector analyses are not used to satisfy WIPP compliance requirements, though they can serve as a useful tool in model troubleshooting and development.

D.2 MODEL CASE DEVELOPMENT

To develop the TBI case, the BRAGFLO model was changed incrementally, and model results were compared for each increment. Changes were introduced incrementally in the BRAGFLO model as shown in Table D.1. After each change, the model was run and the results examined. This incremental approach helped to identify two sets of changes; one set that has little effect on results and another that significantly affects results. This distinction was then used to formulate the intermediate case, termed the TBI, for analysis with a full replicate of 100 vectors. The TBI case only included changes to the grid geometry and removal of the upper DRZ fracture option, both properties that did not generate visible differences in model output. The correction to the molecular weight of cellulose and implementation of the option D panel closures more significantly affected the model results. These cases were tested individually in TBM-c and TBM-d, respectively, with the sum of changes represented in the final TBM case.

Table D.1. Summary of Calculation Subsets Examined with BRAGFLO

Calculation Subset	System Description	Grid	Fracturing in Upper DRZ?	MW (kg/mol)	PCS
TBM-a	BRAGFLO was run with the new grid incorporating the PAVT PCS.	New	Yes	0.030	PAVT
TBI	BRAGFLO was run with the new grid incorporating the PAVT PCS but without fracturing in the upper DRZ.	New	No	0.030	PAVT
TBM-c	BRAGFLO was run with the new grid incorporating the PAVT PCS, no fracturing in the upper DRZ, and the new molecular weight of cellulose.	New	No	0.027	PAVT
TBM-d	BRAGFLO was run with the new grid incorporating the Option D PCS, no fracturing in the upper DRZ, and the old molecular weight.	New	No	0.030	Opt D
TBM	BRAGFLO was run with the new grid incorporating the Option D PCS, no fracturing in the upper DRZ, and the new molecular weight.	New	No	0.027	Opt D

D.3 ANALYSIS OF RESULTS

The single vector chosen here for analysis was PAVT Replicate 1, Vector 008, for scenario S1. Brine saturation, gas generation, and pressure were analyzed for each of the five cases listed in Table 1. For most variables, behavior distinguishing model cases was most pronounced at early times, and therefore many of the plots extent to 1,000 to 6,000 years on the time axis, though the simulations were all run to 10,000 years.

Vector 008 was chosen because it exhibited high pressures in the waste panel in the PAVT. Consequently, the analysis anticipated that pressure in this vector would be sensitive to the changes listed in Table 1. In hindsight, this vector was a poor choice for examining the changes in brine saturation, since saturation remains very low in all cases, obscuring the incremental effect of each change to the system.

D.3.1 Brine Saturation

Figure D-1 shows brine saturation in the waste panel as a function of time. For all cases examined, brine saturations peak at only 4% and quickly fall to near 0% by 1500 years. The small differences among the curves thus give little physical insight into distinctive case behavior. Figure D-2 shows that brine saturation in the rest of repository is very similar to brine saturation in the waste panel; again, the differences between the curves are not meaningful for this particular vector.

Figure D-3 shows brine saturation in the experimental area from 0 to 6,000 years. Although the differences in these curves are again small, they are consistent with the expected effects of the conceptual model changes on brine saturation when the full replicate is examined. When the new grid is introduced, the experimental area becomes slightly more saturated than in the PAVT. This increase in saturation is due to the change in the grid flaring algorithm, which increases the volume of marker beds adjacent to the experimental area. Brine flow from the marker beds into the north end of the repository must pass through the experimental area. With the addition of the option D panel closures, saturation in the experimental area is further increased because gravity-driven brine flow from the experimental area southward, which moves significant volumes of brine in the PAVT, is blocked by the tight panel closures, creating a ponding effect up-gradient of the closure. This ponding effect is realized as an increase in brine saturation in the experimental area.

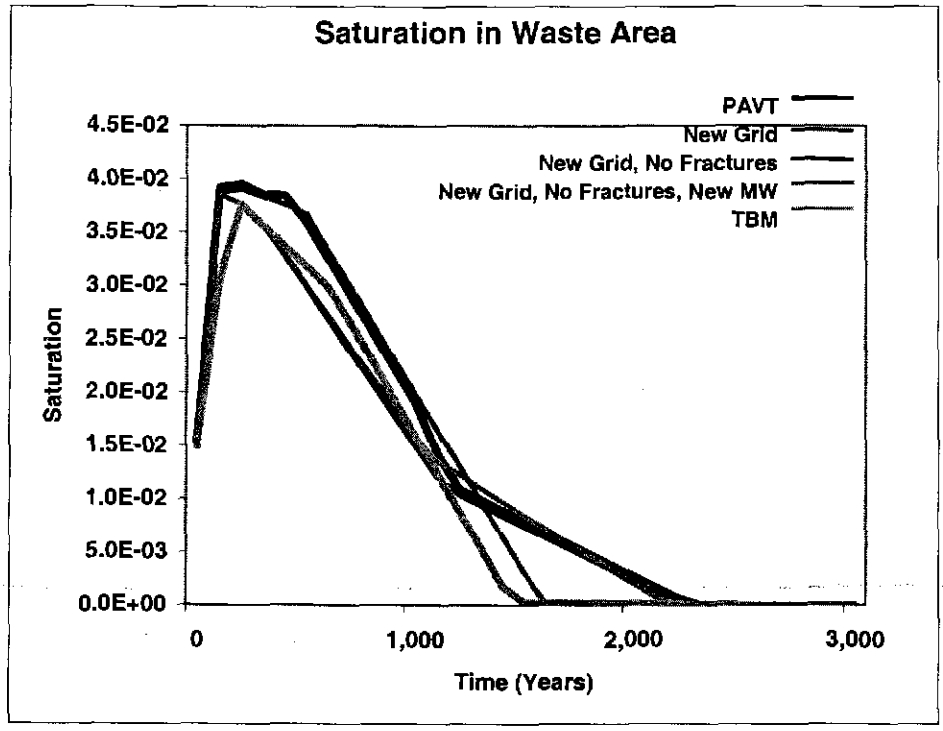

Figure D-1. Undisturbed Scenario (S1); Brine Saturation In The Waste Panel [WAS_SATB], Vector 008

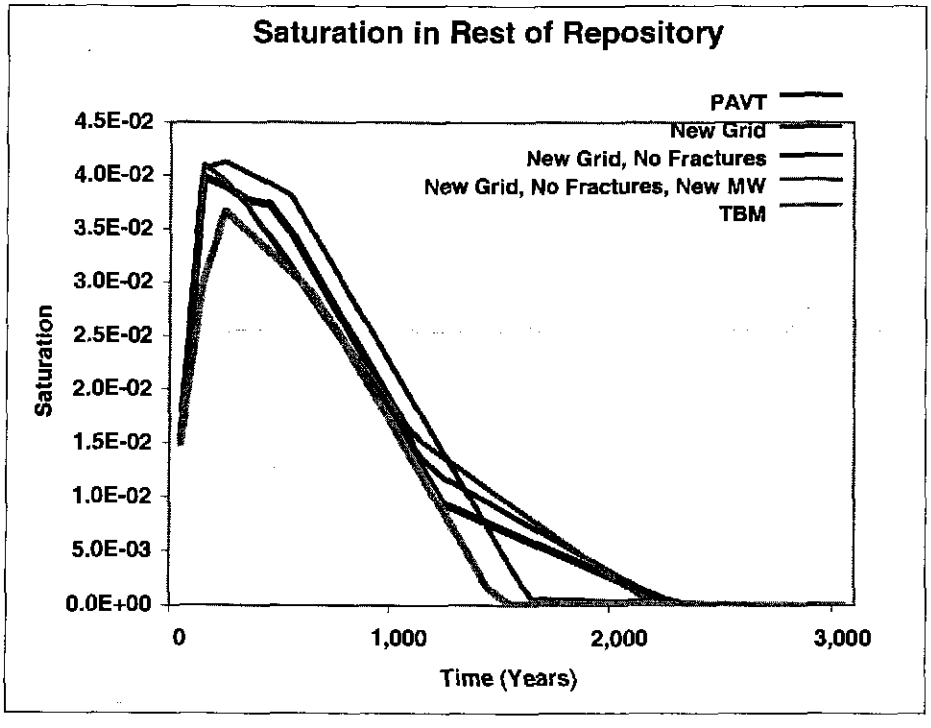

Figure D-2. Undisturbed Scenario (S1); Brine Saturation In The Rest Of Repository [REP_SATB], Vector 008

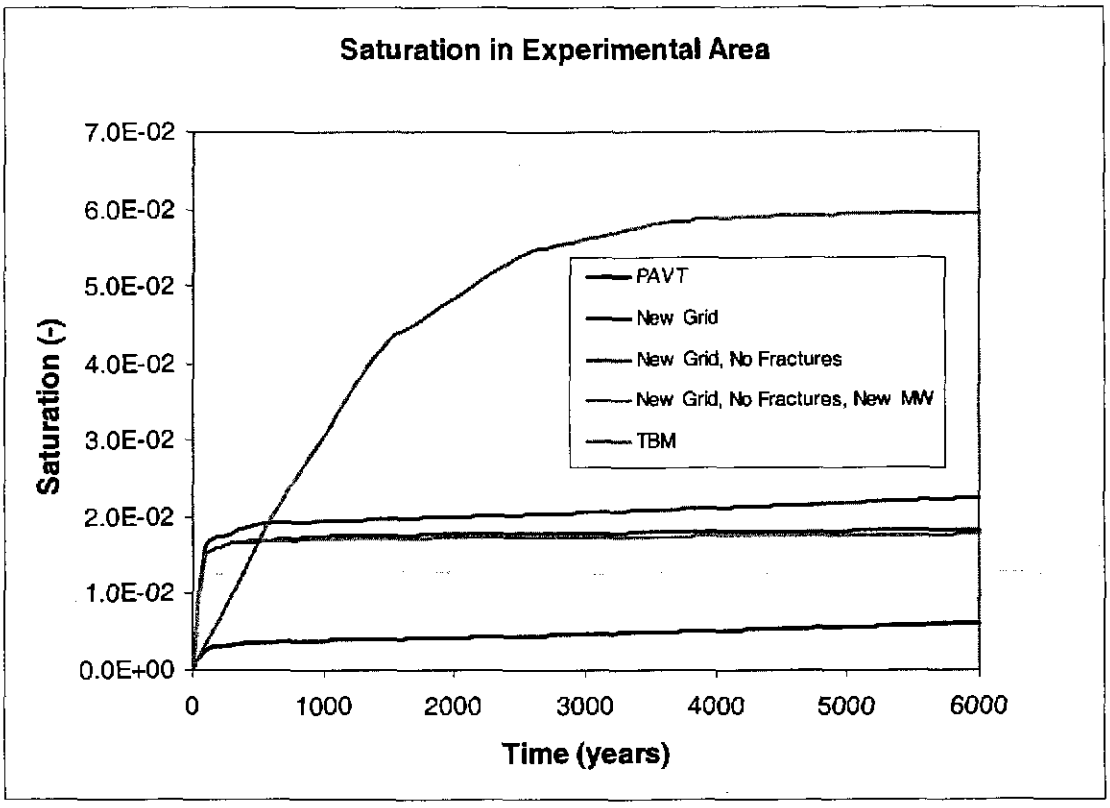

Figure D-3. Undisturbed Scenario (S1); Brine Saturation In The Experimental Area [EXP_SATB], Vector 008

D.3.2 Gas Generation

Gas is generated in the waste regions both by corrosion of steel in brine and degradation of cellulosics by microbial action. As the reactions proceed, both the mass of iron and cellulosics in the repository decrease. Figure D-4 illustrates how the mass of iron remaining in the repository decreases as a function of time for vector 008. There is no distinguishable effect of model changes on the degradation of iron in the repository. This is largely because iron corrosion proceeds only under brine-inundated conditions, and the waste panel saturation was sufficiently low in all cases (WAS_SATB < 0.04) that only 10% of the steel was corroded by 1,500 years when the saturation decreased to nearly zero and effectively shut down corrosion.

Microbial degradation of plastics, rubbers and cellulose also produces gas. Thus, the mass of cellulosics remaining in the repository as a function of time indicates the extent of reaction for microbial degradation (Figure D-5). By 1,000 years, all cases in vector 008 have exhausted the cellulosics.

Figure D-6 shows the moles of gas generated in the repository as a function of time. All model cases predict a rapid increase in moles of gas in the repository reaching a steady-state value at about 1500 years, distinguished by two groupings. The lower steady-state value represents cases

using the PAVT cellulosics molecular weight of 0.030 kg/mol. The higher values represent cases with the new TBM cellulosics molecular weight of 0.027 kg/mole. The reduction in molecular weight from 0.030 kg/mole to 0.027 kg/mol increased the number of moles of gas produced from a fixed mass of cellulosics that is completely degraded by about 10%. Gas production is a primary driver for pressurization of the repository, which is discussed next..

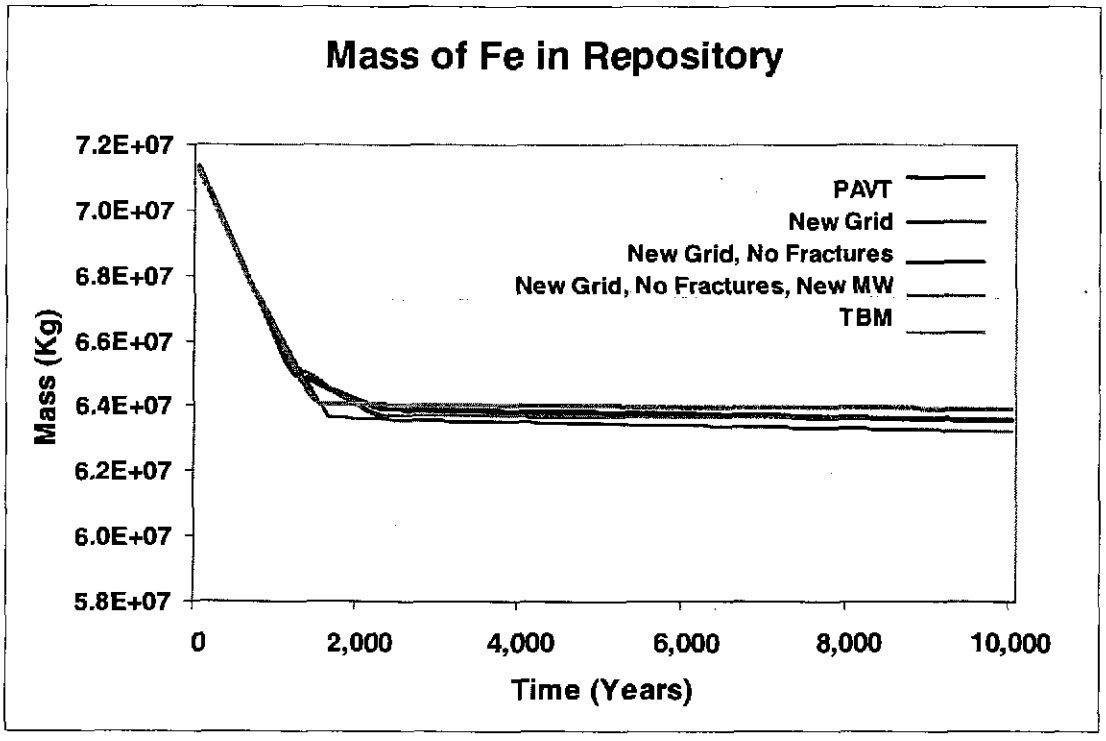

Figure D-4. Undisturbed Scenario (S1); Mass Of Iron In The Repository [FE_KG], Vector 008

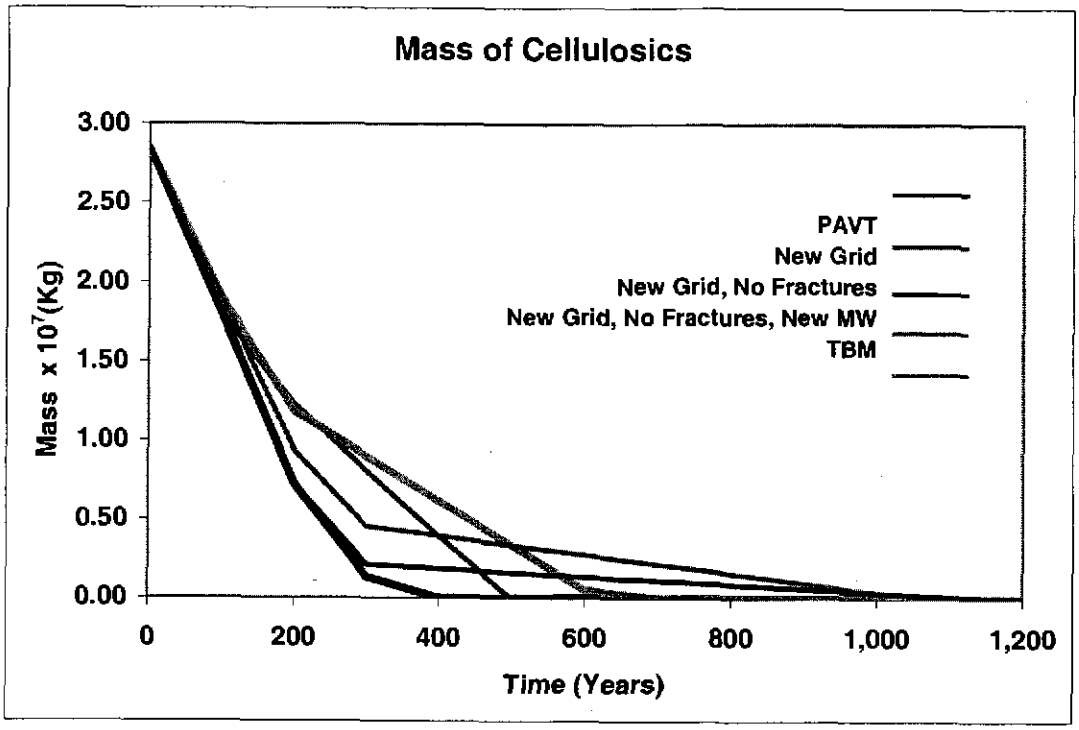

Figure D-5. Undisturbed Scenario (S1), Mass Of Cellulosics In The Repository [CELL_KG], Vector 008

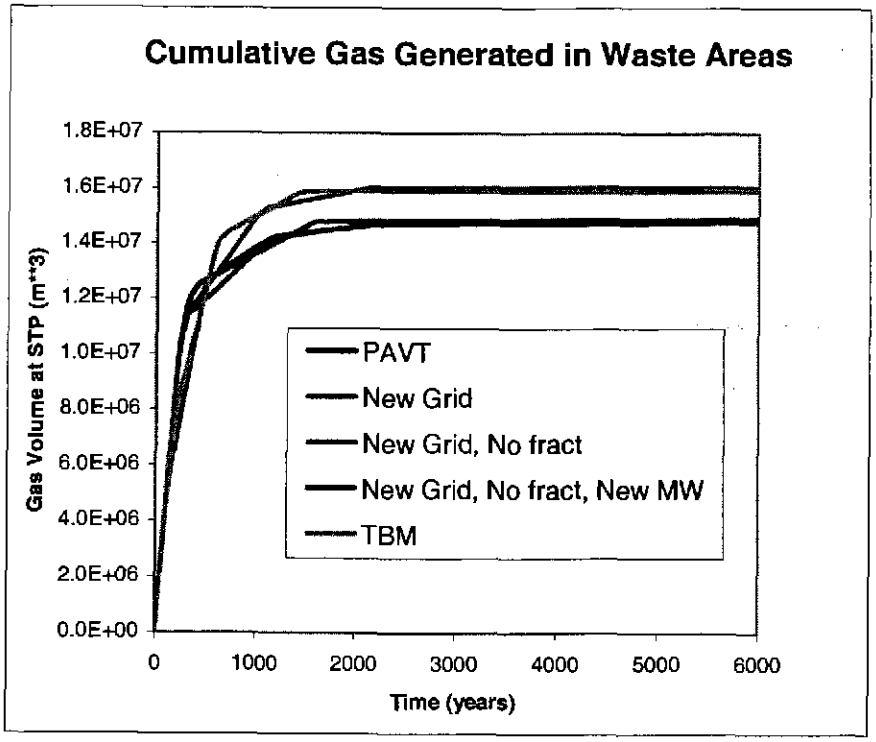

Figure D-6. Undisturbed Scenario (S1); Moles Of Gas Generated In The Waste Regions [GAS_MOLE]; Vector 008

D.3.3 Pressure

Figure D-7 shows the pressure in the waste panel for Scenario S1 as a function of time. All of the cases show a rapid increase in the waste panel pressure reaching a steady-state value at about 1000 years. The primary factors driving this pressure increase are, brine inflow from the upper DRZ and gas generation from the waste regions, and creep consolidation of the host rock. Both have their largest impact within the first 1,000 years after repository closure. Pressure in the undisturbed waste panel therefore typically attains a steady value after 1,000 years determined primarily by the total amount of gas generated. Changing the grid (TBM-a) and removing the upper DRZ fracturing (TBI) increase the steady-state pressure over the PAVT by about 2%. Adding the revised molecular weight of cellulose (TBM-c) and option D panel closures (TBM) raises the 10,000-year pressures by about 8% over the PAVT case.

Noteworthy in the TBM case is the pressure overshoot in the waste panel between 1000-2000 years. The corresponding time lag in pressure rise in the experimental area, shown in Figure D-8, illustrates the dynamic effect of the tight option D panel closures over the loose PAVT representation. This phenomenon was also observed in the replicate analysis and is discussed more in the main body of this report.

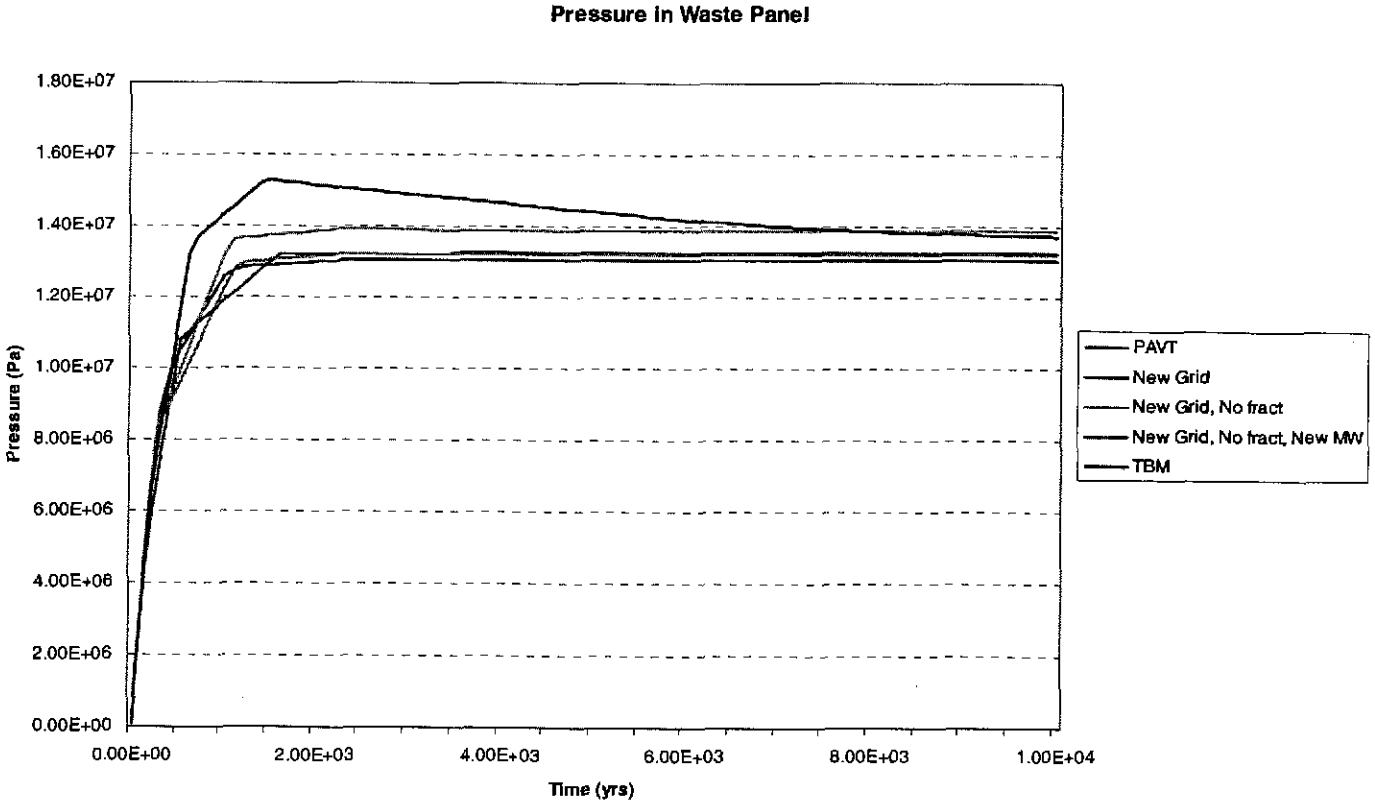

Figure D-7. Undisturbed Scenario (S1); Pressure in the Waste Panel [WAS_PRES]; Vector 008

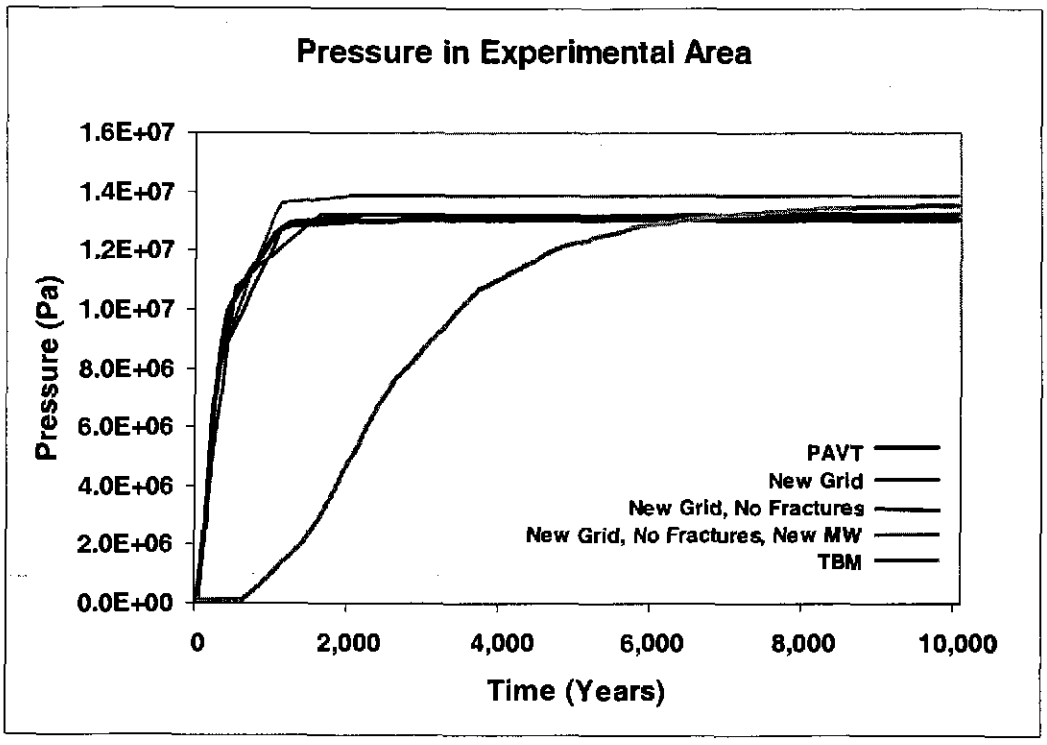

Figure D-6. Undisturbed Scenario (S1); Pressure in the Experimental Area [EXP_PRES]; Vector 008

APPENDIX E
TBM COMPUTATIONAL SUMMARY

E.1 PURPOSE

This appendix contains run control documentation for the BRAGFLO component of the TBM calculation. Similar documentation for the PAVT is provided in Aragon et al, 1997. The information in this appendix ensures reproducibility for the calculation.

E.2 HISTORY OF THE QUALIFIED COMPUTATIONAL ENVIRONMENT

The Technical Baseline Migration calculation is referred to as the TBM calculation in the code management system (CMS) libraries. The intermediate case is also archived in CMS with the descriptor TBI. The calculations were completed between March and May 2002 on Sandia's VAX cluster running Open VMS 7.2.

E.3 SCRIPTS, CODES AND INPUT FILES

The TBM calculation was executed by modifying the run control scripts from the PAVT to account for new code versions and for changes in input files. The TBM calculation used the newest version of BRAGFLO and several other codes. Codes run for this analysis are listed in Table E-1. Since the PAVT, changes in the performance assessment computing system have necessitated modifications to the performance assessment codes. For example, in 2000 the parameter database was migrated to a new data model and the database management software was replaced. The modified codes were tested to ensure that model results were not affected by the changes in the computing system. Lechel and Tisinger 2002 summarize the changes in the performance assessment computing system since the CCA, and the consequent testing of the performance assessment codes.

Input files were provided by Joshua Stein and included new files for each of the three scenarios, S1, S3 and S5. Additionally, a new grid input file, MATSET input file, LHS two input files, ICSET input file and an ALG input file were provided. A POSTALG input file was also provided by David Lord for post processing BF3 results.

E.4 EXPLANATION OF RUN CONTROL TABLES

This appendix contains the run documentation tables for the TBM Calculation. The tables include a heading indicating the code being run, and the process step. Many code sets are broken down into a first step (Step 1) that runs utility codes such as GENMESH (GM), MATSET (MS), and LHS and the second step (Step 2) that runs the primary code along with any pre- and post-processors. Step 1 codes are generally run once, or once per scenario; Step 2 codes are generally run once per vector.

The run control tables are intended to provide all the information normally required to document a calculation. The tables contain six columns:

1. **Code** – the descriptive common code name (ICSET, ALGEBRACDB, BRAGFLO, ...) indicating the row relates to that code, "script" indicating the row relates to the run control system, or blank indicating the row relates to the previous code label. Completely blank rows are for visual separation only.

2. **File name** – VMS file name in the form filename extension. Placeholders are included when multiple scenarios, vectors, time intrusions, etc. are being represented.

3. **File type** – indicates the type of file being identified from the point of view if the current step of the run control system. These include script, script log, executable, input, and output. Note, an output of one step may be the input of another step.

4. **CMS library** – contains the CMS library name where the controlled version of the file can be found, or contains the string "not in CMS." Many files generated by a calculation are for debug purposes, or are intermediate in nature, and are not retained after execution. Files that have been identified as required (by the PA or principal investigator) are always stored in CMS.

5. **Source** – when needed, identifies the source for a file. For example many input files were copied from CCA CMS libraries. Files were copied so that the RH-TRU libraries would be self-contained, enhancing reproducibility.

6. **Comment** – various comments including some run dates, database views, code version numbers, and so on.

Table E-1. Code Versions Used In The TBM Calculations

Code Name	Version	File Spec/Build Date
ALGEBRACDB	2.35	ALGEBRACDB_PA96 – 31-JAN-1996
BRAGFLO	4.10.02	BRAGFLO_QA0410B- 13-JAN-2002
BRAGFLO	4.10.03	BRAGFLO_QA0410C- 12-APRIL-2002
GENMESH	6.08	GM_PA96 - 31-JAN-96
ICSET	2.22	ICSET_PA96 - 1-FEB-1996
LHS	2.41	LHS_PA96_2 - 6-MAR-1996
MATSET	9.10	MATSET_QA0910- 29-NOV-2001
POSTBRAG	4.00	POSTBRAG_PA96 - 6-FEB-1996
POSTLHS	4.07	POSTLHS_PA96 - 7-FEB-1996
PREBRAG	6.00	PREBRAG_PA96 - 6-FEB-1996
PRELHS	2.30	PRELHS_QA0230- 27-NOV-2001

Table E-2. BRAGFLO Calculation

BRAGFLO
Step 1 (BRAGFLO)

Code	File Name	File Type	CMS Library	Source	Comments
Script	eval_bf_tbm_run.com	script	tbm_eval	n/a	Instance Script
	eval_bf_tbm_run_master.com	script	tbm_eval	n/a	Distribution Script
	eval_bf_tbm_step1.inp	script input	tbm_eval	n/a	Parameter_Prod DB
	bf_tbm_r1_s1_step1.log	output	tbm_bfr1sy	n/a	
Genmesh	gm_pa96.exe	executable	gm	Built 1/31/1996	Ver 6.08
	gm_bf_tbm.inp	input	tbm_gm	Provided by JSSTEIN	
	gm_bf_tbm.cdb	output	not in CMS	n/a	
	gm_bf_tbm.dbg	output	not in CMS	n/a	
	gm_bf_tbm_rev1.inp	input	tbm_gm	PER JSSTEIN	Minor change to grid (for records)
Matset	matset_qa0910.exe	executable	ms	Built 11/29/2001	Ver 9.10 (changed from 9.04)
	ms_bf_tbm.inp	input	tbm_ms	Provided by JSSTEIN	
	gm_bf_tbm.cdb	input	not in CMS	intermediate file	
	ms_bf_tbm.cdb	output	not in CMS	n/a	
	ms_bf_tbm.dbg	output	tbm_ms	n/a	
	ms_dbg$output.dat	output	tbm_ms	n/a	
Prelhs	prelhs_qa0230.exe	executable	lhs	Built11/27/2001	Ver 2.30 (changed from 2.24)
	lhs1_bf_tbm_r1.inp	input	tbm_lhs	Provided by JSSTEIN	
	lhs1_bf_tbm_trn_r1.out	output	tbm_lhs	n/a	
	lhs1_bf_tbm_r1.out	output	tbm_lhs	n/a	
	lhs1_bf_tbm.inp	input	tbm_lhs	provided by Josh Stein	
LHS	lhs_pa96.exe	executable	lhs	Built 3/6/1996	Ver 2.41
	lhs1_bf_tbm_trn_r1.out	input	tbm_lhs	n/a	

Code	File Name	File Type	CMS Library	Source	Comments
	lhs2_bf_tbm_trn_r1.out	output	tbm_lhs	n/a	
	lhs2_bf_tbm_dbg_r1.out	output	tbm_lhs	n/a	
PostLHS	postlhs_pa96.exe	executable	lhs	Built 2/7/1996	Ver 4.07
	ms_bf_tbm.cdb	input	tbm_lhs	intermediate file	
	lhs3_bf_tbm.inp	input	tbm_lhs	Provided by JSSTEIN	
	lhs2_bf_tbm_trn_r1.out	input	tbm_lhs	n/a	
	lhs3_bf_tbm_a1_rzzz.cdb	output	tbm_lhs	n/a	To follow LHS requirements and CCA convention, "A1" use rather than "R1" and "rzzz" used rather than "vzzz".
	lhs3_bf_tbm.dbg	output	not in CMS	n/a	
	lhs3_bf_tbm_1.scr	output	not in CMS	n/a	
	lhs3_bf_tbm_2.scr	output	not in CMS	n/a	
Icset	icset_pa96.exe	executable	ic	Built 2/1/1996	Ver 2.22
	lhs3_bf_tbm_a1_rzzz.cdb	input	tbm_lhs	Intermediate file	
	ic_bf_tbm.inp	input	tbm_ic	C97	
	ic_bf_tbm_r1_sy.cdb	output	not in CMS	n/a	
	ic_bf_tbm_r1_sy.dbg	output	not in CMS	n/a	
Algebracdb	algebracdb_pa96.exe	executable	alg	Built 1/31/1996	Ver 2.35
	ic_bf_tbm_r1_sy.cdb	input	not in CMS	Intermediate file	
	alg_bf_postalg_tbm.inp	input	tbm_alg	Provided by DLLORD	Post BF processing
	alg_bf_tbm.inp	input	tbm_alg	Provided by JSSTEIN	
	alg_bf_tbm_r1_vzzz.cdb	output	tbm_alg	n/a	
	alg_bf_tbm_r1_sy.dbg	output	not in CMS	n/a	

- sy – is used to indicate multiple scenarios, where y is 1 through 6.
- vzzz – is used to indicate multiple vectors, where zzz is 1 through 100.
- txxxx – is used to indicate intrusion times., where *xxxx* varies. A list is provided as needed.

- *d* – U for upper or L for lower.

Step 2 (BRAGFLO)

Code	File Name	File Type	CMS Library	Source	Comments
Script	eval_bf_tbm_run.com	script	tbm_eval	n/a	Instance Script
	eval_bf_tbm_run_master.com	script	tbm_eval	n/a	Distribution Script
	eval_bf_tbm_step2.inp	script input	tbm_eval	n/a	Script Input File
	bf_tbm_r1sy_vzzz.log	output	tbm_bfr1sy	Script log file	Script Log File
Prebrag	prebrag_pa96.exe	executable	bf	Built 2/6/1996	Ver 6.00
	bf1_tbm_r1_sy.inp	input	tbm_bfr1sy	Provided by Jim Bean	S1, S3, S5
	alg_bf_tbm_r1_sy_vzzz.cdb	input	tbm_alg	n/a	
	bf1_tbm_r1_sy_vzzz.dbg	output	not in CMS	n/a	
	bf2_tbm_r1_sy_vzzz.inp	output	tbm_bfr1sy	n/a	
Bragflo	bragflo_qa0410b.exe	executable	bf	Built 1/13/2002	Ver 4.10.02
	bf2_tbm_r1_sy_vzzz.inp	input	tbm_bfr1sy	Intermediate file	
	bf2_tbm_r1_sy_vzzz.out	output	not in CMS	n/a	
	bf2_tbm_r1_sy_vzzz.sum	output	not in CMS	n/a	
	bf2_tbm_r1_sy_vzzz.bin	output	not in CMS	n/a	
	bf2_tbm_r1_sy_vzzz.rot	output	not in CMS	n/a	
	bf2_tbm_r1_sy_vzzz.rin	output	not in CMS	n/a	
Postbrag	postbrag_pa96.exe	executable	bf	Built 2/6/1996	Ver 4.00
	bf2_tbm_r1_sy_vzzz.bin	input	not in CMS	Intermediate file	
	alg_bf_tbm_r1_sy.cdb	input	tbm_alg	Intermediate file	
	bf3_tbm_r1_sy_vzzz.cdb	output	tbm_bfr1sy	n/a	
	bf3_tbm_r1_sy_vzzz.dbg	output	not in CMS	n/a	

- sy – is used to indicate multiple scenarios, where y is 1 through 6.
- vzzz – is used to indicate multiple vectors, where zzz is 1 through 100.
- txxxx – is used to indicate intrusion times., where *xxxx* varies. A list is provided as needed.
- *d* – U for upper or L for lower.